Primer Vector Theory in the Design of Optimal Transfers Involving Libration Point Orbits

A Thesis
Submitted to the Faculty

of

Purdue University

by

Julia Lea Bell

In Partial Fulfillment of the
Requirements for the Degree

of

Doctor of Philosophy

December 1995

To Mom, Dad, Jennifer, and Deborah.

ACKNOWLEDGMENTS

Many people throughout my life have provided the opportunities and the preparation that have allowed me to pursue my education at Purdue University, including the work that is presented in this document. I appreciate the contributions of my family, teachers, colleagues, and friends to my life and to this work.

My parents, Dorothy and David Bell, and sisters, Jennifer and Deborah, deserve much more than my thanks for the unlimited support and confidence that they have always shown. For their influence in my life, and for all that they have taught me, I express my gratitude and appreciation. I am honored to be a member of this family.

As a student in the School of Aeronautics and Astronautics of Purdue University, I have benefited from the instruction and guidance of several members of the faculty, staff, and student body. The education and encouragement that I have received from Professor Kathleen Howell, as an advisor, teacher, and role model have shaped my experience. I thank her for her generosity.

I would also like to thank the other members of the faculty who have contribute to this work as members of my graduate committee, Professors Martin Corless, Horatio Espinosa, James Longuski, and Terrence Weisshaar.

Finally, I would like to express my thanks to the people who have assisted in providing the financial support that has enable me to continue my education. Sources of support have included the Purdue University Fellowship Program and the NASA Indiana Space Grant Consortium.

TABLE OF CONTENTS

Page

LIST OF TABLES

Appendix Table

LIST OF FIGURES

ABSTRACT

Bell, Julia Lea. Ph.D., Purdue University, December 1995. Primer Vector Theory in the Design of Optimal Transfers Involving Libration Point Orbits. Major Professor: Dr. Kathleen C. Howell.

Optimal impulsive transfers between libration point orbits associated with the same libration point are considered in the circular and elliptic restricted three-body problems. Existing primer vector theory is applied in conjunction with numerical integration and differential corrections techniques to construct optimal trajectories. The necessary conditions for optimality are stated in terms of the primer vector. Coast arcs and interior impulses are employed simultaneously to improve non-optimal paths. Both superior and inferior optimal transfers in the Sun-Earth problem are achieved for L_1 halo orbits with out-of-plane amplitudes in the range of 110,000 km to 800,000 km.

Unconstrained numerical optimization techniques are used to compute the optimal coast arcs and the optimal timing and location for interior impulses. A gradient-based algorithm is employed where the gradients are evaluated from analytic expressions that are functions of the primer vector and its time derivative. Differential corrections techniques are developed to solve point-to-point targeting problems that occur within the optimization process.

Families of optimal transfers are presented that include various target orbits that are characterized by the out-of-plane amplitude. Two classes of optimal solutions are presented. Optimal solutions requiring two impulses are computed for transfers between L_1 northern halo orbits where the transfer path exists above the plane of primary motion. Optimal solutions requiring three impulses are presented for transfers between L_1 northern orbits where the transfer occurs below the plane of primary motion. The optimal costs are plotted versus the amplitudes of the target orbits. A linear function that approximates the relationship between the transfer cost and the target amplitude is identified for transfers in each class.

I. INTRODUCTION

The regions of space that are explored by libration point orbits offer new perspectives for scientific investigations and satellite communications. Many issues that must be addressed for the consideration of libration point orbits as practical alternatives to traditional body-centered trajectories have been examined in previous studies of solutions in a restricted three-body problem. Lacking an exact analytical solution to the restricted problem, much of the work has focused on the development of numerical solutions. As part of a continuing effort, this work is a numerical analysis of transfer paths between libration point orbits associated with the same libration point.

A. Problem Definition

The optimal impulsive transfer problem is considered under assumptions consistent with the restricted three-body problem, in the context of transfers between libration point orbits in the Sun-Earth system. A gradient-based numerical optimization algorithm is employed with analytic gradients to identify the optimal solution. The trajectory is computed as the solution of a multi-state targeting problem using a differential corrections scheme that targets selected points along the specified paths. All impulses along the optimal trajectory simultaneously satisfy the necessary conditions for optimality.

1. Elliptic Restricted Three-Body Problem

In orbital mechanics, a complete solution for the motion of two gravitationally attracting point masses is available from a dynamic analysis of the two-body system. If, however, an arbitrary third mass is added to the system to form a "three-body problem," the number of independent physical constants that are available is not sufficient to define a complete set of integrals of the motion[1]. For some applications, however, a compromise between the complete three-body structure and a two-body problem is acceptable. A simplified system based on the assumption that one of the particles has infinitesimal mass provides a reasonable approximation for the motion of a spacecraft in a region of space where neither of the two gravitational fields can be neglected. With the assumption of infinitesimal mass for

the third body, the motion of the remaining two primary bodies is governed by the solution to the two-body problem. The motion of the third body can then be investigated using a system that consists of only the third body under the influence of two completely modeled external gravitational fields. This analysis is a study of motion in the "elliptic restricted three-body problem" (ER3BP). A special case of the problem is the circular restricted three-body problem (CR3BP) in which the two primary bodies of finite mass are assumed to move on circular paths. The uniform primary motion that exists in the circular problem simplifies many aspects of the analysis. For this reason, the circular problem is used as a preliminary model for the development of solution techniques that are then extended to the elliptic system. A complete solution is not available for either the elliptic or circular problems, but both models possess equilibrium solutions and approximate solutions associated with the equilibrium conditions that are useful in obtaining solutions in the general problem.

a. Libration Points

The equilibrium solutions that exist in the restricted problem are most easily described in the context of the circular problem, where they are stationary solutions relative to a coordinate system that rotates with the primaries. In this system, five distinct equilibrium locations, called "libration points," exist in the plane defined by the primary motion. Three of the points, called the "collinear points," are located on the line that joins the primaries. Each of the remaining two points is the vertex of an equilateral triangle formed with the primaries. In the elliptic problem, the primaries oscillate along the line that joins the particles in the rotating frame. To compensate for this motion, the collinear points in the elliptic problem also oscillate along that line. Similarly, the triangular points shift in position to maintain the equilateral triangle structure. Thus, while instantaneous equilibrium solutions in the elliptic problem can still be identified relative to the rotating coordinate frame, the solutions are not stationary in this frame.

b. Halo Orbits

Although analytic expressions for the locations of the equilibrium points are available, no closed form solution exists for general motion in the restricted problem. For motion near the libration points, however, both numeric and approximate analytic solutions have been developed. The trajectories represented by such solutions are called "libration point orbits." One type of libration point orbit is a three-dimensional, quasi-periodic solution associated with a collinear libration point, called a "Lissajous trajectory." A periodic class of solutions can be defined if a constraint is imposed on the relative amplitudes of the Lissajous trajectories. Solutions of this type are called "halo orbits." The regions of space in which

halo orbits exist in the Sun-Earth system are useful for studies of solar induced phenomena. The "International Sun-Earth Explorer-3" (ISEE-3) spacecraft, launched in 1978, used the advantages of such an orbit to study the Sun-Earth interplanetary environment[2, 3].

2. Optimal Transfers

The computation of individual libration point orbits is aided by the existence of approximate analytic solutions[4, 5]. Recent studies have used these solutions in the development of transfer paths between libration point orbits; however, numerical approaches that are considered in those works have also been successful[6, 7]. The costs associated with the transfer paths that have been developed are sensitive to the characteristics of the trajectories. Thus, a study of optimal trajectories, in which the characteristics of the transfer are selected according to the optimality criteria, reduces the influence of the procedure and allows a more objective analysis of the feasibility of missions that employ multiple libration point orbits.

The solutions to many optimization problems involve two-point boundary value problems that are expressed in terms of the state variables describing the system and auxiliary variables, called "Lagrange multipliers," that are used to incorporate constraints imposed on the optimization. For the problem considered here, the necessary conditions for optimality are stated in terms of these multipliers. Furthermore, the multipliers provide an analytic expression for the gradient of the cost function that is useful in a numerical optimization procedure.

a. Primer Vector Theory

As developed by Lawden, the optimality conditions for the optimal rocket trajectory problem in a general gravitational field may be expressed in terms of a switching function that governs the thrust magnitude and auxiliary variables that identify the thrust direction[8]. If only impulsive maneuvers are permitted, the necessary conditions for optimality can be expressed in terms of auxiliary variables that are the elements of the "primer vector." Hiday and Howell extended Lawden's solution for use in a statement of the restricted three-body problem that is not consistent with Lawden's assumptions. They also demonstrated techniques by which a non-optimal solution may be improved with the inclusion of coast arcs and interior impulses[6, 7]. The present work follows directly from their development and continues the search for optimal solutions using numerical optimization methods with contributions from an analytic analysis of the necessary conditions for optimality.

b. Numerical Optimization

Many of the numerical optimization techniques that have been developed since the invention of high-speed computers use optimization methods that are based on differential calculus such as those introduced by Newton. Such techniques often require the computation of numerous intermediate solutions, particularly if analytic expressions for the required gradients are not available. The sensitivity of orbital calculations in the restricted problem to relatively small perturbations discourages the computation of significant numbers of solutions; therefore, analytic expressions for the gradients are used to limit the impact of the sensitivities.

In this work, a variable metric numerical optimization routine is used to determine a set of variables that characterize the optimal transfer path. An analytic expression for the gradient associated with the cost function is evaluated as a function of the primer vector. The individual solutions that are required by the method are computed using a differential corrections scheme that satisfies specified endpoint constraints. The optimal number of impulses is determined by sequentially adding impulses to a non-optimal path in a manner consistent with the characteristics of the primer vector; however, the location and timing of all impulsive maneuvers are optimized simultaneously. Thus, the optimal solution is not necessarily a collection of segments that are individually optimal but do not form a complete optimal path; rather, all segments of the solution are considered simultaneously to produce a trajectory that is optimal in its entirety.

B. History of the Problem

The present work incorporates the areas of optimization and trajectory design in an environment that is defined by the restricted three-body problem. Thus, the results of previous studies in each of these areas have identified many of the advantages and difficulties that are associated with work in these fields. The recent investigations of Hiday and Howell, that introduced the classical approach for the optimal rocket trajectory problem to the restricted problem and continued with a numerical study of the optimal paths[6, 7], provides the basis for this study. The targeting approach to trajectory design, employed by Pernicka for the computation of Lissajous trajectories[9], also represents a significant contribution since it inspired many of the trajectory construction techniques that are used here.

1. Restricted Three-Body Problem

Early work on the three-body problem and the restricted three-body problem is primarily attributed to Newton, Euler, Jacobi, and Lagrange in the late 1600's and 1700's. Following

Newton's investigation of the motion of the Sun, Earth, and Moon in 1687[10], work on the restricted problem originated with Euler's investigation of a simplified version of the problem in 1760[11], although the term "restricted" was not specifically applied until 1892 in Poincaré's discussion of the problem as a special case of the three-body problem[11]. The value of Euler's suggestion to seek solutions relative to a rotating coordinate frame is supported by the use of convenient rotating working frames in current studies of the restricted problem. Discussion of equilibrium solutions in the restricted problem by Lagrange in 1772[1, 10] was followed in 1836 by Jacobi's development of an integral of the motion that identifies bounded regions of motion for the particle of interest[11]. During the late 1800's to mid-1900's, work on the restricted problem focused on periodic solutions following Poincaré's conclusion that periodic solutions exist[12]. Periodic solutions were developed by Moulton[11, 13] and Plummer[13] with emphasis on solutions near the collinear libration points; however, the exploration of higher order analytic solutions, including three-dimensional solutions, was limited due to the nature of the computations such work requires.

2. Three-Dimensional Libration Point Orbits

With the introduction of high-speed computers, investigations of numerical solutions and three-dimensional solutions were pursued. In 1967, Szebehely presented numerically integrated solutions to the planar circular problem and extensions of the early work to the elliptic problem[11]. Studies of three-dimensional motion in the late 1960's by Farquhar lead to the identification of periodic three-dimensional orbits, called halo orbits, that repeat exactly with each revolution[14, 15]. Although they are known to exist, the computation of such orbits is difficult without accurate knowledge of their characteristics. Thus, the development of approximate analytic solutions for halo orbits and for a more general class of bounded three-dimensional libration point orbits, called Lissajous trajectories, was an important requirement for further analysis of motion in the restricted problem.

In 1973, Farquhar and Kamel published an analytic approximation for the quasi-periodic orbits that are associated with the libration point on the far side of the Moon in the Earth-Moon system[16]. Additional approximations for both Lissajous and halo orbits have been developed by Richardson and Cary[4, 17] and have been used in subsequent studies to provide the initial approximations that are required by many numerical investigations[6, 9, 18]. More recently, in 1990, Marchal published an approximation for halo orbits, based on a Fourier series expansion, that is used in the present numerical study[5].

In the late 1970's and 1980's, researchers used numerical investigations to seek families of libration point orbits associated with the collinear points. Following Farquhar and Kamel's

investigation of the libration point region on the far side of the Moon, the discovery of a family of orbits in this region by Breakwell and Brown[19] lead to the discovery by Howell of families of orbits associated with each of the collinear points[20, 21]. A significant step for numerical studies of Lissajous and halo orbits was achieved with the publication by Howell and Pernicka of an algorithm to determine Lissajous trajectories for arbitrary primary motion[9, 22]. Their methodology has also been used to compute orbits that retain the general characteristics of halo orbits in cases where precisely periodic halo orbits are not available[6, 18]. The techniques successfully employed in the multi-state targeting scheme discussed in [9] provides the incentive for the use of similar targeting problems in this work.

3. Optimal Transfers

Given the families of libration point orbits that have been discovered thus far, economical transfers between orbits may be useful. The transfer problem can be stated in terms of several different criteria for optimality. For this work, the standard is defined as the minimum change in velocity due to an external force (which corresponds to the minimum fuel consumption for an impulsive maneuver). Hohmann's development of the optimal impulsive solution for transfers between coplanar circular orbits in the two-body problem (1925) is one of the earliest examples of work in the optimal rocket trajectory problem[23]. While Hohmann's original work was presented with a geometrical perspective, a calculus of variations approach provides additional insight into the problem and is more easily generalized to different gravitational environments.

a. Primer Vector Theory

Lawden applied the calculus of variations to the transfer problem in a general gravitational field where the governing differential equations may be expressed as functions of position and time. In his development, the necessary conditions for optimality for impulsive transfers are stated in terms of the adjoint variables associated with the velocity[8]. These variables are denoted as elements of the "primer vector." In 1968, Lion and Handelsman broadened the role of the primer vector as a test for optimality to its use in the improvement of a non-optimal path with the addition of interior impulses and coast arcs on the trajectory[24]. Presented in 1969 and 1970, Prussing applied primer vector theory to the problems of time-fixed, multiple-impulse transfers between close elliptic orbits and close coplanar circular orbits[25, 26].

In Lawden's original development, a general gravitational field is assumed, but the governing differential equations of motion are expressed in a specific form. For applications in the context of the restricted problem, however, the most convenient form in which to

express the equations of motion is not consistent with the particular form considered in Lawden's development of the problem. Investigations of libration point orbits frequently employ a coordinate frame that rotates with the primaries since the libration points are easily identified relative to that frame. When variables that are defined relative to the rotating frame are used to express the equations of motion, terms that are functions of velocity exist that represent the relative motion of the rotating frame. Lawden's derivation does not include terms of this form; however, Hiday and Howell extended the analysis to include the additional terms[6, 7]. Although their derivation differs from that of Lawden, the same necessary conditions for optimality result, although the computation of the primer vector itself differs from the approach in earlier works. Hiday and Howell also developed tools for improving non-optimal solutions in the restricted problem that are similar to those developed by Lion and Handelsman for the two-body case[6]. Optimal impulsive transfers between libration point orbits in the elliptic restricted three-body problem are computed by Hiday and Howell by applying primer vector theory to the transfer problem, in conjunction with a numerical optimization procedure. Although the transfers satisfy the necessary conditions for optimality, the computational algorithm developed in their work yields some deviation from the specified initial and final libration point orbits. Furthermore, coast arcs and interior impulses are not simultaneously optimized. The present work addresses these specific issues.

b. Numerical Optimization

As presented by Hiday, the gradient of the cost function that results from the statement of the optimal transfer problem can be expressed analytically as a function of the primer vector; however, the conditions under which the gradient vanishes (particularly the characteristics of the state variables) are not available from an analytic analysis of the gradient expression. Thus, a gradient-based numerical optimization scheme is suggested. Many optimization algorithms of this type require the calculation of a search direction and an optimal step length in that direction. The descent methods for optimization, traditionally involving the use of first-order derivatives of the objective function, have evolved from Newton's first-order method to quasi-Newton methods that require both first and second-order derivatives to define the desirable search directions. The steepest descent algorithm, first developed by Cauchy, uses the negative of the gradient vector to define the search direction[27]. Variable metric algorithms employ functions of the gradients and optimal step lengths from previous steps to update the search direction. In this way, such methods incorporate the advantages of a quasi-Newton algorithm without requiring the explicit calculation of second-order derivatives. In this study, the Broyden-Fletcher-Goldfarb-Shanno (BFGS) variable metric

method, as incorporated in the Automated Design Synthesis (ADS) optimization package developed by Vanderplatts[28], is used to define appropriate search directions; polynomial interpolation is used to identify optimal step lengths within the procedure.

C. Present Work

Optimal transfer paths between libration point orbits associated with the same libration point are considered in the circular and elliptic restricted three-body problems. A computational algorithm is presented that maintains the specified departure and arrival trajectories during the optimization process. The simultaneous optimization of both coast arcs and interior impulses is achieved using the analytic expressions developed by Hiday for the gradients required in the optimal implementation of coast arcs and interior impulses; however, the number of impulses is optimized sequentially. To constrain the endpoints of the transfer path to the fixed trajectories, the transfers are computed as point-to-point solutions that connect fixed endpoints. Because this technique is employed, the solutions do not depend on any special characteristics of the fixed paths in most cases; therefore, the algorithm may be applied to transfers between any type of libration point orbit, although transfers between halo and near-halo orbits are used as the primary examples. This approach also permits the computation of relatively short duration paths eliminating the need for long numerical integration times that hinder many numerical studies in the restricted problem.

The first step in the algorithm is the optimization of a two-impulse solution over the choice of departure and arrival locations (constrained to the respective libration point orbits). Next, additional impulses are added, as required, to further reduce the transfer cost. As each successive impulse is included, the endpoints of the transfer and all other interior impulses are optimized simultaneously with the new impulse. The magnitude of the primer vector is plotted as a visual representation of the optimality of the solution.

Relationships among optimal transfers between halo orbits of various sizes are examined. Useful characteristics of the optimal solutions are noted, particularly the optimal locations of impulses relative to easily identified locations on the halo orbits. Also, families of optimal transfers are identified that allow the prediction of optimal costs between halo orbits of sizes other than those that are presented in this discussion.

D. Organization

The discussion is arranged as follows:

CHAPTER II: ELLIPTIC RESTRICTED THREE-BODY PROBLEM

The model used to represent the Sun-Earth-Moon dynamic environment is defined. Solutions to the problem are identified.

CHAPTER III: TRAJECTORY OPTIMIZATION

Differential corrections procedures are developed that incorporate the constraints required by the two-point boundary value problems that define the transfer paths. The necessary conditions for optimality and the gradient expressions used in the optimization are presented. The computational algorithm is demonstrated.

CHAPTER IV: OPTIMAL TRANSFER PATHS: CIRCULAR PROBLEM

The original and final orbits are selected to be periodic halo orbits. The optimal transfer paths for these representative departure and arrival orbits in the circular restricted three-body problem are presented. Relationships among the solutions are identified. Useful characteristics of families of optimal solutions are discussed.

CHAPTER V: OPTIMAL TRANSFER PATHS: ELLIPTIC PROBLEM

The timing conditions associated with transfer path computations in the elliptic problem are addressed. Optimal solutions between near-halo orbits in the elliptic restricted three-body problem are presented.

CHAPTER VI: CONCLUSIONS

The conclusions of the study are summarized.

II. ELLIPTIC RESTRICTED THREE-BODY PROBLEM

Spacecraft trajectories in the Sun-Earth system are developed as solutions to a restricted three-body problem. Appropriate kinematic relationships and force models that define the environment provide the mathematical description of the problem. The scalar equations of motion are then derived as the dynamic model. The solution to a matrix differential equation that governs the sensitivity matrix associated with the equations of motion is used to produce numerical solutions that possess specified characteristics. An exact solution to the equations, the set of locations corresponding to the libration points, represents an equilibrium condition about which other solutions, particularly libration point orbits, are defined.

A. Elliptic Restricted Three-Body Problem

Investigations of the three-body problem generally consider solutions for the motion of three particles, each of finite mass, moving under their mutual gravitational attraction; however, the three-body structure does not define a fully integrable problem [1, 11]. If one of the particles is assumed to have infinitesimal mass and, therefore, does not affect the motion of the remaining two massive particles, the resulting problem provides a reasonable approximation for the predicted motion of a spacecraft in the presence of two dominant gravitational fields while providing a partial solution to the general problem. This assumption constrains the remaining two massive particles to elliptical paths as prescribed by the solution to the two-body problem. The motion of the particle of infinitesimal mass is then the solution to the elliptic restricted three-body problem (ER3BP).

1. Geometry

The elliptic restricted model includes descriptions of the motion of three distinct particles including two massive primaries and one particle of infinitesimal mass. The primaries, denoted P_1 and P_2, are defined to have finite masses M_1 and M_2. The spacecraft, represented by the particle of infinitesimal mass, is denoted P (Figure II.1). Two reference frames complete the definition of the system. The $\overline{X}-\overline{Y}-\overline{Z}$ axes represent a right-handed inertial

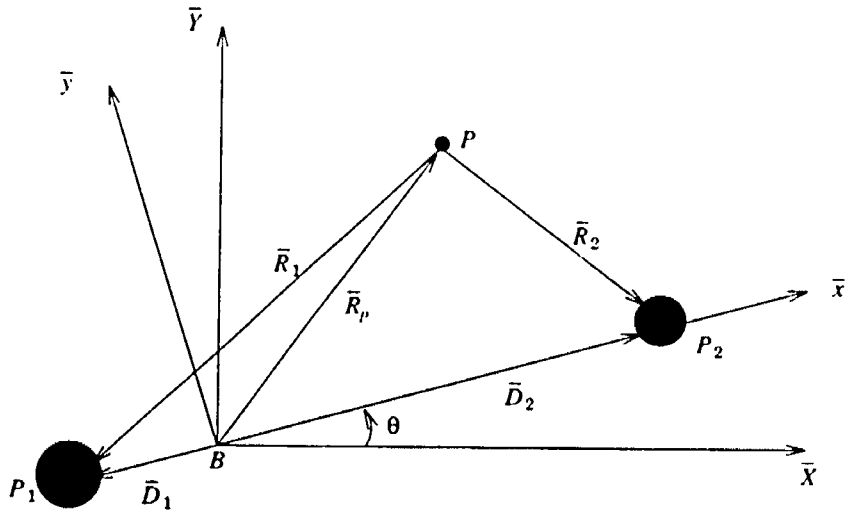

Figure II.1 Geometry and Definitions for the Elliptic Restricted Three-Body Problem.

coordinate system, denoted I, with origin at the barycenter of the primaries, B. (Note that a bar over a letter represents a vector quantity.) The $\overline{X}$-axis is parallel to a vector defined from P_1 toward P_2 at the time of periapsis passage in the primary orbit and is inertially fixed. The $\overline{X}-\overline{Y}$ plane is defined as the plane of primary motion. The $\overline{Z}$ direction completes the right-handed system; that is, $\overline{Z} = \overline{X} \times \overline{Y}$. Frame N denotes a right-handed rotating coordinate system with origin at the barycenter. Represented by the $\bar{x} - \bar{y} - \bar{z}$ axes, frame N is defined by the motion of the primaries. The $\bar{x}$-axis designates an axis that is parallel to a line passing through both primary bodies at all times, directed from the larger toward the smaller primary. The $\bar{y}$-axis is then defined so that the $\bar{x} - \bar{y}$ plane remains in the plane of primary motion. Thus, by definition, $\bar{z}$ and $\overline{Z}$ are always parallel. With these definitions, the rate of change of the angle between the $\bar{x}$ and $\overline{X}$-axes, θ, is the orbital angular rate of the primaries relative to the inertial system; therefore, the rotation rate of the non-inertial frame is equal to the orbital angular rate of the primary system. Finally, the two systems are assumed to be coincident at the time of periapsis passage.

2. Characteristic Quantities

To simplify the calculations, characteristic quantities are used to nondimensionalize the equations. First, characteristic values of mass, length, and time are selected. Characteristic mass, M^*, is defined to be the sum of the primary masses; $M^* = M_1 + M_2$. The average

distance between the primaries is selected as the characteristic length, L^*. Characteristic time, T^*, is defined by

$$T^* = \sqrt{\frac{L^{*3}}{\tilde{G}M^*}} , \qquad \text{[II.1]}$$

where $\tilde{G}$ is the gravitational constant. Next, nondimensional variables are defined to represent the dimensional quantities in the problem. The nondimensional primary masses, m_1 and m_2, are defined as $m_1 = M_1/M^*$ and $m_2 = M_2/M^*$. Thus, $m_1 + m_2 = 1$ in nondimensional units. The average distance between the primaries in the elliptic problem is equal to the semi-major axis of the primary orbit, $\tilde{a}$; therefore, the nondimensional semi-major axis, a, is defined as $a = \tilde{a}/L^*$ and has a value of one. By definition of characteristic time, the nondimensional gravitational constant, G, is also found to be one since $G = \tilde{G}M^*T^{*2}/L^{*3}$. The mean motion of the rotating frame, $\tilde{n}$, is identified by Kepler's modified third law as

$$\tilde{n} = \sqrt{\frac{\tilde{G}(M_1 + M_2)}{\tilde{a}^3}} . \qquad \text{[II.2]}$$

By definition of characteristic time, the nondimensional mean motion is defined $n = \tilde{n}T^*$ and can be written as

$$n = \sqrt{\frac{G(m_1 + m_2)}{a^3}} ; \qquad \text{[II.3]}$$

therefore, the nondimensional mean motion is also equal to one.

3. Gravitational Force Model

The equations of motion for the body of interest will be derived using Newton's Second Law of Motion; therefore, models for the gravitational forces due to the two primaries are necessary. The models for the gravitational forces that act on the particle of interest are written in the form

$$\overline{F}_{P_i} = \frac{\tilde{G}M_i M}{R_i^2}\frac{\overline{R}_i}{R_i} , \qquad \text{[II.4]}$$

where M is the mass of the body of interest, and $\overline{R}_i$ represents the location of the primary, P_i (i=1,2), relative to the body of interest. The variable R_i is the magnitude corresponding to the vector $\overline{R}_i$. In terms of the nondimensional quantities, the force is written as

$$\overline{f}_{P_i} = \frac{Gm_i m}{r_i^2}\frac{\overline{r}_i}{r_i} , \qquad \text{[II.5]}$$

where $\overline{r}_i = \overline{R}_i/L^*$, $m_i = M_i/M^*$ (i = 1,2), and $m = M/M^*$.

4. Equations of Motion

The position vector locating the particle of interest with respect to the barycenter is the vector $\overline{R}_p$ (see Figure II.1). The nondimensional representation of this vector, $\overline{r} = \overline{R}_p/L^*$,

is used in the expression of the vector equation of motion as

$$m\ddot{\bar{r}}^I = \sum_{i=1}^{2} \bar{f}_{P_i} = \frac{Gm_1 m}{r_1^2}\frac{\bar{r}_1}{r_1} + \frac{Gm_2 m}{r_2^2}\frac{\bar{r}_2}{r_2}, \qquad \text{[II.6]}$$

from the application of Newton's Second Law to a free body diagram of the particle of interest. (Dots represent differentiation with respect to nondimensional time.) This expression is simplified with the introduction of a nondimensional mass-ratio parameter, μ, defined as the ratio

$$\mu = \frac{m_2}{m_1 + m_2}. \qquad \text{[II.7]}$$

Using this parameter, the masses of the primaries are expressed nondimensionally as

$$m_1 = 1 - \mu, \qquad \text{[II.8]}$$

and

$$m_2 = \mu. \qquad \text{[II.9]}$$

Given these additional definitions, the nondimensional force summation is rewritten as

$$\ddot{\bar{r}}^I = \frac{(1-\mu)}{r_1^2}\frac{\bar{r}_1}{r_1} + \frac{\mu}{r_2^2}\frac{\bar{r}_2}{r_2}. \qquad \text{[II.10]}$$

The angular velocity of the rotating system with respect to the inertial system, $\bar{\omega}^N$, is introduced in the expansion of the kinematic expression for acceleration, $\ddot{\bar{r}}^I$, as follows,

$$\ddot{\bar{r}}^I = \ddot{\bar{r}}^N + 2\bar{\omega}^N \times \dot{\bar{r}}^N + \dot{\bar{\omega}}^N \times \bar{r} + \bar{\omega}^N \times (\bar{\omega}^N \times \bar{r}). \qquad \text{[II.11]}$$

In terms of the angle, θ, that relates frames I and N, the angular velocity vector is expressed in the form

$$\bar{\omega}^N = \dot{\theta}\hat{z}, \qquad \text{[II.12]}$$

where e is the eccentricity of the primary orbit, and the nondimensional angular rate is evaluated as

$$\dot{\theta} = \frac{\sqrt{1-e^2}}{R^2}. \qquad \text{[II.13]}$$

The symbol $\hat{z}$ represents a unit vector in the direction of $\bar{z}$. In the expression for the angular rate, $\dot{\theta}$, the nondimensional separation distance between the primaries is defined as

$$R = 1 - e\cos E, \qquad \text{[II.14]}$$

where E is the eccentric anomaly which is evaluated from Kepler's equation as a function of time. Next, to evaluate $\dot{\bar{\omega}}^N$ for equation II.11, the angular rate is differentiated to produce an expression for the magnitude of the angular acceleration as

$$\ddot{\theta} = \frac{-2\,e\sin E\,\sqrt{1-e^2}}{R^4}. \qquad \text{[II.15]}$$

To represent the position of the particle of interest relative to the primary barycenter, nondimensional components of distance, represented as x, y, z, are used to define the position as

$$\bar{r} = x\hat{x} + y\hat{y} + z\hat{z} . \qquad \text{[II.16]}$$

Thus, the acceleration of the particle P relative to the rotating frame is written

$$\ddot{\bar{r}}^N = \ddot{x}\hat{x} + \ddot{y}\hat{y} + \ddot{z}\hat{z} . \qquad \text{[II.17]}$$

Relative to the inertial system, the acceleration of P can now be expressed in terms of the vector variable of interest, $\bar{r}$, with components x, y, z as

$$\ddot{\bar{r}}^I = (\ddot{x} - x\dot{\theta}^2 - 2\dot{y}\dot{\theta} - y\ddot{\theta})\,\hat{x} + (\ddot{y} - y\dot{\theta}^2 + 2\dot{x}\dot{\theta} + x\ddot{\theta})\,\hat{y} + \ddot{z}\,\hat{z} . \qquad \text{[II.18]}$$

To reduce the kinetic terms on the right hand side of equation II.10 to their three scalar components, r_1 and r_2 are expressed in terms of the components of $\bar{r}$ and any additional known quantities that are appropriate. The position of each primary body relative to the center of mass is defined in terms of the overall separation distance, R, and the individual masses as

$$\bar{d}_1 = -R\mu\hat{x} , \qquad \text{[II.19]}$$

and

$$\bar{d}_2 = R(1-\mu)\hat{x} , \qquad \text{[II.20]}$$

where $\bar{d}_1 = \bar{D}_1/L^*$ and $\bar{d}_2 = \bar{D}_2/L^*$; therefore, $\bar{r}_1$ and $\bar{r}_2$ can be expressed as

$$\bar{r}_1 = \bar{d}_1 - \bar{r} , \qquad \text{[II.21]}$$

and

$$\bar{r}_2 = \bar{d}_2 - \bar{r} . \qquad \text{[II.22]}$$

The combination of equations II.10, II.16–II.18, II.21, and II.22 yields the three scalar equations of motion written in terms of the rotating coordinates, x, y, z, with origin at the primary barycenter as

$$\ddot{x} - x\dot{\theta}^2 - 2\dot{y}\dot{\theta} - y\ddot{\theta} = \frac{1-\mu}{r_1^3}(-R\mu - x) + \frac{\mu}{r_2^3}[R(1-\mu) - x] , \qquad \text{[II.23]}$$

$$\ddot{y} - y\dot{\theta}^2 + 2\dot{x}\dot{\theta} + x\ddot{\theta} = -\left(\frac{1-\mu}{r_1^3} + \frac{\mu}{r_2^3}\right) y , \qquad \text{[II.24]}$$

$$\ddot{z} = -\left(\frac{1-\mu}{r_1^3} + \frac{\mu}{r_2^3}\right) z , \qquad \text{[II.25]}$$

where

$$r_1 = \left\{(x + R\mu)^2 + y^2 + z^2\right\}^{1/2} , \qquad \text{[II.26]}$$

$$r_2 = \left\{ [x - R(1 - \mu)]^2 + y^2 + z^2 \right\}^{1/2} . \qquad \text{[II.27]}$$

Equations II.23 through II.25 may be expressed in a simpler form by definition of a pseudo-potential, U, such that

$$U = \frac{1}{2}\dot{\theta}^2(x^2 + y^2) + \frac{(1 - \mu)}{r_1} + \frac{\mu}{r_2} . \qquad \text{[II.28]}$$

Using this definition, the equations of motion are rewritten as

$$\ddot{x} - 2\dot{y}\dot{\theta} = \frac{\partial U}{\partial x} + y\ddot{\theta} , \qquad \text{[II.29]}$$

$$\ddot{y} + 2\dot{x}\dot{\theta} = \frac{\partial U}{\partial y} - x\ddot{\theta} , \qquad \text{[II.30]}$$

$$\ddot{z} = \frac{\partial U}{\partial z} . \qquad \text{[II.31]}$$

This form of the equations of motion is particularly convenient in the analysis of equilibrium solutions.

Recall that primary motion in the elliptic restricted model is assumed to be periodic. Thus, it may be possible for the motion of the particle of interest to be periodic as well; however, this is neither required nor possible in all cases. The gravitational force models that are employed assume periodic motion of the primaries; however, no constraints on the motion of the third particle are introduced in the development of the equations of motion.

In the special case of circular primary motion, a constant, first determined by Jacobi in 1836, is available that identifies bounded regions of motion in the circular problem[29]. In terms of the pseudo-potential, U, the expression for the constant can be written in the form

$$C = 2U - (\dot{x}^2 + \dot{y}^2 + \dot{z}^2) . \qquad \text{[II.32]}$$

The quantity is not constant in the elliptic problem due to the variations introduced by the time varying angular rate in the pseudo-potential expression.

5. State Transition Matrix

The differential corrections process that is used to perform trajectory calculations employs the 6×6 state transition matrix, $\Phi(t, t_o)$, that is associated with the equations of motion. The state transition matrix is governed by thirty-six first-order scalar differential equations that are represented by the single matrix differential equation

$$\frac{d}{dt}\Phi(t, t_o) = A(t)\Phi(t, t_o) , \qquad \text{[II.33]}$$

where

$$A(t) = \left[\begin{array}{c|c} 0_3 & I_3 \\ \hline U_{XX} + \ddot{\theta}\Omega & 2\dot{\theta}\Omega \end{array}\right], \qquad \text{[II.34]}$$

$$\Omega = \begin{bmatrix} 0 & 1 & 0 \\ -1 & 0 & 0 \\ 0 & 0 & 0 \end{bmatrix}, \qquad \text{[II.35]}$$

and

$$U_{XX} = \begin{bmatrix} \partial^2 U/\partial x^2 & \partial^2 U/\partial x \partial y & \partial^2 U/\partial x \partial z \\ \partial^2 U/\partial x \partial y & \partial^2 U/\partial y^2 & \partial^2 U/\partial y \partial z \\ \partial^2 U/\partial x \partial z & \partial^2 U/\partial y \partial z & \partial^2 U/\partial z^2 \end{bmatrix}. \qquad \text{[II.36]}$$

The notation '0_n' represents the $n \times n$ matrix of zeroes, and 'I_n' represents the $n \times n$ identity matrix. The initial condition associated with this differential equation is $\Phi(t_o, t_o) = I_6$. Differentiating equation II.28 and using equations II.26 and II.27, the individual elements associated with the symmetric matrix U_{XX} can be derived and expressed in the form

$$\frac{\partial^2 U}{\partial x^2} = \dot{\theta}^2 + 3\left[\frac{(1-\mu)(-x-R\mu)^2}{r_1^5} + \frac{\mu[-x+R(1-\mu)]^2}{r_2^5}\right] - \left[\frac{(1-\mu)}{r_1^3} + \frac{\mu}{r_2^3}\right], \qquad \text{[II.37]}$$

$$\frac{\partial^2 U}{\partial x \partial y} = -3y\left[\frac{(1-\mu)(-x-R\mu)}{r_1^5} + \frac{\mu[-x+R(1-\mu)]}{r_2^5}\right] - \left[\frac{(1-\mu)}{r_1^3} + \frac{\mu}{r_2^3}\right], \qquad \text{[II.38]}$$

$$\frac{\partial^2 U}{\partial x \partial z} = -3z\left[\frac{(1-\mu)(-x-R\mu)}{r_1^5} + \frac{\mu[-x+R(1-\mu)]}{r_2^5}\right] - \left[\frac{(1-\mu)}{r_1^3} + \frac{\mu}{r_2^3}\right], \qquad \text{[II.39]}$$

$$\frac{\partial^2 U}{\partial y^2} = \dot{\theta}^2 + 3y^2\left[\frac{(1-\mu)}{r_1^5} + \frac{\mu}{r_2^5}\right] - \left[\frac{(1-\mu)}{r_1^3} + \frac{\mu}{r_2^3}\right], \qquad \text{[II.40]}$$

$$\frac{\partial^2 U}{\partial y \partial z} = 3yz\left[\frac{(1-\mu)}{r_1^5} + \frac{\mu}{r_2^5}\right], \qquad \text{[II.41]}$$

$$\frac{\partial^2 U}{\partial z^2} = 3z^2\left[\frac{(1-\mu)}{r_1^5} + \frac{\mu}{r_2^5}\right] - \left[\frac{(1-\mu)}{r_1^3} + \frac{\mu}{r_2^3}\right]. \qquad \text{[II.42]}$$

Since the matrix A in equation II.33 is a function of time (through the states and the angular rates), numerical integration is generally required to produce a solution for the state transition matrix.

Given a set of initial conditions for the state vector, defined as $\overline{X} = \{x\ y\ z\ \dot{x}\ \dot{y}\ \dot{z}\}^T$, where superscript T indicates matrix transpose, numerical integration of the equations of motion alone is sufficient to produce the numerical representation of the trajectory. However, the simultaneous integration of both the equations of motion (equations II.23–II.25) and the differential equation that governs the state transition matrix (equation II.33) is required to construct trajectories with specific characteristics. Thus, the production

of the numerical solutions presented in this work requires the simultaneous integration of forty-two differential equations.

The elements of the state transition matrix represent relationships between the linearized states at the two instants of time for which the matrix is defined as

$$\Phi(t,t_o) = \frac{\partial \overline{X}(t)}{\partial \overline{X}(t_o)} = \begin{bmatrix} \partial x(t)/\partial x(t_o) & \partial x(t)/\partial y(t_o) & \cdots & \partial x(t)/\partial \dot{z}(t_o) \\ \partial y(t)/\partial x(t_o) & \partial y(t)/\partial y(t_o) & \cdots & \partial y(t)/\partial \dot{z}(t_o) \\ \vdots & \vdots & \ddots & \vdots \\ \partial \dot{z}(t)/\partial x(t_o) & \partial \dot{z}(t)/\partial y(t_o) & \cdots & \partial \dot{z}(t)/\partial \dot{z}(t_o) \end{bmatrix}. \quad \text{[II.43]}$$

This relationship is used extensively in the development of the differential corrections algorithms that are used to compute transfer trajectories.

6. Sun-Earth/Moon Barycenter Model

The assumption of two gravitational fields provides a reasonable model for motion in the Sun-Earth system; however, for motion in the vicinity of the libration points that are close to the Earth, a more realistic model can be constructed that retains the structure of the restricted problem. Contributions of the Moon's gravity field to the total force cannot be included directly in the Sun-Earth model as presented for the elliptic restricted problem because of the limitation of two primary bodies; however, an artificial system can be defined that satisfies the constraints of the R3BP while retaining the Moon's mass in the model. This system yields a more accurate model for motion near the collinear points in the Sun-Earth system[30]. The "Sun-Earth/Moon barycenter system" is formed by assuming that the mass of the smaller primary is equal to the combined mass of the Earth/Moon system and that the particle is located at the barycenter of the Earth and Moon. Thus, the two primaries are defined to be the Sun and a particle with the combined Earth/Moon mass located at the Earth/Moon barycenter. This system is used in the remainder of this discussion to define the environment in which the motion of the spacecraft is considered.

The parameters that are associated with the smaller primary in the Sun-Earth restricted problem are redefined to construct the Sun-Earth/Moon barycenter system. The new definitions are represented in Figure II.2. In the Sun-Earth/Moon barycenter model, the smaller primary, P_2, represents the combined Earth/Moon system with mass M_2 equal to the sum of the masses of the Earth and Moon. Thus, the system barycenter is defined to be the barycenter of the Sun and the Earth/Moon system. The vector $\overline{R}_2$ is defined to be the position of the center of mass of the Earth and Moon relative to the spacecraft ("S/C"). Similarly, the location of the center of mass of the Earth and Moon relative to the system barycenter is defined by the vector $\overline{D}_2$. The $\overline{X} - \overline{Y}$ plane is still defined as the plane of

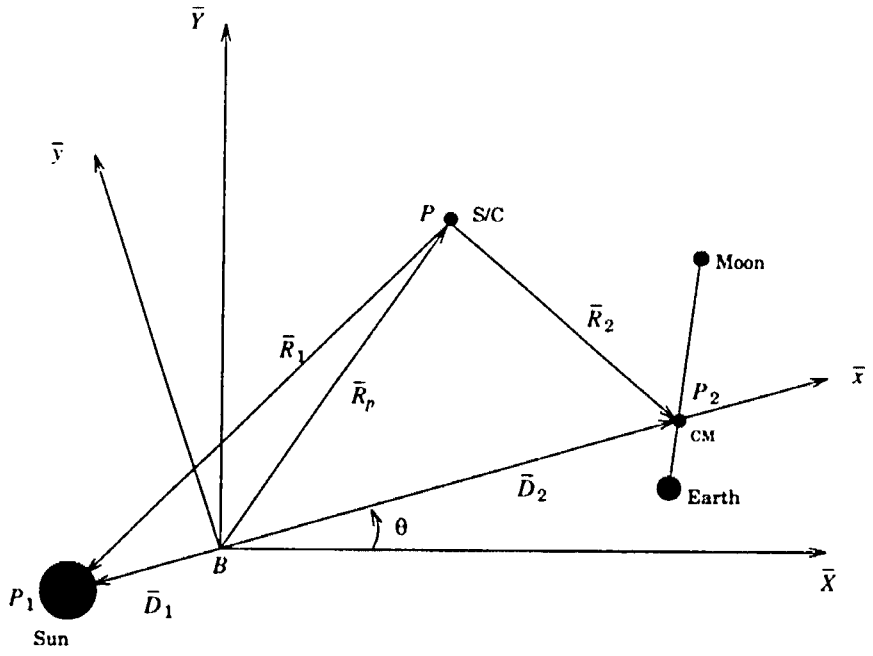

Figure II.2 Sun-Earth/Moon Barycenter Geometry.

primary motion; however, with the primaries defined as P_1 and P_2, only the location of the center of mass of the Earth and Moon is constrained to this plane — not the individual locations of the Earth and Moon. With these modifications, the equations developed for the dynamic model associated with the Sun-Earth elliptic restricted problem also govern motion in the Sun-Earth/Moon barycenter system.

B. Libration Points

A complete analytic solution to the elliptic restricted three-body problem does not exist; however, particular solutions that satisfy specific conditions are available. Bounded motion in the vicinity of the particular solutions is also possible. Periodic solutions of this type are used in this study to demonstrate the techniques that are developed.

1. Libration Point Definitions

The equilibrium solutions comprise the set of locations at which the instantaneous summation of all forces acting in the elliptic restricted problem (including the centrifugal force) is zero. These five points are also called the Lagrange or libration points. Expressions for computing the positions of these points are available from the equilibrium condition associated with the equations of motion, equations II.29–II.31; that is, $\partial U/\partial x = \partial U/\partial y = \partial U/\partial z = 0$.

Figure II.3 shows the locations of the five libration points in the circular problem as they appear in the rotating frame. Three of the solutions, the collinear points, lie along the

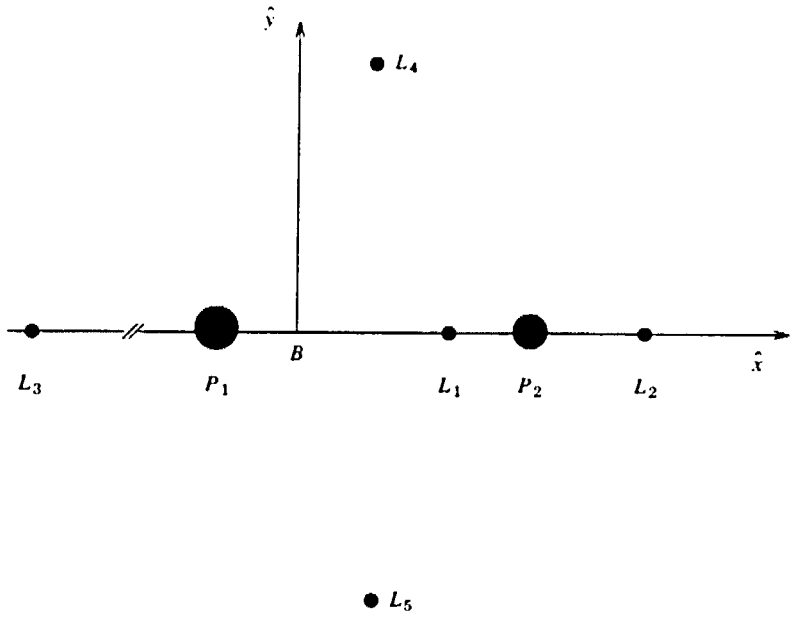

Figure II.3 Libration Point Locations.

$\hat{x}$-axis. The interior point, between the primaries, is labeled L_1; the point on the far side of the smaller primary relative to the barycenter is labeled L_2; the point on the far side of the larger primary is denoted L_3. The remaining two points, in conjunction with the primaries, are the vertices of equilateral triangles positioned with one edge along the $\hat{x}$-axis. Thus, L_4 and L_5 are called the triangular points. In the circular problem, where the primary bodies are separated by a constant distance, each libration point is stationary with respect to the rotating frame and is located at a constant distance from the barycenter. In the more general problem of elliptic primary paths, the collinear equilibrium points still exist, but they oscillate along the $\hat{x}$-axis. The triangular points also exist in the elliptic restricted problem where they shift to maintain the equilateral triangular shape.

The libration point location is frequently used as a point of reference for numerical solutions; therefore, a coordinate system relative to the libration point of interest is convenient. (In this study, only one libration point is assumed to be relevant for any solution.) Consequently, a third frame of reference, denoted by axes $\dot{x} - \dot{y} - \dot{z}$, is defined with origin at the libration point and the $\dot{x}$-axis parallel to $\hat{x}$ (frame P). Note that $\dot{y} = \hat{y}$ and $\dot{z} = \hat{z}$. Thus,

the rotation rate of frame P is equal to that of the previously defined non-inertial frame, $\hat{x} - \hat{y} - \hat{z}$ (frame N).

2. Bounded, Three-Dimensional Libration Point Orbits

The existence of the libration points suggests the possible presence of other solutions in their vicinity. Unbounded motion that passes near the libration points is possible but is not of interest here. Solutions that represent bounded motion in the vicinity of a libration point are called libration point orbits. One type of libration point orbit, called a Lissajous trajectory, is a bounded, three-dimensional, quasi-periodic path in the vicinity of the libration point. A significant step in the numerical computation of these trajectories, especially those of relatively long duration, is the approach discussed in [9] and [22]. Howell and Pernicka developed a strategy for the computation of three-dimensional bounded solutions, including Lissajous trajectories, near the collinear points for an arbitrary, but predetermined, number of revolutions.

a. Lissajous Trajectories

One example of a Lissajous trajectory is presented in Figure II.4. For convenience, this three-dimensional trajectory is presented in three two-dimensional (planar) projections, each with origin at L_1. The coordinates x, y, z represent components in the rotating frame with origin at the libration point (frame P); the dot in each view identifies the libration point location; arrows denote the general direction of motion. The upper left plot represents the projection of the trajectory onto the $\hat{x} - \hat{y}$ plane; that is, the view of an observer looking down the $\hat{z}$-axis. The projection onto the $\hat{x} - \hat{z}$ plane is represented in the lower left corner. This is subsequently labeled the "front view." The lower right plot is the projection onto the $\hat{y} - \hat{z}$ plane. This trajectory completes approximately fifteen revolutions and was computed using the algorithm developed by Howell and Pernicka for the computation of long duration Lissajous trajectories[9, 22]. Clearly, the path does not repeat with each revolution and is not periodic within the time interval of interest. The exploration of a large region of the space, as represented by this type of trajectory, may be useful for some missions; however, the contraction of the Lissajous shape near the origin in the $y - z$ projection physically represents the vehicle crossing between the Sun and Earth in front of the solar disk. Since this may interfere with communications and scientific experiments, Pernicka and Howell developed a method of z-axis control to compute Lissajous trajectories that avoid this region[31]; however, periodic solutions that avoid the region without external control are also possible under special conditions.

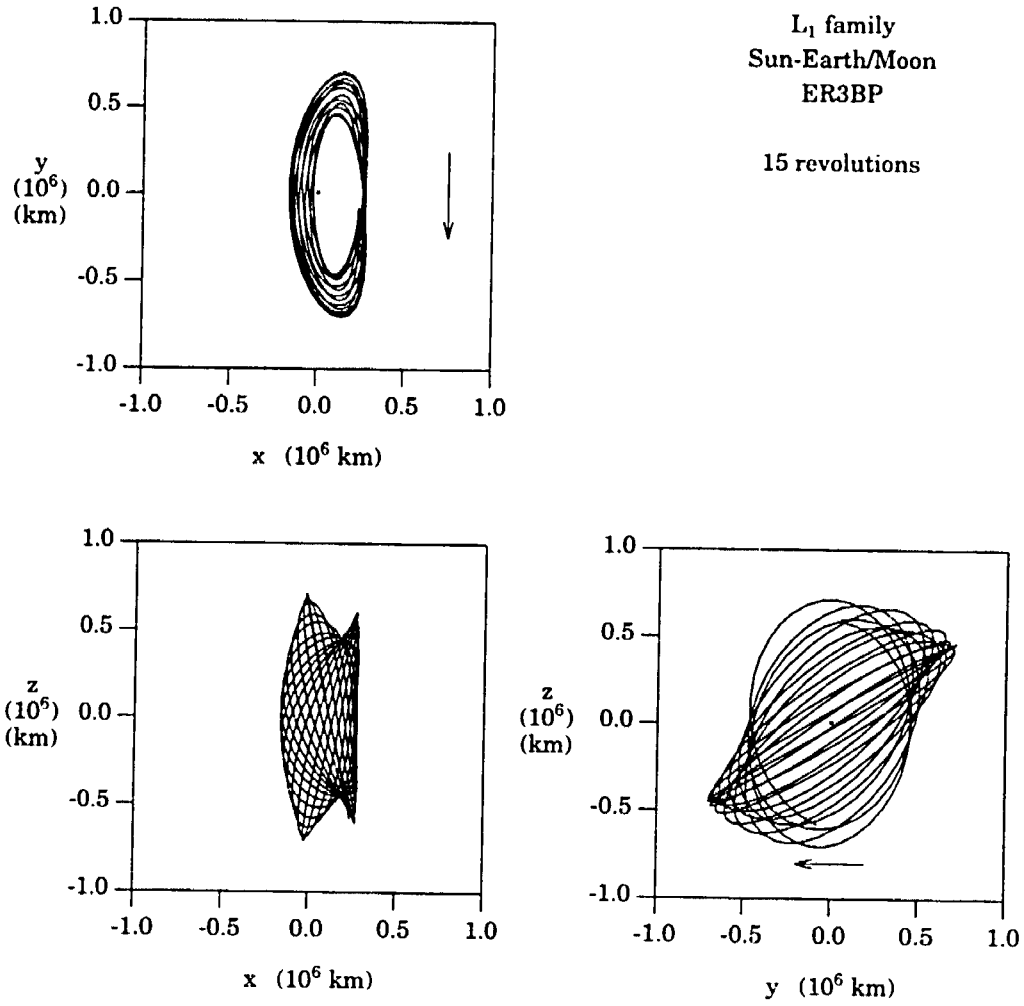

Figure II.4 Example of a Lissajous Trajectory in the Sun-Earth/Moon Barycenter ER3BP.

b. Halo Orbits

With appropriate constraints, a class of closed, periodic solutions near the collinear points may exist that repeat exactly with each revolution. A halo orbit is defined as a Lissajous trajectory in which the rotation of the in-plane (x or y) to the out-of-plane (z) amplitudes are equal to a specified value that is not arbitrary. The trajectory is periodic, and the period is commensurate with the period of the primary orbit. Families of halo orbits are associated with each of the collinear points.

An example of a numerically computed halo orbit for the Sun-Earth/Moon barycenter system is presented in Figure II.5. This particular orbit was computed as a solution to the circular restricted problem and has a period of approximately 177.1 days. The magnitude of the largest excursion in the direction of a particular coordinate axis is defined as the amplitude of the trajectory relative to that axis. For example, in Figure II.5, the largest z-excursion is approximately 600,000 km (in a positive z direction). Thus, this orbit is a 600,000 km A_z amplitude orbit.

In the elliptic restricted problem, a truly periodic orbit may not be available with the specific combination of amplitudes that is required to produce a halo orbit. In this case, a path that approximates a halo orbit is used and is identified as a near-halo orbit. Although it does have special characteristics not found in a general Lissajous trajectory, a near-halo orbit can be computed using an algorithm developed for the computation of the more general Lissajous solution under special constraints. The algorithm developed by Howell and Pernicka[9, 22] has been modified to compute the near-halo orbits that are used as the fixed departure and arrival paths in the elliptic problem in this study.

c. Branches of Libration Point Orbits

Families of periodic, collinear libration point orbits exist in the restricted problem along two main branches, known as northern and southern families, that are defined by the characteristics of the orbit. For the halo orbit presented in Figure II.5, the solution proceeds in a clockwise direction in both the $x-y$ and $y-z$ projections. Furthermore, the largest z-excursion occurs in the positive $\hat{z}$ direction relative to the $\hat{x}-\hat{y}$ plane. Trajectories near L_1 with these characteristics are identified as being members of a "northern family." A second type of periodic orbit exists in which motion proceeds in the clockwise direction in the $x-y$ projection but in the counterclockwise direction in the $y-z$ projection. L_1 orbits with these characteristics are categorized as being part of a "southern family." Under special conditions, a southern trajectory can be constructed as a mirror image of the corresponding northern trajectory as seen in the $x-z$ and $y-z$ projections (Figure II.6). The two types

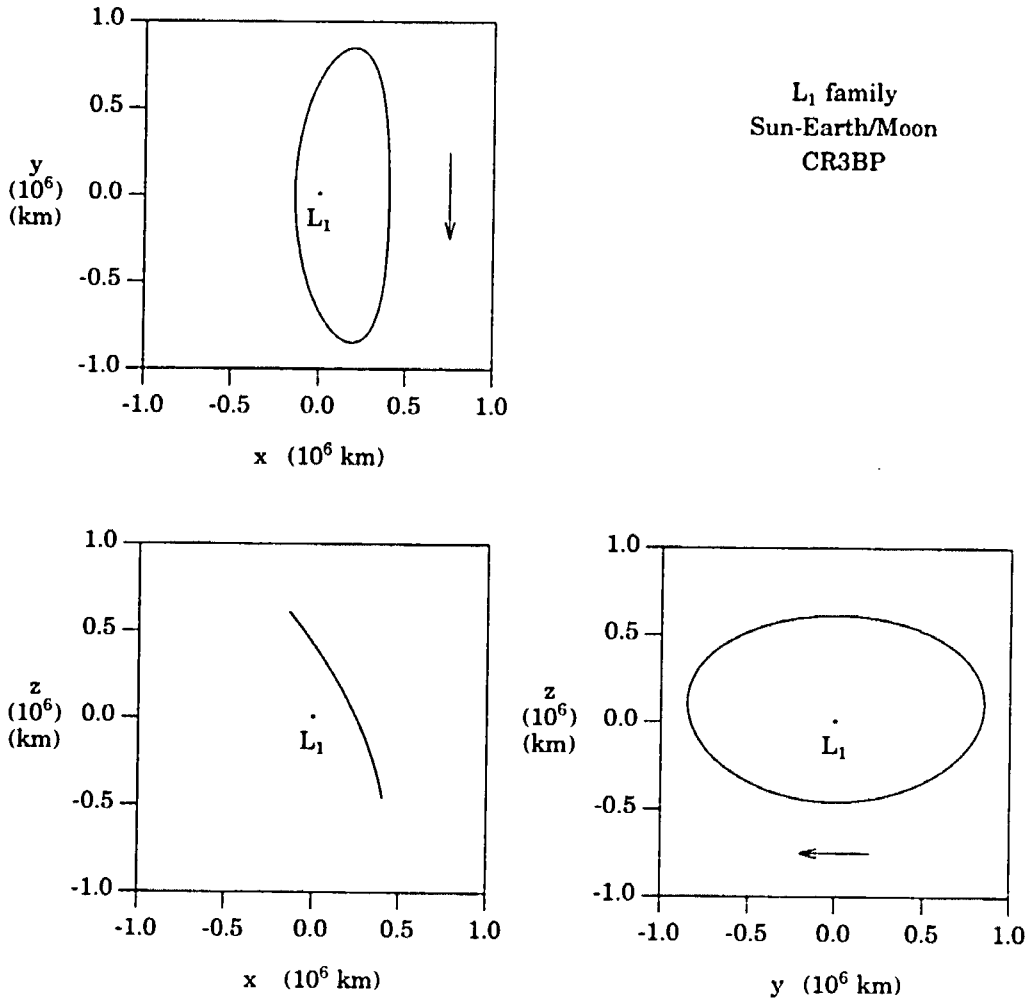

Figure II.5 Example of a Halo Orbit in the Sun-Earth/Moon Barycenter CR3BP.

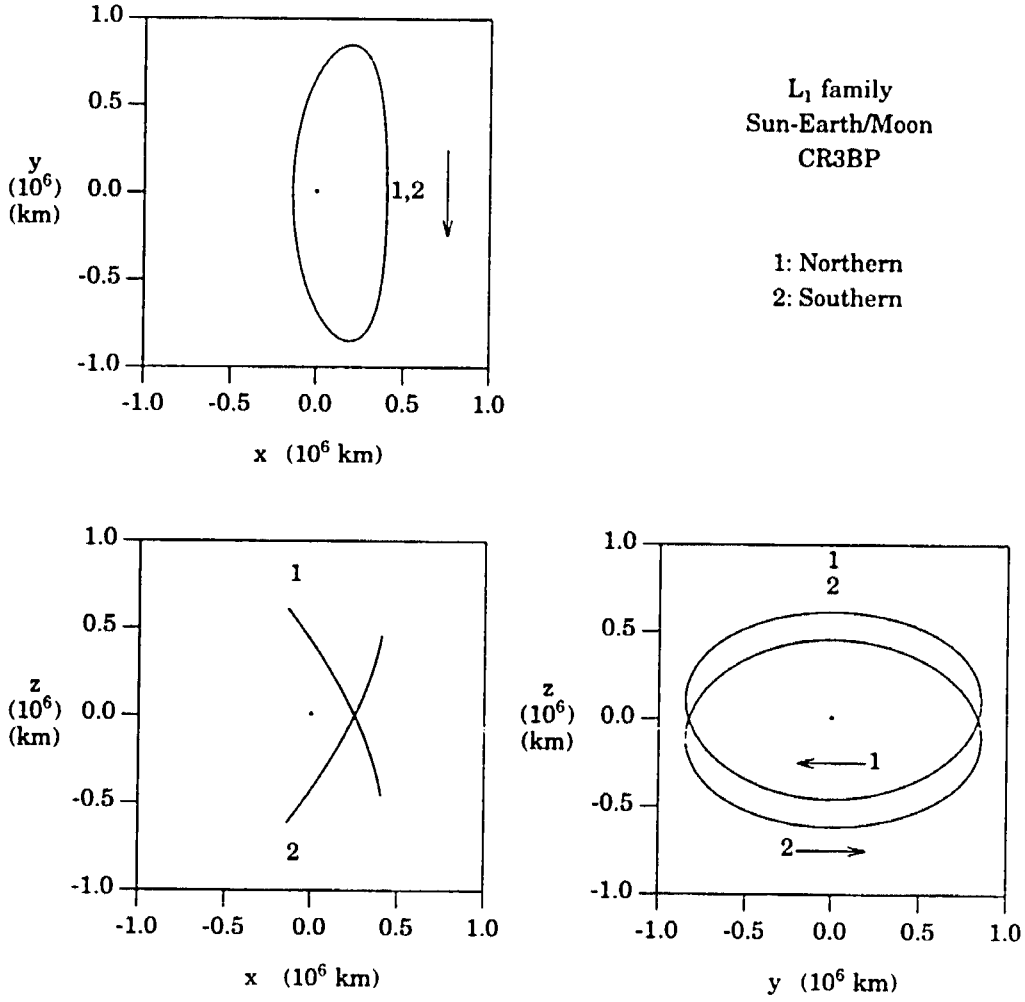

Figure II.6 Northern and Southern Orbits with Similar Characteristics in the CR3BP.

of halo orbits, as mirror image trajectories, are discussed by Farquhar and Kamel[16] and in more detail by Richardson[17] where they are denoted class I and class II orbits. For the L_1 family, Richardson denotes northern orbits, as defined here, as class I and southern orbits as class II. For the L_2 family, he again denotes orbits with clockwise rotation in the $y-z$ projection as class I and orbits with counterclockwise rotation in that projection as class II; however, L_2 orbits with clockwise rotation in the $y-z$ projection have a maximum z-excursion in a negative $\dot{z}$ direction. Thus, in terms of the direction of maximum z-excursion, L_2 northern orbits correspond to class II orbits, and L_2 southern orbits correspond to class I. Lissajous trajectories also exist in mirror image families; however, since a maximum excursion criterion may not be applicable in all cases, categories defined by the direction of motion may be more appropriate for discussion of Lissajous paths.

III. TRAJECTORY OPTIMIZATION

Solving the optimal transfer problem requires the ability to identify the desired characteristics of the optimal solution and to compute a transfer with those characteristics. A numerical optimization routine, supported by a first-order primer vector development, is used to select the optimal characteristics. Differential corrections in conjunction with numerical integration is used to compute the solutions. The details associated with these two procedures, as applied in this work, are presented below. The algorithm is demonstrated for a transfer between two L_1 halo orbits in the Sun-Earth/Moon barycenter circular restricted problem.

A. Differential Corrections

A path computed under the assumptions of the elliptic restricted problem is defined by a single state, that is, initial position and velocity of the particle of interest, and the relative orientation of the primaries at the time associated with that state; therefore, the path can be modified to meet a set of desired characteristics by changing any or all of these conditions. For example, initial conditions that yield unbounded motion can be modified to produce a periodic solution in the circular problem. To construct a solution that satisfies a set of specified characteristics, an iterative search algorithm can be developed that is based on a mathematical description of the desired solution and the state transition matrix. Such an algorithm is one type of differential corrections procedure. In the process, a current set of conditions is improved with corrections that are computed as functions of the error in the current solution relative to specified characteristics and appropriate elements of the state transition matrix. Since the state transition matrix represents a linear relationship between variations in states at two different times, an iterative process is generally required to achieve convergence of the actual states to the desired values.

Although trajectories in this work are presented in libration point centered coordinates (frame P), all computations use barycenter rotating (frame N) coordinates. Thus, the differential correctors are derived in terms of barycenter rotating coordinates. The vector $\overline{X}(t)$ is the six-dimensional vector of nondimensional barycenter rotating coordinates and

their derivatives defined in the form $\overline{X} = \{x\ y\ z\ \dot{x}\ \dot{y}\ \dot{z}\}^T$. The differential corrections algorithms are constructed by expanding $\overline{X}(t)$ about a nominal solution, $\overline{X}_n(t)$, in a Taylor series as

$$\overline{X}(t) - \overline{X}_n(t) = \frac{\partial \overline{X}(t)}{\partial \overline{X}(t_o)} \left[\overline{X}(t_o) - \overline{X}_n(t_o)\right] + \dot{\overline{X}}(t_n)(t - t_n) , \qquad \text{[III.1]}$$

where only first-order terms are retained. The coefficients, $\partial \overline{X}(t)/\partial \overline{X}(t_o)$, in this expression are identical to the elements of the state transition matrix (see equation II.43); therefore, equation III.1 may be expressed in the form

$$\overline{X}(t) - \overline{X}_n(t) = \Phi(t, t_o) \left[\overline{X}(t_o) - \overline{X}_n(t_o)\right] + \dot{\overline{X}}(t_n)(t - t_n) . \qquad \text{[III.2]}$$

Transfer paths are computed as the solutions to targeting problems that connect two fixed states. Depending on the specific problem under consideration, components of the vectors $\overline{X}$ and $\overline{X}_n$ identify desired position or velocity states that define the targeting problem. Other elements of these vectors represent unknown quantities that are determined as the result of the differential corrections procedure.

1. Single Segment Differential Corrections

One type of transfer is a continuous trajectory that connects two fixed end positions. The construction of such a path is defined as the single position targeting problem. The path is labeled a single segment trajectory since it is assumed to be a path that is continuous in both position and velocity and can, therefore, be represented by a single initial state. Given a specified initial position, $\bar{r}_o = \{x_o, y_o, z_o\}^T$, the problem is to determine the initial velocity, $\bar{v}_o = \{\dot{x}_o, \dot{y}_o, \dot{z}_o\}^T$, that is required to arrive at a specified final position, $\bar{r}_f = \{x_f, y_f, z_f\}^T$, where the notation $\bar{r} = \{x\ y\ z\}^T$ represents a three element position vector, and $\bar{v} = \{\dot{x}\ \dot{y}\ \dot{z}\}^T$ represents a velocity vector. In the following discussion, the subscript 'o' is used to denote an initial condition; subscript 'f' indicates a final condition; subscript 'k' defines a current value; and subscript '$k+1$' denotes an updated value.

The algorithm requires initial guesses for the velocity, $\bar{v}_{o_k}$, and for the time of flight, t_{f_k}, that are appropriate for the application. A desired initial position is known, $\bar{r}_o$; therefore, this is specified as the initial position in all iterations, $\bar{r}_{o_k} = \bar{r}_o$. Next, given the initial guess for all six elements of the state vector $\overline{X}_{o_k}$, defined as $\overline{X}_{o_k} = \overline{X}_k(t_o) = \{\bar{r}_{o_k}\ \ \bar{v}_{o_k}\}^T$, the equations of motion (equations II.23–II.25) are integrated simultaneously with the state transition matrix differential equation (equation II.33) from the time t_o to the time t_{f_k}. The final state resulting from the integration is defined as $\overline{X}_{f_k} = \overline{X}_k(t_{f_k}) = \{\bar{r}_{f_k}\ \ \bar{v}_{f_k}\}^T$. If the constraint on the final position is not satisfied ($\bar{r}_{f_k} \neq \bar{r}_f$), some modification of the initial velocity and possibly the time of flight is required. The appropriate changes are

computed as the solution to a set of linear equations that are derived in terms of elements of the state transition matrix and the difference between the specified states and the states that are achieved in the current iteration. The goal is to select an improved initial state, $\overline{X}_{o_{k+1}} = \{\bar{r}_{o_{k+1}} \;\; \bar{v}_{o_{k+1}}\}^T$, and time of flight, $t_{f_{k+1}}$, such that the position at the new final time in the next iteration, $\bar{r}_{f_{k+1}}$, equals the desired position, $\bar{r}_f$.

For evaluation in III.2, the trajectory denoted by 'k' represents the nominal solution, $\overline{X}_n$. The trajectory that results from the modified velocity and time of flight, denoted with the subscript '$k+1$', corresponds to the solution $\overline{X}$. Thus, the states in this example are substituted into equation III.2 to yield

$$\left(\overline{X}_{f_{k+1}} - \overline{X}_{f_k}\right) = \Phi(t_{f_k}, t_o)\left(\overline{X}_{o_{k+1}} - \overline{X}_{o_k}\right) + \dot{\overline{X}}_k(t_{f_k})(t_{f_{k+1}} - t_{f_k}) \,. \qquad \text{[III.3]}$$

Expanding this equation in terms of separate position and velocity vectors, the first three rows can be written in the form

$$\bar{r}_{f_{k+1}} - \bar{r}_{f_k} = \left[\begin{array}{cc} \phi_{11} & \phi_{12} \end{array}\right]_{(t_{f_k}, t_o)} \left\{\begin{array}{c} \bar{r}_{o_{k+1}} - \bar{r}_{o_k} \\ \bar{v}_{o_{k+1}} - \bar{v}_{o_k} \end{array}\right\} + \bar{v}_{f_k}(t_{f_{k+1}} - t_{f_k}) \,, \qquad \text{[III.4]}$$

where the ϕ_{ij} represent partitioned 3×3 submatrices of the state transition matrix. Recall, a desired final position is specified, but a final velocity is not defined in this application; therefore, the remaining rows of equation III.3 provide no useful information when targeting only the final position.

To represent the desired characteristics, any quantities on the updated trajectory that can be expressed in terms of the prescribed states (not through linear approximations) are assumed to satisfy those expressions. Thus, the new initial position is defined as

$$\bar{r}_{o_{k+1}} = \bar{r}_{o_k} = \bar{r}_o \,, \qquad \text{[III.5]}$$

and the new final position is assumed to satisfy

$$\bar{r}_{f_{k+1}} = \bar{r}_f \,. \qquad \text{[III.6]}$$

With these definitions, equation III.4 is rewritten as

$$\bar{r}_f - \bar{r}_{f_k} = \left[\begin{array}{c|c} \phi_{12}(t_{f_k}, t_o) & \bar{v}_{f_k} \end{array}\right] \left\{\begin{array}{c} \bar{v}_{o_{k+1}} - \bar{v}_{o_k} \\ t_{f_{k+1}} - t_{f_k} \end{array}\right\} , \qquad \text{[III.7]}$$

where the only remaining unknowns are $\bar{v}_{o_{k+1}}$ and $t_{f_{k+1}}$. This vector equation represents three scalar equations in four unknowns. Thus, the targeting problem, as defined, is under-constrained; an infinite number of solutions exist.

The use of a minimum norm solution may be appropriate, or a specific constraint may be imposed on the solution to equation III.7 to achieve an additional desired characteristic.

Consistent with the goal of achieving low cost transfers, the transfer costs that result from a variety of additional requirements are used to evaluate the most useful constraints. Different solutions to equation III.7 represent different transfer paths that can be parameterized by the time of flight; however, an analytic constraint representing the optimal time is not available as a function of the terminal conditions. Also, the minimum norm solution does not necessarily yield the optimal transfer time. Thus, to produce the best solution between the specified endpoints, a numerical optimization routine is used to select the optimal time of flight. The problem is posed as a one parameter optimization problem where the variable of interest is the transfer time, t_f; therefore, solutions to equation III.7 that constrain time are required.

A constraint on the final time is imposed in the solution of equation III.7 as

$$t_{f_{k+1}} = t_{f_k} = t_f \ , \qquad \text{[III.8]}$$

where it is assumed that the initial guess is equal to the desired value. In this case, the corrected value for the initial velocity is computed by inverting equation III.7 such that

$$\bar{v}_{o_{k+1}} = \bar{v}_{o_k} + \phi_{12}^{-1}(t_f, t_o)(\bar{r}_f - \bar{r}_{f_k}) \ , \qquad \text{[III.9]}$$

assuming ϕ_{12} is invertible. Then, the improved path is computed using the updated initial state vector, $\overline{X}_{o_{k+1}} = \{\bar{r}_{o_{k+1}} \ \ \bar{v}_{o_{k+1}}\}^T$. This process continues until a trajectory that includes the desired initial and final positions is constructed with the specified time of flight.

2. Multi-Segment Differential Corrections

The single segment differential corrections scheme is designed to solve the single position targeting problem as defined in the previous discussion. This problem may be extended to a multi-segment (or multiple segment) trajectory where constraints are imposed at locations other than the departure and arrival positions. The label "n-segment trajectory" implies that the specification of state vectors at n locations along the path is required for a complete definition of the solution. It is not possible to construct a multi-segment path, continuous in both position and velocity, that satisfies arbitrary constraints on position and velocity; therefore, specific constraints that can be satisfied are considered. Three definitions help to clarify the terminology that is used in this work: all trajectories are assumed to be continuous in position; individual segments along a trajectory are assumed to be continuous in both position and velocity; velocity discontinuities that exist along a path are denoted as instantaneous $\Delta\bar{v}$'s. Finally, since multi-segment paths are constructed to satisfy constraints that are appropriate to the application under consideration, individual segments do not necessarily share any common characteristics such as shape or duration.

Consistent with the discussion of the single segment differential corrector, 'o' is used to denote initial conditions; 'f' denotes final conditions; 'k' denotes a current value; and '$k+1$' denotes updated conditions. Other notation necessary for a two-segment solution includes the following: subscript 'm' denotes an interior point that occurs at a time between the initial and final times; superscript '$-$' denotes conditions just prior to a $\Delta\bar{v}$; and '$+$' denotes conditions immediately after a $\Delta\bar{v}$. Each two-segment problem is considered in terms of one segment that connects points o and m and a second segment that connects points m and f, where it is assumed that constraints are imposed at points o, m, and f. For this development, all integrations are performed forward in time. Thus, the segments are defined by the corresponding initial state vectors, $\overline{X}_o = \{\bar{r}_o\ \bar{v}_o\}^T$ and $\overline{X}_{m^+} = \{\bar{r}_{m^+}\ \bar{v}_{m^+}\}^T$, and the two times of flight defined by the quantities $t_m - t_o$ and $t_f - t_m$, where t_o is the time corresponding to $\overline{X}_o$, t_m corresponds to the interior state $\overline{X}_{m^+}$, and t_f corresponds to the final state $\overline{X}_f$.

As in the single segment development, first-order Taylor series expansions still form the basis of the derivation. Equation III.3 is extended for a two-segment trajectory as

$$\overline{X}_{m_{k+1}^-} - \overline{X}_{m_k^-} = \Phi(t_{m_k}, t_o)(\overline{X}_{o_{k+1}} - \overline{X}_{o_k}) + \dot{\overline{X}}_{m_k^-}(t_{m_{k+1}} - t_{m_k}) , \qquad \text{[III.10]}$$

and

$$\overline{X}_{f_{k+1}} - \overline{X}_{f_k} = \Phi(t_{f_k}, t_{m_k})(\overline{X}_{m_{k+1}^+} - \overline{X}_{m_k^+}) + \dot{\overline{X}}_{f_k}(t_{f_{k+1}} - t_{f_k}) . \qquad \text{[III.11]}$$

These expressions are used in each of the two-segment differential correctors developed in this section. Two different algorithms are discussed. One corrector assumes a fixed interior position. The second corrector constrains the $\Delta\bar{v}$ at the interior point. Both correctors are derived with the assumption that the initial and final positions are fixed.

a. Fixed Interior Position

The differential corrector based on a fixed interior position is designed to construct a two-segment trajectory that includes both specified initial and final positions, $\bar{r}_o$ and $\bar{r}_f$, and one specified interior position, $\bar{r}_m$. Since it may not be possible to construct such a path to be continuous in both position and velocity, an unspecified velocity discontinuity may exist at the specified interior position, denoted as $\Delta\bar{v}_m$. The unknowns are the initial velocities on each segment, $\bar{v}_o$ and $\bar{v}_{m^+}$, and the times t_m and t_f, assuming a given initial time, t_o.

As a first step, initial guesses for the state vectors are selected and denoted $\overline{X}_{o_k} = \{\bar{r}_{o_k}\ \bar{v}_{o_k}\}^T$ and $\overline{X}_{m_k^+} = \{\bar{r}_{m_k^+}\ \bar{v}_{m_k^+}\}^T$. Initial guesses corresponding to the times of interest are denoted by t_{m_k} and t_{f_k}. Initial values of the velocities and times are selected from other information that is available in a particular application. Constraints on the positions

are incorporated in the corrector as $\bar{r}_{o_k} = \bar{r}_o$ and $\bar{r}_{m_k^+} = \bar{r}_m$. The equations of motion and the differential equation governing the state transition matrix are simultaneously integrated from time t_o to t_{m_k} with initial conditions $\overline{X}_{o_k}$ and $\Phi(t_o, t_o) = I_6$. The final state along the first segment is denoted $\overline{X}_{m_k^-} = \left\{\bar{r}_{m_k^-} \;\; \bar{v}_{m_k^-}\right\}^T$, where '$k$' denotes a current value and '$-$' indicates that the state occurs before any $\Delta\bar{v}$. Next, the equations of motion and the matrix differential equation for Φ are integrated from t_{m_k} to t_{f_k} with initial conditions $\overline{X}_{m_k^+}$ and $\Phi(t_{m_k}, t_{m_k}) = I_6$. (Note that the initial guess, $\bar{v}_{m_k^+}$, is not necessarily equal to $\bar{v}_{m_k^-}$ since it is assumed that a velocity discontinuity may occur at the interior position.) The final state along the second segment is denoted $\overline{X}_{f_k} = \{\bar{r}_{f_k} \;\; \bar{v}_{f_k}\}^T$. If the two final positions that are achieved, $\bar{r}_{m_k^-}$ and $\bar{r}_{f_k}$, do not equal the desired states, $\bar{r}_m$ and $\bar{r}_f$, respectively, the velocities, $\bar{v}_{o_k}$ and $\bar{v}_{m_k^+}$, and possibly the integration times are modified. A set of linear equations is developed to compute the appropriate changes.

To begin the development, any known or desired quantities on the updated trajectory are identified. The derivation assumes that the improved trajectory will satisfy the constraints; therefore, since initial, interior, and final positions are constrained, the new positions are specified as

$$\begin{aligned} \bar{r}_{o_{k+1}} &= \bar{r}_{o_k} = \bar{r}_o \; ; \\ \bar{r}_{m_{k+1}^-} &= \bar{r}_m \; ; \\ \bar{r}_{m_{k+1}^+} &= \bar{r}_{m_k^+} = \bar{r}_m \; ; \\ \bar{r}_{f_{k+1}} &= \bar{r}_f \; . \end{aligned} \qquad \text{[III.12]}$$

Using these constraints and neglecting equations that provide no useful information in this application, equations III.10 and III.11 reduce to the following

$$\begin{Bmatrix} \bar{r}_m - \bar{r}_{m_k^-} \\ \bar{r}_f - \bar{r}_{f_k} \end{Bmatrix} = \begin{bmatrix} \phi_{12}(t_{m_k}, t_o) & 0_3 & \bar{v}_{m_k^-} & 0_{3\times 1} \\ 0_3 & \phi_{12}(t_{f_k}, t_{m_k}) & 0_{3\times 1} & \bar{v}_{f_k} \end{bmatrix} \begin{Bmatrix} \bar{v}_{o_{k+1}} - \bar{v}_{o_k} \\ \bar{v}_{m_{k+1}^+} - \bar{v}_{m_k^+} \\ t_{m_{k+1}} - t_{m_k} \\ t_{f_{k+1}} - t_{f_k} \end{Bmatrix}, \qquad \text{[III.13]}$$

where $0_{3\times 1} = \{0 \;\; 0 \;\; 0\}^T$. In this expression, the remaining unknowns are $\bar{v}_{o_{k+1}}$, $\bar{v}_{m_{k+1}^+}$, $t_{m_{k+1}}$, and $t_{f_{k+1}}$. Thus, equation III.13 represents six scalar equations in eight unknowns; the system is underconstrained. A minimum norm solution does not necessarily yield the lowest cost transfer containing the selected positions; therefore, two additional constraints are imposed that are useful for particular applications. Since different solutions can be parameterized by the times of flight for each segment, a numerical optimization routine is used to identify the optimal values for the times. To compute a solution that satisfies time requirements selected by the numerical method, constraints are applied as

$$t_{m_{k+1}} = t_{m_k} = t_m \; , \qquad \text{[III.14]}$$

and

$$t_{f_{k+1}} = t_{f_k} = t_f \ , \qquad \text{[III.15]}$$

resulting in a unique solution for equation III.13. Thus, for the applications here, the use of constraints other than time in the corrector that fixes the interior position are not employed.

Given the constraints on time, equation III.13 is written as

$$\begin{Bmatrix} \bar{r}_m - \bar{r}_{m_k^-} \\ \bar{r}_f - \bar{r}_{f_k} \end{Bmatrix} = \begin{bmatrix} \phi_{12}(t_m, t_o) & 0_3 \\ 0_3 & \phi_{12}(t_f, t_m) \end{bmatrix} \begin{Bmatrix} \bar{v}_{o_{k+1}} - \bar{v}_{o_k} \\ \bar{v}_{m_{k+1}^+} - \bar{v}_{m_k^+} \end{Bmatrix} . \qquad \text{[III.16]}$$

The form of this expression indicates that this type of targeting problem is separable; the two segments may be computed independently. Thus, the updated velocities are evaluated from

$$\bar{v}_{o_{k+1}} = \bar{v}_{o_k} + \phi_{12}^{-1}(t_m, t_o)(\bar{r}_m - \bar{r}_{m_k^-}) \ , \qquad \text{[III.17]}$$

and

$$\bar{v}_{m_{k+1}^+} = \bar{v}_{m_k^+} + \phi_{12}^{-1}(t_f, t_m)(\bar{r}_f - \bar{r}_{f_k}) \ , \qquad \text{[III.18]}$$

where each solution is expressed completely in terms of conditions associated with a single segment. These updated velocities are used to define the initial states to again integrate the equations of motion and the state transition matrices, and the process is repeated until the conditions $\bar{r}_{m_k^-} = \bar{r}_m$ and $\bar{r}_{f_k} = \bar{r}_f$ are satisfied to within an acceptable tolerance. These requirements, and the assumption that $\bar{r}_{m_k^+} = \bar{r}_m$ at each iteration, guarantee position continuity for the trajectory at point m. Since the constraint $\bar{v}_{m_{k+1}^+} = \bar{v}_{m_{k+1}^-}$ was *not* imposed, a velocity discontinuity may exist at the patch point of the two segments. This discontinuity can be represented as $\Delta\bar{v}_m = \bar{v}_{m_{k+1}^+} - \bar{v}_{m_{k+1}^-}$. To impose a velocity constraint creates an overconstrained problem (even if the two time constraints are abandoned) since it represents three additional scalar equations, although only two additional constraints may be imposed on the solution of equation III.13 to define a unique solution.

This derivation was presented for a two-segment trajectory; however it can be expanded to any number of segments with the result that each segment can be computed separately. In this way, a trajectory that includes several specified positions can be constructed with unspecified velocity discontinuities at those fixed points. Thus, the shape of a trajectory can be specified; however, impulses may be required to produce it.

b. Fixed Interior $\Delta\bar{V}$

A second multi-segment differential corrector is one that matches initial and final positions and constrains the interior velocity discontinuity, $\Delta\bar{v}_m$. The specified quantities are $\bar{r}_o$, $\bar{r}_f$, and the quantity $\bar{v}_{m+} - \bar{v}_{m-} = \Delta\bar{v}_m$, although neither of the individual velocities

are constrained. The unknown quantities are the velocities $\bar{v}_o$ and $\bar{v}_{m^+}$, the position $\bar{r}_m$, and the times t_m and t_f. As in the case of the fixed interior position, initial guesses for the unknown quantities are selected and denoted with subscript 'k'. Then, given states $\overline{X}_{o_k}$, $\overline{X}_{m_k^+}$, and times t_{m_k}, t_{f_k}, the first segment is integrated forward in time from $\overline{X}_{o_k}$ to t_{m_k}; the second segment is integrated forward from $\overline{X}_{m_k^+}$ to time t_{f_k}. If the resulting velocity discontinuity does not equal the prescribed value ($\bar{v}_{m_k^+} - \bar{v}_{m_k^-} \neq \Delta\bar{v}_m$), position continuity at the patch point is not satisfied ($\bar{r}_{m_k^-} \neq \bar{r}_{m_k^+}$), or the desired final position is not achieved ($\bar{r}_{f_k} \neq \bar{r}_f$), the initial velocity, $\bar{v}_{o_k}$, and both the position and velocity of the interior point, $\bar{r}_{m_k^+}$ and $\bar{v}_{m_k^+}$, may be adjusted. (Changing the integration times is also an option, but the times are assumed to be fixed for this example, consistent with its use in the numerical optimization process. Thus, the times are constrained by $t_{m_{k+1}} = t_{m_k} = t_m$ and $t_{f_{k+1}} = t_{f_k} = t_f$.)

To develop an expression to represent the corrector, any known values for the updated quantities are identified. To satisfy the endpoint constraints, the updated initial and final positions are defined by

$$\begin{aligned} \bar{r}_{o_{k+1}} &= \bar{r}_{o_k} = \bar{r}_o \ ; \\ \bar{r}_{f_{k+1}} &= \bar{r}_f \ . \end{aligned} \qquad \text{[III.19]}$$

A velocity discontinuity equal to the prescribed value, $\Delta\bar{v}_m$, is represented in terms of the new initial velocity of the second segment as

$$\bar{v}_{m_{k+1}^+} = \bar{v}_{m_{k+1}^-} + \Delta\bar{v}_m \ . \qquad \text{[III.20]}$$

Finally, to guarantee position continuity at the patch point, the interior position is required to satisfy the equality

$$\bar{r}_{m_{k+1}^-} = \bar{r}_{m_{k+1}^+} \ , \qquad \text{[III.21]}$$

although this position is not required to equal either of the current interior positions, $\bar{r}_{m_k^-}$ or $\bar{r}_{m_k^+}$, since no interior position is specified. Using these constraints in equations III.10 and III.11, and neglecting equations that offer no useful information, a set of linear expressions is formed as

$$\begin{Bmatrix} \bar{r}_{m_{k+1}^+} - \bar{r}_{m_k^-} \\ (\bar{v}_{m_{k+1}^+} - \Delta\bar{v}_m) - \bar{v}_{m_k^-} \end{Bmatrix} = \begin{bmatrix} \phi_{12}(t_m, t_o) \\ \phi_{22}(t_m, t_o) \end{bmatrix} (\bar{v}_{o_{k+1}} - \bar{v}_{o_k}) \ , \qquad \text{[III.22]}$$

and

$$(\bar{r}_f - \bar{r}_{f_k}) = [\phi_{11}(t_f, t_m) \ \ \phi_{12}(t_f, t_m)] \begin{Bmatrix} \bar{r}_{m_{k+1}^+} - \bar{r}_{m_k^+} \\ \bar{v}_{m_{k+1}^+} - \bar{v}_{m_k^+} \end{Bmatrix} . \qquad \text{[III.23]}$$

The coupling of the unknown quantities $\bar{r}_{m_{k+1}^+}$ and $\bar{v}_{m_{k+1}^+}$ between the equations complicates the solution; however, rearranging the equations does yield an expression in the form

$$\begin{Bmatrix} \bar{v}_{o_{k+1}} \\ \bar{r}_{m_{k+1}^+} \\ \bar{v}_{m_{k+1}^+} \end{Bmatrix} = \begin{Bmatrix} \bar{v}_{o_k} \\ \bar{r}_{m_k^+} \\ \bar{v}_{m_k^+} \end{Bmatrix} + \begin{bmatrix} \begin{bmatrix} \phi_{12_{mo}} \\ \phi_{22_{mo}} \end{bmatrix} & [-I_6] \\ [0_3] & [\phi_{11_{fm}} \quad \phi_{12_{fm}}] \end{bmatrix}^{-1} \begin{Bmatrix} \bar{r}_{m_k^+} - \bar{r}_{m_k^-} \\ (\bar{v}_{m_k^+} - \bar{v}_{m_k^-}) - \Delta\bar{v}_m \\ \bar{r}_f - \bar{r}_{f_k} \end{Bmatrix}. \tag{III.24}$$

This form is convenient since the difference $\bar{r}_{m_k^+} - \bar{r}_{m_k^-}$ represents any position discontinuity at the patch point in the current iteration. Similarly, other differences in equation III.24 also represent the current deviation from the prescribed characteristics. Using equation III.24, the initial velocity and the complete interior state (both position, $\bar{r}_{m_k^+}$, and velocity, $\bar{v}_{m_k^+}$) are updated, and the corrections process is continued until the solution converges to the desired end positions with position continuity at the patch point and the prescribed interior impulse. In the Sun-Earth/Moon barycenter problem, a tolerance of approximately 0.15 millimeters is designated for all targeted positions including positions at patch points. This value is approximately equal to 1×10^{-15} times the characteristic length used in the computations.

As mentioned for the solution with a fixed interior position, equation III.24 may be extended to include additional segments. For a three-segment trajectory with fixed endpoints and two fixed interior $\Delta\bar{v}$'s, the solution takes the form

$$\begin{Bmatrix} \bar{v}_{o_{k+1}} \\ \bar{r}_{m_{k+1}^+} \\ \bar{v}_{m_{k+1}^+} \\ \bar{r}_{n_{k+1}^+} \\ \bar{v}_{n_{k+1}^+} \end{Bmatrix} = \begin{Bmatrix} \bar{v}_{o_k} \\ \bar{r}_{m_k^+} \\ \bar{v}_{m_k^+} \\ \bar{r}_{n_k^+} \\ \bar{v}_{n_k^+} \end{Bmatrix} \tag{III.25}$$

$$+ \begin{bmatrix} \begin{bmatrix} \phi_{12_{mo}} \\ \phi_{22_{mo}} \end{bmatrix} & [-I_6] & [0_6] \\ \begin{bmatrix} [0_3] \\ [0_3] \end{bmatrix} & [\Phi_{nm}] & [-I_6] \\ [0_3] & [0_3 \quad 0_3] & [\phi_{11_{fn}} \quad \phi_{12_{fn}}] \end{bmatrix}^{-1} \begin{Bmatrix} \bar{r}_{m_k^+} - \bar{r}_{m_k^-} \\ (\bar{v}_{m_k^+} - \bar{v}_{m_k^-}) - \Delta\bar{v}_m \\ \bar{r}_{n_k^+} - \bar{r}_{n_k^-} \\ (\bar{v}_{n_k^+} - \bar{v}_{n_k^-}) - \Delta\bar{v}_n \\ \bar{r}_f - \bar{r}_{f_k} \end{Bmatrix},$$

where 'n' denotes a second interior point that is located between points 'm' and 'f' (in time); 'mo' indicates the state transition matrix $\Phi(t_m, t_o)$; 'nm' denotes the state transition matrix $\Phi(t_n, t_m)$; and 'fn' represents the state transition matrix $\Phi(t_f, t_n)$. This form is easily expanded to include additional segments. In this way, a trajectory can be constructed

that is continuous in position with specified endpoints and specified velocity discontinuities along the path. The $\Delta\bar{v}$'s may be defined to be zero in order to construct a path that is continuous in both position and velocity; however, the interior positions cannot be specified in the process as developed. Thus, the shape of the path cannot be defined; only the endpoints can be specified.

In the development of both correctors for use in a two-segment trajectory, only two additional assumptions are possible. Thus, even if the fixed time assumptions are eliminated, neither corrector can constrain both the interior position and the interior $\Delta\bar{v}$ since either additional requirement represents three scalar constraints. It is not possible to match arbitrary initial, final, and interior positions, and an interior $\Delta\bar{v}$ simultaneously since these requirements define an overconstrained problem.

3. Differential Corrections in Initial Condition Selection

In addition to providing corrections to an initial guess, the state transition matrix can also be used to determine an initial guess for the calculation of a new trajectory based on the difference between the new desired characteristics and an existing solution. Although the equations required for this use of the state transition matrix are similar to those employed for modifying an existing guess as discussed above, the use of the matrix in the *selection* of an appropriate initial guess represents an alternative use of differential corrections. Improving the initial guess through algebraic relationships before using it to integrate equations of motion may reduce the number of iterations required to converge to a solution. It can also result in convergence of subsequent differential corrections procedures that update the initial guess when convergence was previously not achieved due to a poor initial guess.

In the optimization algorithm, candidate trajectories are identified relative to a nominal solution by differences in the times of flight along individual segments and differences in the positions at both endpoints of each segment of a trajectory. The state transition matrix is used in conjunction with these relative differences to suggest appropriate changes to the nominal initial conditions; that is, to compute a guess for the initial velocity along each segment of the perturbed transfer. Thus, the problem is similar to the fixed position targeting problems discussed earlier, but, in this case, the meaning associated with the states is modified. For example, as opposed to representing an error relative to some desired state, the final position from the first iteration represents the final position along the nominal path; the desired final position along the improved solution represents the final position along the perturbed path. Also, unlike the targeting examples discussed in previous sections, a change in the initial position is considered in this application.

Endpoints associated with a nominal transfer path are identified as points o and f with associated state vectors $\overline{X}_o = \{\bar{r}_o \;\; \bar{v}_o\}^T$ and $\overline{X}_f = \{\bar{r}_f \;\; \bar{v}_f\}^T$. Points o_p and f_p define the endpoints of a perturbed transfer path with associated state vectors $\overline{X}_{o_p} = \{\bar{r}_{o_p} \;\; \bar{v}_{o_p}\}^T$ and $\overline{X}_{f_p} = \{\bar{r}_{f_p} \;\; \bar{v}_{f_p}\}^T$. The state transition matrix associated with the nominal solution is identified as $\Phi(t_f, t_o)$ using the nominal final time, t_f. The time dt defines the change in the transfer time that is required. Thus, in terms of the notation used in the previous discussion, the nominal solution represents the current iteration, denoted k, and the updated solution, connecting o_p and f_p, is denoted $k+1$. Using equation III.4, with the appropriate definitions for the subscripts k and $k+1$, the nominal and perturbed positions at the new final time, given by $t_{f_p} = t_f + dt$, are related, to first order, by

$$\bar{r}_{f_p} - \bar{r}_f \;=\; [\phi_{11} \;\; \phi_{12}]_{(t_f, t_o)} \begin{Bmatrix} \bar{r}_{o_p} - \bar{r}_o \\ \bar{v}_{o_p} - \bar{v}_o \end{Bmatrix} + \bar{v}_f dt \; . \qquad \text{[III.26]}$$

The desired quantity is the value of the velocity on the new transfer, that is $\bar{v}_{o_p}$, since the position $\bar{r}_{o_p}$ is known as the desired initial position for the new transfer. Solving equation III.26 for the unknown velocity yields

$$\bar{v}_{o_p} \;=\; \bar{v}_o \;+\; \phi_{12}^{-1}(t_f, t_o) \left[\bar{r}_{f_p} - \bar{r}_f - \phi_{11}(t_f, t_o)(\bar{r}_{o_p} - \bar{r}_o) - \bar{v}_f(dt_f - dt_o)\right] \; . \qquad \text{[III.27]}$$

Given the improved initial guess, the equations of motion are integrated over a time interval equal to $t_{f_p} - t_o$ with the initial condition $\overline{X}_{o_p} = \{\bar{r}_{o_p} \;\; \bar{v}_{o_p}\}^T$. The differential correctors discussed previously are then used to modify this improved guess to produce the desired characteristics.

Although this development is only presented for a single segment, it is used to update the initial conditions separately for each segment of a multi-segment transfer. In this way, an organized approach is employed to determine the initial conditions for the computation of a perturbed transfer. This perturbed transfer serves to initiate a new corrections cycle.

B. Primer Vector

Differential correctors of the type discussed in the previous sections are used to produce trajectories that possess sets of specified characteristics, but a conventional numerical optimization routine is employed to identify the characteristics that correspond to an optimal solution. Since a numerical procedure may require many iterations that involve expensive calculations, any operation that reduces the number of required computations is beneficial. An analytic solution for a step in the process is one option. Given the dependence of many optimization methods on the gradient of the cost function, an analytic expression for this

quantity represents a partial solution that can substantially reduce the number of computations. In addition, an examination of the conditions that must exist in an optimal solution provides insight into the problem.

In the optimal transfer problem, the primer vector, defined by Lawden as the adjoint vector to the velocity, is an important element in a discussion of the necessary conditions for optimality and in the development of an analytic expression for the gradient of the cost function. This principle was extended to the restricted problem by Hiday and Howell and was demonstrated for transfers between libration point orbits in the elliptic restricted problem[6, 7]. The conditions for optimality applied to impulsive transfers can be defined in terms of the characteristics of the primer vector. Also, this vector can be used to modify the endpoints of a transfer and to add interior impulses in an effort to reduce the cost. The following discussion follows from Hiday's derivation of the necessary conditions for optimality for impulsive transfers in the ER3BP and her development of tools for improving non-optimal paths[6].

1. Euler-Lagrange Equations

Following Hiday[6], the second-order scalar equations of motion in the restricted three-body problem are written in a first-order form in terms of the vectors $\bar{r} = \{x, y, z\}^T$ and $\bar{v} = \{\dot{x}, \dot{y}, \dot{z}\}^T$ representing position and velocity components in barycenter rotating coordinates. The thrust is introduced in terms of the thrust magnitude, T, a unit vector in the thrust direction, $\hat{u}_T$, and the effective exhaust velocity, c. With these definitions, the governing differential equations are expressed in terms of the state variables $\bar{r}$, $\bar{v}$, and m (vehicle mass) and control variables $\hat{u}_T$ and T as

$$\dot{\bar{r}} = \bar{v} , \qquad \text{[III.28]}$$

$$\dot{\bar{v}} = \frac{T}{m}\hat{u}_T + \bar{g} , \qquad \text{[III.29]}$$

$$\dot{m} = -\frac{T}{c} , \qquad \text{[III.30]}$$

where $\bar{g}$ includes all acceleration terms, except the external thrust term, as

$$\bar{g} = \begin{Bmatrix} 2\dot{y}\dot{\theta} + y\ddot{\theta} + \partial U/\partial x \\ -2\dot{x}\dot{\theta} - x\ddot{\theta} + \partial U/\partial y \\ \partial U/\partial z \end{Bmatrix} . \qquad \text{[III.31]}$$

Constraints on the control variables are stated as

$$|\hat{u}_T| = 1 , \qquad \text{[III.32]}$$

and

$$0 \leq T \leq \tilde{T} , \qquad \text{[III.33]}$$

where $\tilde{T}$ is a maximum allowable thrust magnitude.

The scalar cost function is defined in terms of the initial and final masses as

$$J = c \ln\left[\frac{m_o}{m_f}\right] . \qquad \text{[III.34]}$$

This is equivalent to the definition of the cost as the sum of the maneuver magnitudes ($\sum_i |\Delta\bar{v}_i|$) assuming only impulsive maneuvers are permitted. Since this function contains no path dependent term, the Hamilton is expressed as a linear combination of the state equations in the form

$$H = \bar{\lambda}_r^T \bar{v} + \bar{\lambda}_v^T \left(\frac{T}{m} \hat{u}_T + \bar{g} \right) - \lambda_m \frac{T}{c} , \qquad \text{[III.35]}$$

with Lagrange multipliers $\bar{\lambda}_r$, $\bar{\lambda}_v$, and λ_m. The adjoint differential equations are then derived from the Euler-Lagrange equations as

$$\dot{\bar{\lambda}}_r^T = -\frac{\partial H}{\partial \bar{r}} = -\bar{\lambda}_v^T \frac{\partial \bar{g}}{\partial \bar{r}} , \qquad \text{[III.36]}$$

$$\dot{\bar{\lambda}}_v^T = -\frac{\partial H}{\partial \bar{v}} = -\bar{\lambda}_r^T - \bar{\lambda}_v^T \frac{\partial \bar{g}}{\partial \bar{v}} , \qquad \text{[III.37]}$$

$$\dot{\lambda}_m = -\frac{\partial H}{\partial m} = \frac{T}{m^2} \bar{\lambda}_v^T \hat{u}_T , \qquad \text{[III.38]}$$

where

$$\frac{\partial \bar{g}}{\partial \bar{r}} = U_{XX} + \ddot{\theta}\Omega , \qquad \text{[III.39]}$$

and

$$\frac{\partial \bar{g}}{\partial \bar{v}} = 2\dot{\theta}\Omega , \qquad \text{[III.40]}$$

with Ω and U_{XX} defined in equations II.35 and II.36, respectively. Lawden developed the solution to the problem in terms of coordinates that are defined relative to an inertial reference frame; therefore, the vector $\bar{g}$ in his derivation is a function of position and time only. Thus, the term $\partial\bar{g}/\partial\bar{v}$ is zero in his derivation. This term exists when the equations associated with the restricted problem are written relative to the rotating coordinate frame ($\dot{\theta}$ is the angular rate of the rotating frame) and is included in Hiday's derivation. The additional requirements that result from the Euler-Lagrange necessary conditions are written in terms of a Lagrange expression, F, formed from the Hamiltonian and the constraints as

$$F = \sigma_1[T(\tilde{T} - T) - q^2] + \sigma_2[|\hat{u}_T|^2 - 1] - H , \qquad \text{[III.41]}$$

where σ_1 and σ_2 are additional Lagrange multipliers, and a control variable, q, is employed to incorporate the inequality constraint on the thrust magnitude. In terms of this expression, the remaining Euler-Lagrange equations require that

$$\frac{\partial F}{\partial \hat{u}_T} = 0 = 2\sigma_2 \hat{u}_T - \frac{T}{m} \bar{\lambda}_v ; \qquad \text{[III.42]}$$

$$\frac{\partial F}{\partial T} = 0 = \sigma_1(\tilde{T} - 2T) - \frac{1}{m}\bar{\lambda}_v^T \bar{u}_T + \frac{1}{c}\lambda_m \; ; \qquad \text{[III.43]}$$

$$\frac{\partial F}{\partial q} = 0 = -2\sigma_1 q \; . \qquad \text{[III.44]}$$

Consistent with Pontryagin's Maximum Principle, the Hamiltonian is maximized over the choice of control variables that satisfy the constraints to minimize the cost. With terms evaluated on the optimal trajectory indicated by '*', this requires

$$\left[\frac{1}{m}\bar{\lambda}_v^{*T}\bar{u}_T^* - \frac{\lambda_m^*}{c}\right]T^* \geq \left[\frac{1}{m}\bar{\lambda}_v^{*T}\bar{u}_T - \frac{\lambda_m^*}{c}\right]T \; , \qquad \text{[III.45]}$$

since other terms in the Hamiltonian expression are not affected by changes in the controls. This inequality is recognized as the Weierstrass condition. Across an impulse, that represents a discontinuity in the velocity states (a corner), the Hamiltonian and the multipliers are required to satisfy the Weierstrass-Erdmann corner conditions. Thus, it is required that

$$\bar{\lambda}_r^{-*} = \bar{\lambda}_r^{+*} \; , \qquad \text{[III.46]}$$

$$\bar{\lambda}_v^{-*} = \bar{\lambda}_v^{+*} \; , \qquad \text{[III.47]}$$

$$\lambda_m^{-*} = \lambda_m^{+*} \; , \qquad \text{[III.48]}$$

and

$$H^{-*} = H^{+*} \; , \qquad \text{[III.49]}$$

where '−' indicates a condition immediately prior to an impulse, and '+' denotes a condition immediately after an impulse. Finally, assuming specified initial and final positions, velocities, times, and initial mass, the transversality condition requires that

$$\lambda_m^*(t_f) = \frac{\partial J}{\partial m_f} \; , \qquad \text{[III.50]}$$

or

$$\lambda_m^*(t_f) = \frac{c}{m_f} \; . \qquad \text{[III.51]}$$

An analysis of equations III.36–III.38, III.42–III.49, and III.51 yields a partial solution to the optimal impulsive transfer problem.

2. Necessary Conditions for Optimality

An examination of the Euler-Lagrange equations and the corner conditions yields several conditions that must be satisfied by the multiplier $\bar{\lambda}_v$ along an optimal trajectory. Consistent with other studies, this vector is relabeled $\bar{p}$ ($\bar{\lambda}_v = \bar{p}$) and is denoted as the primer vector. One result of the Euler-Lagrange equations, particularly equation III.42, is that the primer vector must be parallel to the thrust direction when the thrust is not zero. The

corner conditions also provide two immediate conclusions. First, as explicitly required by equation III.47, the primer vector must be continuous across an impulse. Then, with the matrix $\partial g/\partial \bar{v}$ completely defined by the motion of the primaries (see equation III.40) and the continuity of $\bar{\lambda}_r$ and $\bar{p}$ as required by the corner conditions, equation III.37 requires that the derivative of the primer vector must also be continuous across an impulse since it can be expressed as a function of variables that are themselves continuous. Using equation III.37 to express $\bar{\lambda}_r$ and assuming the primer vector is parallel to u_T on the optimal path, as found in previous results, the Hamiltonian can be rewritten in the form

$$H^* = \bar{p}^{*T}\bar{g} + \left(\frac{p^*}{m} - \frac{\lambda_m^*}{c}\right)T^* - \left(\dot{\bar{p}}^{*T} + \bar{p}^*\frac{\partial \bar{g}}{\partial \bar{v}}\right)\bar{v} \,. \qquad \text{[III.52]}$$

The Hamiltonian can only be continuous across an impulse, where the thrust is discontinuous, if the coefficient of the thrust magnitude is zero in this expression. With this simplification, equation III.49 can be expressed as $H^{+*} - H^{-*} = 0$ and reduced to the form

$$H^{+*} - H^{-*} = -\dot{\bar{p}}^{*T}(\bar{v}^+ - \bar{v}^-) = -\dot{\bar{p}}^{*T}\Delta\bar{v} = 0 \,, \qquad \text{[III.53]}$$

using continuity of the primary motion, the position of the vehicle, and the primer vector at the corner. Then, since the primer vector and the thrust direction are parallel on the optimal path, this corner condition requires that $\dot{\bar{p}}^{*T}\bar{p}^* = 0$ at the time of the impulse.

The Weierstrass condition imposes additional requirements on the primer vector along the optimal path. By considering limiting conditions in which strict equality is satisfied and employing parallel primer and thrust vectors, Hiday develops the following conditions for the two extreme cases. In the case of zero thrust, inequality III.45 is reduced to the expression

$$\frac{cp^*}{m} - \lambda_m^* \leq 0 \,. \qquad \text{[III.54]}$$

In the case of maximum thrust, the inequality requires that

$$\frac{cp^*}{m} - \lambda_m^* \geq 0 \,. \qquad \text{[III.55]}$$

An impulsive thrust, as the instantaneous intersection of an interval of maximum thrust preceded and followed by finite intervals of zero thrust, requires that

$$\frac{cp^*}{m} - \lambda_m^* = 0 \,. \qquad \text{[III.56]}$$

Further analysis of this condition is considered in terms of the thrust magnitude switching function, S, defined as the function

$$S = \frac{cp^*}{m} - \lambda_m^* \,. \qquad \text{[III.57]}$$

Over a coast arc, where $T = 0$, equation III.38 requires λ_m to be constant; therefore, the expression for S over a coast arc can be written as

$$S = \frac{cp^*}{m} - \text{constant} , \qquad \text{[III.58]}$$

where the constant is undetermined to this point. If the coast arc joins two impulsive thrusts with $S = 0$ at each of those two instants as required by equation III.56, the value of the constant at a time immediately after the first impulse is evaluated from equation III.56 as cp_o^*/m_o. At the final time, the switching function is evaluated from the equation

$$S_f = 0 = \frac{cp_f^*}{m_f} - \frac{cp_o^*}{m_o} ; \qquad \text{[III.59]}$$

therefore, the initial and final values of the primer magnitude must be equal since the final mass on a coast arc equals the initial mass on that arc. Using the transversality condition, equation III.51, the switching function at the beginning of a coast arc that follows the final impulse can be expressed as

$$S_f = 0 = \frac{cp_f^*}{m_f} - \frac{c}{m_f} . \qquad \text{[III.60]}$$

Thus, the final value of p (and, therefore, the initial value) must be one. Finally, the magnitude of $\bar{p}$ must be less than its initial value over the coast arc for inequality III.54 to be satisfied. Thus, the initial and final values of p must be one, and p must be less than one over the entire coast arc. Return now to the consequence of continuity of the Hamiltonian ($(\dot{\bar{p}}^T \bar{p})^* = 0$), and use the expression $p\dot{p} = \dot{\bar{p}}^T \bar{p}$. Since p is non-zero at a corner, $\dot{p}$ must be zero for $(\dot{\bar{p}}^T \bar{p})^* = 0$ to be valid at an interior impulse.

The results of the above discussion, as a summary of Hiday's derivation of the necessary conditions for optimality, can be stated as:

a. The magnitude of the primer vector must be one at the instant of impulse and less than one elsewhere.

b. The thrust vector must be aligned with the direction of the primer vector.

c. The primer vector and its first derivative must be continuous.

d. The derivative $\dot{p}$ must be zero at all interior impulses; also, the primer vector and its first derivative must be orthogonal at those times.

These conditions are used to identify non-optimal solutions and to identify initial conditions for the computation of the primer vector.

3. Primer Vector Computation

Although equations III.36 and III.37 are first-order vector differential equations that could be numerically integrated for the values of the adjoint vectors, $\overline{\lambda}_r$ and $\overline{p}$, given appropriate initial conditions, numerical results that represent the solution for $\overline{p}$ are available from other information in the problem. Numerical integration of equations III.36 and III.37 is not required. A derivation of the expression for the primer vector, developed by Hiday, begins with the differentiation of equation III.37 in the form

$$\ddot{\overline{p}}^T = \overline{p}^T \left[\frac{\partial \overline{g}}{\partial \overline{r}} - \frac{d}{dt} \left(\frac{\partial \overline{g}}{\partial \overline{v}} \right) \right] - \dot{\overline{p}}^T \frac{\partial \overline{g}}{\partial \overline{v}} , \qquad \text{[III.61]}$$

where equation III.36 is used to represent $\dot{\overline{\lambda}}_r$. Incorporating the derivative of equation III.40, and writing $\partial \overline{g} / \partial \overline{r}$ in the form of equation III.39, the difference in equation III.61 can be expressed as

$$\frac{\partial \overline{g}}{\partial \overline{r}} - \frac{d}{dt} \left(\frac{\partial \overline{g}}{\partial \overline{v}} \right) = U_{XX} - \ddot{\theta} \Omega . \qquad \text{[III.62]}$$

The symmetry of U_{XX} and the skew-symmetry of Ω are employed to write the transpose of equation III.61 in the form

$$\ddot{\overline{p}} = \frac{\partial \overline{g}}{\partial \overline{r}} \overline{p} + \frac{\partial \overline{g}}{\partial \overline{v}} \dot{\overline{p}} . \qquad \text{[III.63]}$$

A solution for this second-order differential equation is available from an analysis of the variational equations for the barycenter rotating coordinates.

The variational expression for the position and velocity is

$$\begin{Bmatrix} \delta \dot{\overline{r}}(t) \\ \delta \dot{\overline{v}}(t) \end{Bmatrix} = A(t) \begin{Bmatrix} \delta \overline{r}(t) \\ \delta \overline{v}(t) \end{Bmatrix} , \qquad \text{[III.64]}$$

where $A(t)$ is defined in equation II.34. This equation can be written in a second-order form as

$$\delta \ddot{\overline{r}} = \delta \dot{\overline{v}} = \frac{\partial \overline{g}}{\partial \overline{r}} \delta \overline{r} + \frac{\partial \overline{g}}{\partial \overline{v}} \delta \overline{v} . \qquad \text{[III.65]}$$

The solution to this differential equation is known to be of the form

$$\begin{Bmatrix} \delta \overline{r}(t) \\ \delta \overline{v}(t) \end{Bmatrix} = \Phi(t, t_o) \begin{Bmatrix} \delta \overline{r}(t_o) \\ \delta \overline{v}(t_o) \end{Bmatrix} , \qquad \text{[III.66]}$$

using the state transition matrix, Φ. The differential equation for the primer vector is equivalent in form to the variational equation for the barycenter rotating coordinates; therefore, the solution for the primer vector takes a form equivalent to that of the solution to the variational equation. Specifically, the solution is expressed in terms of the state transition matrix, $\Phi(t, t_o)$, as

$$\begin{Bmatrix} \overline{p}(t) \\ \dot{\overline{p}}(t) \end{Bmatrix} = \begin{bmatrix} \phi_{11}(t, t_o) & \phi_{12}(t, t_o) \\ \phi_{21}(t, t_o) & \phi_{22}(t, t_o) \end{bmatrix} \begin{Bmatrix} \overline{p}(t_o) \\ \dot{\overline{p}}(t_o) \end{Bmatrix} , \qquad \text{[III.67]}$$

where Φ is partitioned into four 3×3 submatrices denoted by the ϕ_{ij}. Equation III.67 can be used to compute the primer vector at any time for which the state transition matrix is available, given initial conditions for the primer vector and its derivative.

For the case of impulsive maneuvers, the necessary conditions require the thrust vector to be aligned with the primer vector. Also, the magnitude of the primer on the optimal transfer at the impulse times must be one. These requirements define the initial and final conditions of the primer vector as

$$\bar{p}(t_o) = \frac{\Delta\bar{v}_o}{|\Delta\bar{v}_o|} , \qquad \text{[III.68]}$$

and

$$\bar{p}(t_f) = \frac{\Delta\bar{v}_f}{|\Delta\bar{v}_f|} , \qquad \text{[III.69]}$$

where the velocity discontinuities represented by $\Delta\bar{v}_o$ and $\Delta\bar{v}_f$ are defined by the velocities at departure (t_o) and arrival (t_f) on the initial and final trajectories and the associated velocities on the transfer. Given $\bar{p}(t_o)$ and $\bar{p}(t_f)$, the value of $\dot{\bar{p}}(t_o)$ is determined by evaluating equation III.67 at the time of the final impulse. Assuming ϕ_{12} is invertible, the resulting expression for $\dot{\bar{p}}(t_o)$ is

$$\dot{\bar{p}}(t_o) = \phi_{12}^{-1}(t_f,t_o)\,[\,\bar{p}(t_f) - \phi_{11}(t_f,t_o)\bar{p}(t_o)\,] . \qquad \text{[III.70]}$$

Thus, all required initial conditions are available for computation of the primer vector and its derivative at any point along the transfer path using equations III.67 through III.70. The characteristics of the primer vector and its derivative can then be compared with the necessary conditions to determine if the associated trajectory is optimal.

4. Adjoint Equation

Hiday developed an additional expression involving the primer vector that is used to derive other results that are employed in this work; that is, the adjoint equation. By subtracting the product of $\delta\bar{r}^T$ and equation III.63 from the product of $\bar{p}^T$ and equation III.65, Hiday constructs an exact differential equation of the form

$$\bar{p}^T\delta\dot{\bar{v}} + \dot{\bar{p}}^T\delta\bar{v} - \ddot{\bar{p}}^T\delta\bar{r} - \dot{\bar{p}}^T\delta\dot{\bar{r}} - \dot{\bar{p}}^T\frac{\partial\bar{g}}{\partial\bar{v}}\delta\bar{r} - \bar{p}^T\frac{d}{dt}\left(\frac{\partial\bar{g}}{\partial\bar{v}}\right)\delta\bar{r} - \bar{p}^T\frac{\partial\bar{g}}{\partial\bar{v}}\delta\dot{\bar{r}} = 0 . \qquad \text{[III.71]}$$

Integrating this expression yields the equation

$$\bar{p}^T\delta\bar{v} - \left[\dot{\bar{p}}^T + \bar{p}^T\frac{\partial\bar{g}}{\partial\bar{v}}\right]\delta\bar{r} = \text{constant} , \qquad \text{[III.72]}$$

called the adjoint equation. This relationship is used by Hiday in the development of the gradient expressions that are required in the numerical optimization problems considered in this work.

C. Improving Non-Optimal Paths

In addition to its role in the evaluation of the optimality of a transfer (through the necessary conditions), the primer vector can also be useful in the improvement of a non-optimal solution. The gradient of the cost function with respect to each of a variety of different variables that characterize the solution can be expressed analytically in terms of the primer vector and its derivative. One set of representative variables is the set of departure and arrival positions on the fixed orbits. A second set of variables describes the timing and location of interior impulses.

1. Time-Free Solutions

The time-free problem is the simultaneous search for the optimal departure location (constrained to the departure trajectory) and the optimal arrival location (constrained to the arrival trajectory) for transfer between two specified trajectories. The initial trajectory, or departure trajectory, is denoted as orbit 'O'. The final trajectory, or arrival trajectory, is denoted as orbit 'F'. (The departure and arrival paths are not required to be closed orbits; however, the terminology of transferring between "orbits" is convenient.) A nominal transfer path is identified by endpoints denoted as 'o' and 'f' on trajectories O and F, respectively. Endpoints identified as 'o_p' and 'f_p' that are also on trajectories O and F denote the terminal points of a perturbed solution. Each of the fixed paths (the departure and arrival orbits) can be parameterized by time; that is, given an initial state, a specified time interval defines a position on the path. Since an exact analytical representation of the path is not available, the parameterization cannot be expressed analytically. If, however, the nominal and perturbed states are sufficiently close, a first-order approximation, that is, a linear expression, in terms of the time between the points may be assumed. The six-dimensional state vector on the departure trajectory associated with point o is $\overline{X}_{o-} = \{\overline{r}_o \;\; \overline{v}_{o-}\}^T$. The state vector on the arrival orbit associated with point f is $\overline{X}_{f+} = \{\overline{r}_f \;\; \overline{v}_{f+}\}^T$. If the time to travel from point o to point o_p along orbit O is dt_o, the position of o_p ($\overline{r}_{o_p}$) can be approximated as $\overline{r}'_{o_p} = \overline{r}_o + \overline{v}_{o-} dt_o$. Similarly, the position of f_p ($\overline{r}_{f_p}$) can be approximated as $\overline{r}'_{f_p} = \overline{r}_f + \overline{v}_{f+} dt_f$, where dt_f is the time to travel from f to f_p along orbit F. With these assumptions, the problem of finding the optimal end positions, defined by six scalar quantities (the elements of $\overline{r}'_{o_p}$ and $\overline{r}'_{f_p}$), is replaced with the problem of finding the optimal times (dt_o and dt_f), that is, two scalars. In addition, although the position coordinates that are selected as optimal must satisfy the constraints that define the trajectory, the times are not constrained. Thus, the time-free problem is developed as an unconstrained minimization problem in two variables. Although first-order assumptions are used to develop the problem,

the actual positions that result from integrating through the time intervals dt_o and dt_f ($\bar{r}_{o_p}$ and $\bar{r}_{f_p}$) are used in this work. In this way, the endpoints remain on the "true" fixed paths although the positions $\bar{r}'_{o_p}$ and $\bar{r}'_{f_p}$ do not. Thus, the first-order approximations are not maintained in the implementation of the result.

The improvement in the cost achieved by transferring between the perturbed endpoints o_p and f_p versus the nominal transfer cost for endpoints o and f was developed by Hiday as a dual coast problem that simultaneously optimizes over some initial and final coast times. The term "coast" applies to the use of a coast arc between a nominal endpoint along a specified orbit and a position along the same orbit that is the terminal position for a perturbed transfer. The objective is to express the change in cost, to first-order, that results from modifying the endpoints as a function of information available from the nominal solution. The departure state on orbit O is defined by the state vector $\overline{X}_{o-} = \{\bar{r}_o \;\; \bar{v}_{o-}\}^T$; the departure state vector on the transfer is given by $\overline{X}_{o+} = \{\bar{r}_o \;\; \bar{v}_{o+}\}^T$; the arrival state vector on the transfer is $\overline{X}_{f-} = \{\bar{r}_f \;\; \bar{v}_{f-}\}^T$; the arrival state vector on orbit F is identified by the state vector $\overline{X}_{f+} = \{\bar{r}_f \;\; \bar{v}_{f+}\}^T$. In terms of the appropriate velocity vectors, the nominal transfer cost is defined by the expression

$$J = |\bar{v}_{o+} - \bar{v}_{o-}| + |\bar{v}_{f+} - \bar{v}_{f-}| \,. \qquad \text{[III.73]}$$

The transfer cost on the perturbed path is defined as

$$J_p = |\bar{v}_{o_p+} - \bar{v}_{o_p-}| + |\bar{v}_{f_p+} - \bar{v}_{f_p-}| \,, \qquad \text{[III.74]}$$

where the subscript 'p' is used to identify a condition on the perturbed path. The variation in cost is, therefore, defined to be

$$\delta J = J_p - J \,. \qquad \text{[III.75]}$$

For the perturbed solution to represent an improvement in cost, δJ must be negative.

An initial coast is considered first where the departure position is altered, but the arrival position is fixed. The velocity vectors on the perturbed path are written in terms of the vectors along the nominal solution and terms that represent the differences in the corresponding velocities. A contemporaneous variation in velocity, denoted as $\delta\bar{v}$, represents the change in velocity at one endpoint of a transfer due to a change in the position at the opposite end. A noncontemporaneous variation, indicated by $d\bar{v}$, represents the change in a velocity vector at one end of a transfer that results from a coast arc applied at that same end. For example, if an initial coast is applied to change the departure position, the velocity at departure on the fixed halo path is expressed as $\bar{v}_{o_p^-} = \bar{v}_{o-} + d\bar{v}_{o-}$; the departure

velocity on the perturbed transfer is written as $\bar{v}_{o_p+} = \bar{v}_{o+} + d\bar{v}_{o+}$. The arrival velocity on the perturbed transfer is defined by $\bar{v}_{f_p-} = \bar{v}_{f-} + \delta\bar{v}_{f-}$, and the arrival velocity on the fixed destination path is unchanged. Using these velocity variations and approximating a difference of the form $|\bar{x} \pm \delta\bar{x}| - |\bar{x}|$ (from a binomial expansion) as $\pm\delta\bar{x}^T\bar{x}/|\bar{x}|$, the variation in cost resulting from an initial coast can be expressed as

$$\delta J_i = \bar{p}_o^T(d\bar{v}_{o+} - d\bar{v}_{o-}) - \bar{p}_f^T\delta\bar{v}_{f-} \ . \qquad \text{[III.76]}$$

In this expression, the primer vectors on the nominal path, $\bar{p}_o$ and $\bar{p}_f$, are introduced to represent velocity ratios such as those in equations III.68 and III.69 that result from approximating differences of the form $|\bar{v}_{o_p+} - \bar{v}_{o_p-}| - |\bar{v}_{o+} - \bar{v}_{o-}|$ using the binomial expansion as $(d\bar{v}_{o+} - d\bar{v}_{o-})^T(\bar{v}_{o+} - \bar{v}_{o-})/|(\bar{v}_{o+} - \bar{v}_{o-})|$. Next, since the nominal transfer is a coast arc, the adjoint equation is applied at times t_{o+} and t_{f-} to produce an expression for the product $\bar{p}_f^T\delta\bar{v}_{f-}$ in terms of information at the initial time. Finally, the contemporaneous variations are expressed in terms of noncontemporaneous variations in velocity and the coast time dt_o to yield an expression for the change in cost in the form

$$\delta J_i = \dot{\bar{p}}_o^T d\bar{r}_o - \dot{\bar{p}}_o^T \bar{v}_{o+} dt_o \ , \qquad \text{[III.77]}$$

called the initial coast transversality condition. Given a linear approximation for the change in the initial position ($d\bar{r}_o = \bar{v}_{o-}dt_o$), equation III.77 is simplified to the form

$$\delta J_i = -\dot{\bar{p}}_o^T(\bar{v}_{o+} - \bar{v}_{o-})dt_o \ . \qquad \text{[III.78]}$$

A similar analysis in the case of a final coast produces the final coast transversality condition, expressed as

$$\delta J_f = -\dot{\bar{p}}_f^T d\bar{r}_f + \dot{\bar{p}}_f^T \bar{v}_{f-} dt_f \ . \qquad \text{[III.79]}$$

This can also be written in the form

$$\delta J_f = -\dot{\bar{p}}_f^T(\bar{v}_{f+} - \bar{v}_{f-})dt_f \ , \qquad \text{[III.80]}$$

using the linear approximation $d\bar{r}_f = \bar{v}_{f+}dt_f$. Then, if initial and final coasts are applied simultaneously, the variation in cost represented by equation III.75 is equivalent to the sum

$$\delta J = \delta J_i + \delta J_f \ , \qquad \text{[III.81]}$$

which can also be written in the form

$$\delta J = -\dot{p}_o \Delta v_o dt_o - \dot{p}_f \Delta v_f dt_f \ . \qquad \text{[III.82]}$$

In this expression, scalar derivatives of the primer are evaluated as

$$\dot{p} = \dot{\bar{p}}^T \frac{\bar{p}}{p} . \qquad \text{[III.83]}$$

Equation III.82 describes the change in the cost (to first-order) that results from changes in the variables of interest (dt_o and dt_f). Expressed in a vector form, in which the gradient expression that is required for a numerical optimization technique is identified, equation III.82 is rewritten as

$$\delta J = \nabla J \cdot \overline{dt} , \qquad \text{[III.84]}$$

where

$$\nabla J = \begin{bmatrix} -\dot{p}_o \Delta v_o \\ -\dot{p}_f \Delta v_f \end{bmatrix} , \qquad \text{[III.85]}$$

and

$$\overline{dt} = \begin{Bmatrix} dt_o \\ dt_f \end{Bmatrix} . \qquad \text{[III.86]}$$

If the slopes of the primer magnitudes ($\dot{p}_o$ and $\dot{p}_f$) are not zero at the initial and final impulse locations, the gradient in equation III.85 is used in a gradient-based optimization scheme to search for a trajectory that satisfies the zero slope conditions. Thus, on the optimal time-free path, the slopes of the primer must be zero at both endpoints.

If a transfer is not optimal, the sense (+ of −) of the primer derivative at each endpoint indicates the appropriate direction to shift the respective endpoint to reduce the cost (within the limitations of the first-order assumptions used to develop the gradient expression). For example, consider a nominal primer history in which $\dot{p}_o > 0$. To reduce the cost, δJ must be negative; therefore, the transfer can be improved by choosing $dt_o > 0$ so that $\delta J < 0$ (see equation III.82). A positive value for dt_o represents an initial coast on the departure trajectory (a delayed departure). Thus, if $\dot{p}_o > 0$, an initial coast is suggested. Similarly, if $\dot{p}_o$ is negative, dt_o should also be selected to be negative, consistent with an early departure, to achieve a reduction in the cost. Next, if $\dot{p}_f > 0$, dt_f should be positive indicating a final coast along the final trajectory (a late arrival) to make δJ negative. Also, if $\dot{p}_f < 0$, an early arrival, indicated by negative dt_f, should be applied to reduce the cost. These conditions are incorporated into the optimization algorithm to predict appropriate search directions that are represented by the coast times on the fixed orbits. Then, numerical integration (forward or backward in time) through the intervals dt_o and dt_f along the fixed trajectories is used to accurately identify the improved endpoints suggested by the numerical optimization routine.

2. Additional Impulse Solutions

In addition to modifying the endpoints, a trajectory can be improved in some cases by including additional impulses that redistribute the total cost more effectively. If the magnitude of the primer vector associated with a transfer exceeds one anywhere along the path, Hiday demonstrates through a first-order analysis that an additional impulse will reduce the cost. Thus, the location and time at which to apply an additional maneuver represents a second set of variables that characterize an optimal path. Given a nominal transfer to which an additional impulse is to be added, the primer vector associated with the nominal solution is used to predict the appropriate additional impulse; however, the resulting transfer may not satisfy all of the conditions for optimality for an interior maneuver. Thus, the location and time at which the impulse is applied is optimized using a gradient-based numerical optimization routine. The result is a transfer in which the derivative of the primer vector is continuous across the interior impulse and equal to zero at the impulse time, as required by the necessary conditions for optimality of an interior impulse.

a. Nominal Three-Impulse Transfer Construction

Obtaining an optimal three-impulse transfer begins with the construction of a nominal three-impulse solution. A two-impulse transfer is assumed to exist that connects points o and f along trajectories O and F, respectively. Within this discussion, the two-impulse path is denoted as the reference solution to distinguish it from the three-impulse path that is labeled the nominal solution, consistent with its use in subsequent optimization procedures. The magnitude of the primer vector is assumed to be greater than one at some time along the two-impulse transfer path. The additional impulse is added when the primer reaches its maximum (and, therefore, the derivative is zero), defined by the time t_m.

Since the reference solution (the two-impulse path) is continuous in position and velocity, it can be computed as a single segment with the initial condition $\overline{X}_{o+} = \{\bar{r}_o \;\; \bar{v}_o\}^T$; however, intermediate conditions are required for further computations. Therefore, it is useful to define the trajectory in terms of two distinct segments: one segment contains points o and m, denoted by position vectors $\bar{r}_o$ and $\bar{r}_m$; the second segment contains points m and f, denoted by position vectors $\bar{r}_m$ and $\bar{r}_f$, where the assumption of position continuity at the patch point is implicit. The state on the reference transfer at the point where the primer reaches its maximum value is denoted as $\overline{X}_m = \{\bar{r}_m \;\; \bar{v}_m\}^T$. The primer vector on the reference path at t_m is $\bar{p}_m$.

To reduce the cost, an additional impulse is included at time t_m in the direction of the primer vector associated with the reference two-impulse path (consistent with the necessary

condition that the thrust vector is aligned with the primer vector); however, since the two-impulse transfer that includes positions $\bar{r}_o$, $\bar{r}_m$, and $\bar{r}_f$ does not require an interior impulse, the interior position for a three-impulse transfer, that includes positions $\bar{r}_o$ and $\bar{r}_f$ and an interior impulse, must differ from $\bar{r}_m$. The perturbed interior position is given by $\tilde{\bar{r}}_m = \bar{r}_m + \delta\bar{r}_m$, where $\delta\bar{r}_m$ represents the change in the position. Thus, the objective is to determine the best position for the application of the impulse and the magnitude of the maneuver. The direction of the impulse is defined to be parallel to $\bar{p}_m$. To determine the best magnitude and the location (relative to the nominal point) at which to apply the maneuver, Hiday considers the difference between the costs associated with the two-impulse path and a perturbed path that includes three-impulses. Since the interior position along the perturbed path ($\tilde{\bar{r}}_m$) differs from the nominal position ($\bar{r}_m$), the velocities at the endpoints of the reference solution must change to produce a path that includes the modified interior position. In the following discussion, the tilde is used to indicate a state on the three-impulse transfer that differs from a corresponding state on the two-impulse path. For example, $\bar{r}_m$ denotes the position at t_m along the two-impulse path; $\tilde{\bar{r}}_m$ indicates the position at t_m along the three-impulse transfer. Similarly, $\tilde{\bar{v}}_{m-}$, the velocity immediately before the interior impulse on the three-impulse path, is defined as $\tilde{\bar{v}}_{m-} = \bar{v}_{m-} + \delta\bar{v}_{m-}$, where $\delta\bar{v}_m^-$ represents a perturbation relative to the reference velocity at t_m.

The reference two-impulse cost is given by

$$J = |\Delta\bar{v}_o| + |\Delta\bar{v}_f| , \qquad \text{[III.87]}$$

where $\Delta\bar{v}_o = \bar{v}_{o+} - \bar{v}_{o-}$ and $\Delta\bar{v}_f = \bar{v}_{f+} - \bar{v}_{f-}$ are expressed using the previous definitions for the departure and arrival velocity vectors. The cost associated with a perturbed path that includes an impulse at t_m is expressed as

$$J_p = |\Delta\bar{v}_o + \delta\bar{v}_o| + |\tilde{\bar{v}}_{m+} - \tilde{\bar{v}}_{m-}| + |\Delta\bar{v}_f + \delta\bar{v}_f| . \qquad \text{[III.88]}$$

The variation in cost, defined as $\delta J = J_p - J$, can be written as

$$\delta J = \bar{p}_o^T\delta\bar{v}_o + |\delta\bar{v}_{m+} - \delta\bar{v}_{m-}| - \bar{p}_f^T\delta\bar{v}_f , \qquad \text{[III.89]}$$

using binomial expansions similar to those employed in the development of the time-free problem and noting that $\tilde{\bar{v}}_{m+} - \tilde{\bar{v}}_{m-} = \delta\bar{v}_{m+} - \delta\bar{v}_{m-}$ since the reference path contains no impulse at m. Next, Hiday employs continuity of $\bar{p}_m$ and $\dot{\bar{p}}_m$ on the reference path, continuous primary motion, and position continuity at the interior impulse time, in conjunction with the adjoint equation, applied first at times t_o and t_{m-} and next at times t_{m+} and t_f, to produce the expression

$$\bar{p}_o^T\delta\bar{v}_o - \bar{p}_f^T\delta\bar{v}_f = \bar{p}_m^T(\delta\bar{v}_{m-} - \delta\bar{v}_{m+}) . \qquad \text{[III.90]}$$

Consistent with the requirement that the impulse is aligned with the primer, the interior impulse is defined as

$$\delta\bar{v}_{m+} - \Delta\bar{v}_{m-} = \Delta\tilde{v}_m \frac{\bar{p}_m}{p_m} , \qquad \text{[III.91]}$$

where $\Delta\tilde{v}_m$ is the magnitude of the interior impulse ($\Delta\tilde{v}_m > 0$). The variation in cost is then written as

$$\delta J = \Delta\tilde{v}_m \left(1 - \bar{p}_m^T \frac{\bar{p}_m}{p_m}\right) . \qquad \text{[III.92]}$$

This equation supports the requirement that p_m must be greater than one for the three-impulse path to have a lower cost than the reference trajectory ($\delta J < 0$).

An alternate expression for δJ is obtained by considering the variations at m as functions of the changes at o and f through the state transition matrix relationships as represented in equation III.66. Changes in the initial velocity on the reference transfer ($\delta\bar{v}_o$), due to variations in the interior position and velocity states on the reference path (immediately before t_m), are related to $\delta\bar{r}_m$ and $\delta\bar{v}_{m-}$ through the state transition matrix $\Phi(t_m, t_o)$ computed for the first segment. On the second segment, variations in the reference position ($\delta\bar{r}_m$) and velocity ($\delta\bar{v}_{m+}$) after t_m are related to $\delta\bar{v}_f$ through the state transition matrix $\Phi(t_m, t_f)$. In this way, the interior impulse is expressed as

$$\delta\bar{v}_{m+} - \delta\bar{v}_{m-} = D\delta\bar{r}_m , \qquad \text{[III.93]}$$

where

$$D = \phi_{22}(t_m, t_f)\phi_{12}^{-1}(t_m, t_f) - \phi_{22}(t_m, t_o)\phi_{12}^{-1}(t_m, t_o) . \qquad \text{[III.94]}$$

Equating the expression for the impulse in equation III.93 with equation III.91 yields an expression for the change in the interior position as

$$\delta\bar{r}_m = \Delta\tilde{v}_m D^{-1} \frac{\bar{p}_m}{p_m} . \qquad \text{[III.95]}$$

Then, replacing the variable $\delta\bar{r}_m$ in the relationships for $\delta\bar{v}_o$ and $\delta\bar{v}_f$ developed in terms of the appropriate state transition matrices and writing the magnitudes as the square root of the sum of the squares, equation III.88 is written in the form

$$\begin{aligned} J_p = & \sqrt{\Delta\bar{v}_o^T\Delta\bar{v}_o + 2\Delta\tilde{v}_m\bar{\alpha}^T\Delta\bar{v}_o + \Delta\tilde{v}_m^2\bar{\alpha}^T\bar{\alpha}} \\ & + \sqrt{\Delta\bar{v}_f^T\Delta\bar{v}_f + 2\Delta\tilde{v}_m\bar{\beta}^T\Delta\bar{v}_f + \Delta\tilde{v}_m^2\bar{\beta}^T\bar{\beta}} + \Delta\tilde{v}_m , \end{aligned} \qquad \text{[III.96]}$$

where

$$\bar{\alpha} = \phi_{12}^{-1}(t_m, t_o)D^{-1}\frac{\bar{p}_m}{p_m} , \qquad \text{[III.97]}$$

$$\bar{\beta} = \phi_{12}{}^{-1}(t_m, t_f)D^{-1}\frac{\bar{p}_m}{p_m} . \qquad \text{[III.98]}$$

The terms $\phi_{ij}(t_m, t_o)$ represent 3×3 submatrices of $\Phi(t_m, t_o)$, and the terms $\phi_{ij}(t_m, t_f)$ represent 3×3 submatrices of $\Phi(t_m, t_f)$, both computed for the reference two-impulse path. (The matrix $\Phi(t_m, t_f)$ is computed as the inverse of $\Phi(t_f, t_m)$; and, $\Phi(t_f, t_m)$ results from integrating forward in time from t_m to t_f on the reference path with initial condition $\Phi(t_m, t_m) = I_6$.) Note that all quantities in equations III.96 through III.98 are evaluated on the reference trajectory with the exception of $\Delta\tilde{v}_m$. This variable is computed by iteratively solving for the value of $\Delta\tilde{v}_m$ that minimizes J_p. Then, the interior impulse is defined to be

$$\Delta\tilde{\bar{v}}_m = \Delta\tilde{v}_m \frac{\bar{p}_m}{p_m} . \qquad \text{[III.99]}$$

One additional issue must be addressed with respect to the construction of the nominal three-impulse path given the goal of maintaining the fixed original and destination trajectories. The first-order analysis suggests that the three-impulse solution should contain positions $\bar{r}_o$, $\bar{r}_m + \delta\bar{r}_m$, and $\bar{r}_f$ with an impulse specified as $\Delta\tilde{\bar{v}}_m$ applied at time t_m. However, as discussed in the development of the multi-segment differential correctors, this represents an overconstrained problem. The departure and arrival positions, $\bar{r}_o$ and $\bar{r}_f$, must be included to constrain the endpoints to the selected orbits. Of the remaining options, only the interior position *or* the interior impulse may be specified. For transfers between halo orbits, a solution that constraints the interior impulse to the computed value, $\Delta\tilde{\bar{v}}_m$, generally yields a lower cost solution than a trajectory that contains the perturbed interior position, $\bar{r}_m + \delta\bar{r}_m$. Thus, the corrector that fixes the interior $\Delta\overline{V}$ is used to construct a path that contains positions $\bar{r}_o$ and $\bar{r}_f$ at times t_o and t_f with an interior impulse equal to $\Delta\tilde{\bar{v}}_m$ at time t_m, where the position $\tilde{\bar{r}}_m = \bar{r}_m + \delta\bar{r}_m$ is used only as the initial guess for the determination of the interior position. The solution that results from the differential corrections process is the nominal three-impulse transfer. It is used as the first guess in a numerical optimization routine that identifies the optimal location and the time at which to apply an interior maneuver.

b. Three-Impulse Transfer Optimization

On the nominal three-impulse path, continuity of the primer vector is guaranteed by the definitions of the primer vectors at the interior point ($\tilde{\bar{p}}_{m-}$ and $\tilde{\bar{p}}_{m+}$) in terms of the interior impulse; however, the derivative of the primer vector is not guaranteed to be continuous ($\dot{\tilde{\bar{p}}}_{m-} \neq \dot{\tilde{\bar{p}}}_{m+}$). Also, the Hamiltonian may not be continuous across the impulse. Thus, although the nominal three-impulse transfer generally has a lower cost than the reference two-impulse solution, it may not be an optimal solution. To achieve continuity in the desired quantities, the location and time of the interior impulse are perturbed to search for a trajectory that satisfies these requirements.

As developed by Hiday, the improvement achieved by shifting the interior point from $\tilde{\bar{r}}_m$ at time t_m to position $\tilde{\bar{r}}_{m'}$ at time $t_{m'}$ is examined by defining the perturbed path to be the result of initial and final coasts applied to the beginning of the second segment and to the end of the first segment, respectively. (Note that the interior position on the nominal path may be changed from $\tilde{\bar{r}}_m$ in the differential corrections process; however, the vector $\tilde{\bar{r}}_m$ is still used here to refer to the location at t_m on the nominal path.) If the final coast transversality condition (equation III.79) is evaluated at t_{m-} and the initial coast transversality condition (equation III.77) is evaluated at t_{m+}, the variation in cost due to the change in the interior position and time can be expressed in the form

$$\delta J = \left(\dot{\tilde{\bar{p}}}_{m+}^T - \dot{\tilde{\bar{p}}}_{m-}^T\right) d\bar{r}_m + \left(\dot{\tilde{\bar{p}}}_{m-}^T \tilde{\bar{v}}_{m-} - \dot{\tilde{\bar{p}}}_{m+}^T \tilde{\bar{v}}_{m+}\right) dt_m \ . \qquad \text{[III.100]}$$

The first term in this expression is a function of the discontinuity in the derivative of the primer vector. Similarly, the second term in this equation can be expressed in terms of the discontinuity in the Hamiltonian that exists on a non-optimal trajectory. On a coast arc, T=0 in equation III.52; therefore, using continuity in the motion of the primaries and evaluating the Hamiltonian immediately before and immediately after the impulse, the discontinuity in H is written

$$\tilde{H}_{m+} - \tilde{H}_{m-} = \dot{\tilde{\bar{p}}}_{m-}^T \tilde{\bar{v}}_{m-} - \dot{\tilde{\bar{p}}}_{m+}^T \tilde{\bar{v}}_{m+} \ . \qquad \text{[III.101]}$$

Then, the change in the cost can be expressed as

$$\delta J = \left(\dot{\tilde{\bar{p}}}_{m+}^T - \dot{\tilde{\bar{p}}}_{m-}^T\right) d\bar{r}_m + \left(\tilde{H}_{m+} - \tilde{H}_{m-}\right) dt_m \ , \qquad \text{[III.102]}$$

where the derivatives of the primer vector and the Hamiltonian are evaluated on the nominal three-impulse path. The quantity $d\bar{r}_m$ represents the change in the position of the interior position as

$$\tilde{\bar{r}}_{m'} = \tilde{\bar{r}}_m + d\bar{r}_m \ . \qquad \text{[III.103]}$$

Similarly, dt_m represents the change in time as

$$t_{m'} = t_m + dt_m \ . \qquad \text{[III.104]}$$

Given the form of δJ, the gradient of the cost function with respect to the location and time of the additional impulse is written as

$$\nabla J = \begin{Bmatrix} \dot{\tilde{\bar{p}}}_{m+} - \dot{\tilde{\bar{p}}}_{m-} \\ \tilde{H}_{m+} - \tilde{H}_{m-} \end{Bmatrix} . \qquad \text{[III.105]}$$

Thus, the requirements that both the derivative of the primer vector and the Hamiltonian must be continuous across an impulse are consistent with the zero gradient condition that

indicates an optimal solution. The Hamiltonian can be continuous only if the derivative of the magnitude of the primer is zero; therefore, in addition to being continuous, the derivative of the primer must have a value of zero at the impulse time.

This gradient is used in a numerical optimization procedure to determine the optimal time and location at which to apply an interior impulse. At each iteration in the optimization procedure, a candidate position and time for the optimal impulse is selected. Then, a transfer is constructed that contains the fixed endpoints and the selected interior position with integration times that are determined from the selected interior time. This problem satisfies the assumptions employed in the derivation of the differential corrector that fixes the interior position with a specified interior time; therefore, additional constraints required to impose a specified $\Delta\overline{V}$ cannot be incorporated under the current structure. The interior $\Delta\overline{V}$, approximated in equation III.99, is only used in the computation of the nominal solution and is abandoned in the optimization of the transfer. Thus, using the gradient defined in equation III.105, a numerical optimization routine is employed to identify the optimal interior position and time. The differential corrector that fixes the interior position is used to evaluate the cost function at each iteration. Given the optimal position and time at which to apply an interior impulse, the optimal interior impulse is determined as the change in velocity required at the interior point to patch the two segments together.

D. Optimization Algorithm

The gradients derived for incorporating coast arcs and interior impulses are used in a numerical optimization routine to compute optimal transfers between fixed orbits. To illustrate the optimization algorithm developed in this study, the computation of an optimal impulsive transfer between two northern L_1 halo orbits is discussed below. Although periodic orbits are used in this example, the algorithm does not require periodicity nor any other characteristic that is unique to a halo orbit. The goal of this example is a transfer path that connects any point along the departure orbit to any point along the arrival orbit and satisfies all of the requirements for optimality. In terms of the primer vector associated with the optimal transfer, the magnitude of the primer vector must be equal to one at all impulse times and less than one elsewhere, and the slope of the primer must be zero at all impulse times.

In the circular restricted problem, any path is completely defined by initial position and velocity vectors. In the elliptic problem, however, the location of the primaries at the initial time must also be defined. The time of periapsis passage in the primary orbit is one convenient representation of this information. Thus, while departure and arrival

paths in the circular problem can be defined without regard to time of periapsis, their definition in an elliptic system is time dependent. This introduces an additional constraint on transfers computed in the elliptic problem: the solution must connect two selected points with departure and arrival times that coincide with the appropriate periapsis times of the primaries. This additional requirement yields a unique solution to the problem of connecting two fixed points. For this reason, optimal transfers in the circular problem are used to select times of periapsis passage for departure and arrival orbits in the elliptic problem in the absence of mission requirements that define these times. This example considers transfers in the circular problem; extension to the elliptic problem is discussed in a later chapter.

1. Nominal Two-Impulse Path

The procedure begins with the construction of a nominal two-impulse path that connects selected endpoints along the two halo orbits. Given the nominal solution, the optimal endpoints corresponding to a two-impulse transfer are computed as the solution to the time-free problem, where optimality is indicated by a primer history that includes zero slopes at the endpoints. Next, a nominal three-impulse transfer is constructed that connects the endpoints determined for the optimal two-impulse solution. Then, the endpoints for the three-impulse solution and the timing and location of the interior impulse are optimized simultaneously to yield the optimal three-impulse transfer. Finally, any additional impulses that may be required are added one at a time. As each maneuver is added, the timing and location of the additional impulse are optimized simultaneously with the timing and location of all other interior impulses and the endpoint locations. The terminology "optimal two-impulse transfer" denotes the best solution that can be achieved with two-impulses, although a transfer with a lower cost may be possible if additional impulses are included. In general, the phrase "optimal n-impulse transfer" denotes the best solution that can be achieved with n impulses. A solution that cannot be improved with additional impulses or coast arcs is identified as an "optimal impulsive transfer." (The necessary conditions that are employed to test the optimality of each solution only indicate a local optimum. Thus, although a transfer may be denoted as an optimal impulsive solution, the possible existence of other solutions with lower costs is not excluded.)

The target orbits used in this example are halo orbits computed in the Sun-Earth/Moon circular restricted three-body problem. The orbits are plotted in three, two-dimensional projections, each with origin at L_1 as shown in Figure III.1. The departure orbit, denoted as orbit O, has a z-amplitude of 110,000 km and a period of 177.9 days. The arrival orbit, denoted as orbit F, has a z-amplitude of 600,000 km and a period of 177.1 days. The transfer from orbit O to orbit F is identified as a superior transfer since it transfers from

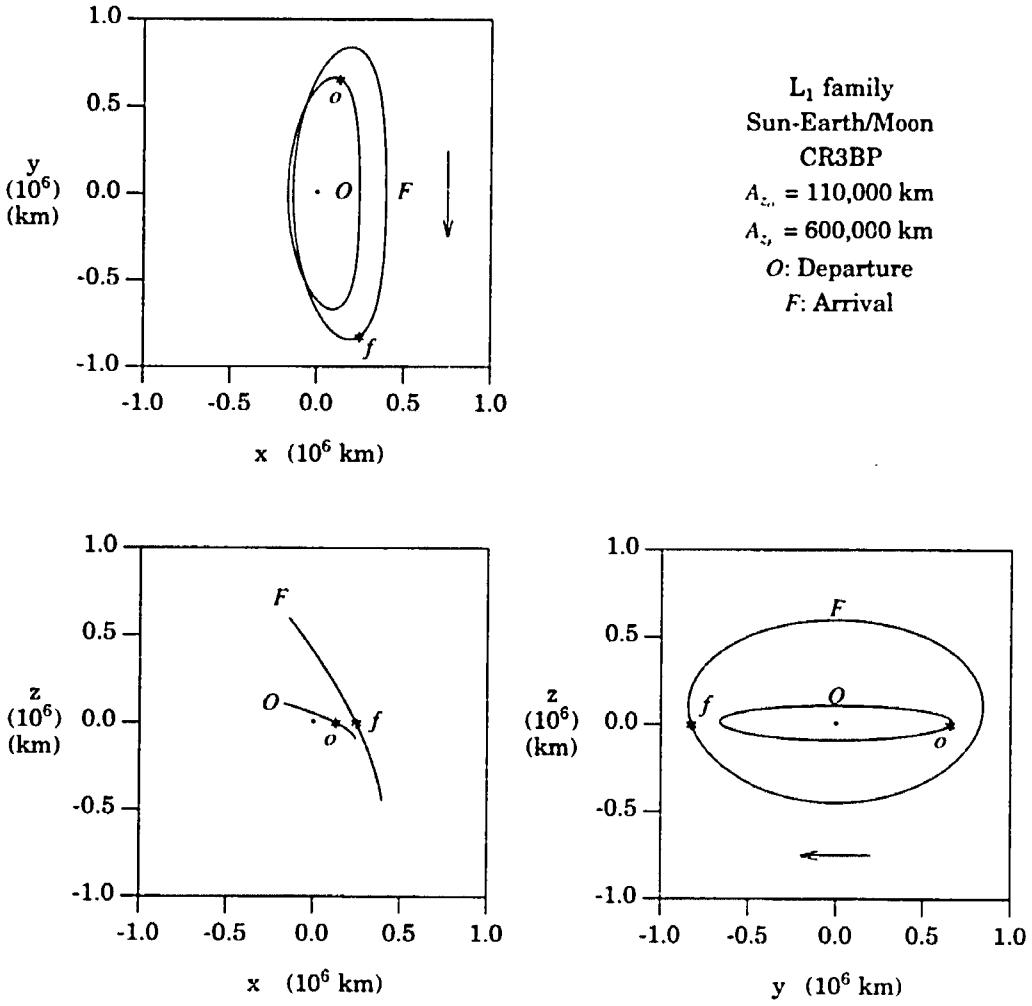

Figure III.1 Departure and Arrival Orbits.

the halo of smaller amplitude to the orbit of larger amplitude. Transfers from the orbit of larger amplitude to one with a smaller amplitude are designated as inferior transfers. For this example, the nominal departure and arrival points are selected at locations where z is zero on the two orbits. (Recall, y=y, and z=z.) The selected departure point is denoted 'o'. The selected arrival point is denoted 'f'. Thus, given two fixed points, o and f, a path that connects these points, and is continuous in both position and velocity, is computed using the time-fixed differential corrector developed for the single segment targeting problem.

The velocity on orbit O at the departure point is used as the initial guess for the velocity on the transfer at departure; therefore, the transfer path is initially assumed to be the departure halo orbit (the "initial guess"). Although the departure and arrival points are separated by approximately one-half revolution in the $y-z$ projection, assuming the time of flight on the transfer to be one-half the period of either orbit O or orbit F generally does not yield convergence with these endpoints, given the initial guess for the velocity that is suggested above. A shorter time, approximately eighty-five percent of the half-period, is usually required to achieve a solution that includes the selected endpoints with a fixed transfer time. Given these starting values for the departure velocity and the transfer time, the differential corrector is then used to compute the actual departure velocity along a path that is continuous in position and velocity and includes points o and f, that is, the nominal two-impulse transfer. The nominal transfer cost is then computed as the sum of the two impulses required at the endpoints to match the velocities on the fixed paths.

The resulting nominal transfer path and selected segments of the departure and arrival halo orbits are presented in Figure III.2, where stars indicate the endpoints of the transfer. Note that, although approximately one-half revolution along each halo is included in the figure to indicate the orientation of the transfer relative to the fixed paths, only one point of each trajectory is used to compute the transfer. By integrating the transfer apart from the halo orbits, the duration of the numerical integration process is limited to the length of the transfer. Thus, relatively short integration times are an advantage of the point-to-point solution approach. The transfer time from point o to point f is the selected (fixed) time of 75.6 days. The required initial ΔV is 208.8 m/s; the final ΔV is 96.4 m/s; therefore, the total cost for the transfer is 305.2 m/s.

Before coast arcs are employed to reduce the cost, modifying the transfer time of flight is considered. The transfer time of flight is selected arbitrarily as any time for which convergence can be achieved; however, since the halo orbits are defined without regard to the time of periapsis passage in the primary orbit, any transfer time that yields a solution may be acceptable. Furthermore, different times of flight may yield lower cost transfers between the same nominal endpoints. Since an analytic expression for the optimal transfer

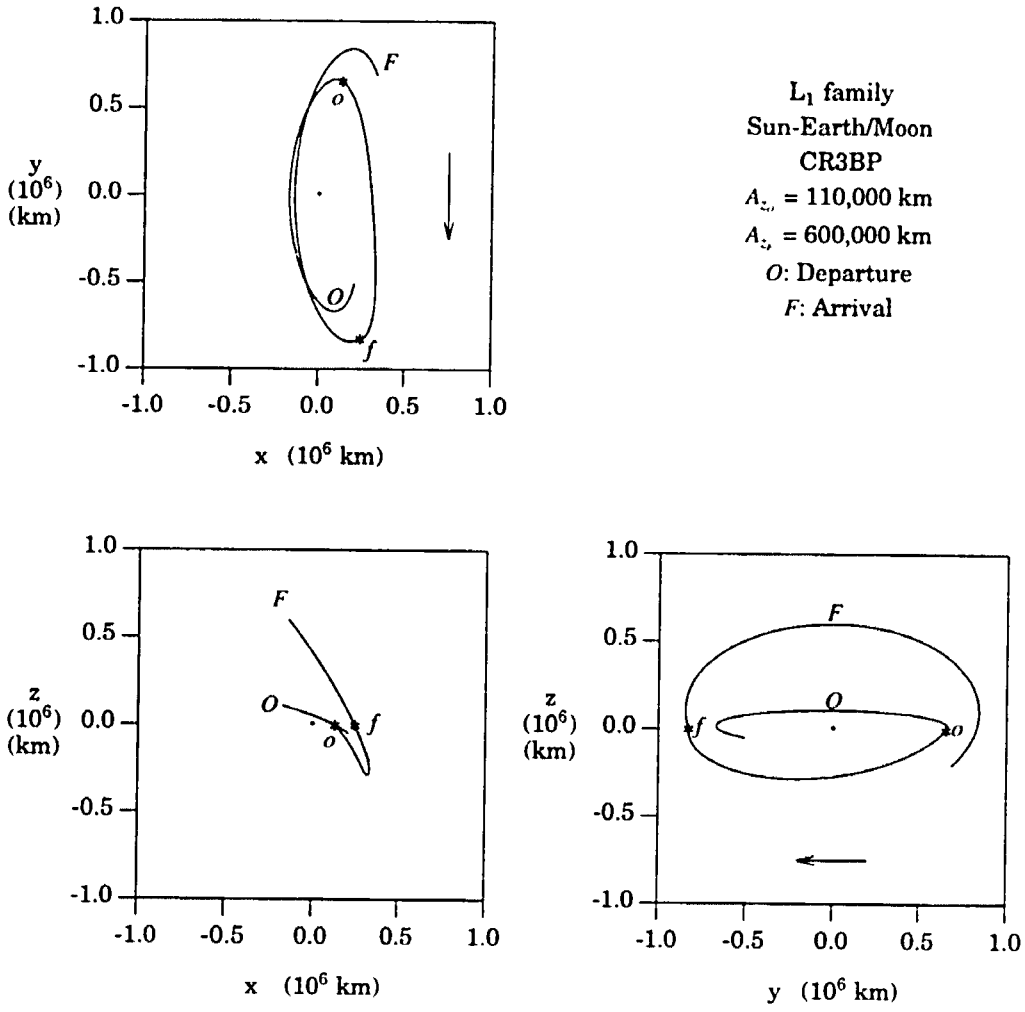

Figure III.2 Example: Nominal Two-Impulse Transfer.

time for fixed endpoints is not available, an intermediate optimization step is used in the circular problem to compute the optimal transfer times. This defines a new optimization problem. The search for the optimal path between the current endpoints with the current number of impulses is called the "variable-time optimization problem." Although several variables may be used to define the new problem, the transfer time is one of the most convenient parameters with which to consider this intermediate one parameter optimization problem. The objective of the problem is to compute the transfer time that yields the lowest ΔV solution between the current set of endpoints. The time-fixed differential corrector is used in conjunction with a polynomial interpolation optimization routine to evaluate the desired time of flight. The y – z projection of the "improved" nominal transfer is presented in Figure III.3 where points o and f denote the same nominal endpoints as those shown in Figure III.2 (only the transfer time is changed). In this case, the improved transfer time, denoted t_f, is equal to 74.8 days. The cost associated with the improved nominal transfer is 256.1 m/s with a 132.1 m/s impulse at departure and a 124.0 m/s impulse at arrival. Thus, changing only the transfer time reduces the cost by 49.1 m/s. For the remainder of the discussion, in the circular problem, the label "nominal solution" actually refers to the improved nominal solution unless otherwise stated.

The free variable represented by the variable-time optimization problem is evident in the development of the necessary conditions for optimality in the definition of the transversality condition. If the final time is not fixed, an additional transversality condition exists that requires the Hamiltonian at the final time to be zero on the optimal path. Solving the variable-time optimization problem at each iteration of the time-free problem yields this requirement without explicitly considering the nonlinear constraint represented by the Hamiltonian expression.

2. Optimal Two-Impulse Path

Given the nominal solution, the departure and arrival positions are modified to search for the optimal locations (the time-free optimization problem). Since improvements in the transfer cost due to coast arcs are functions of the slope of the primer vector magnitude at the endpoints, a plot of the magnitude of the primer is useful for evaluating the solution. The magnitude of the primer vector that is associated with the (improved) nominal transfer is included in Figure III.3. The slopes at the endpoints are not zero; therefore, this is not an optimal time-free solution. Using the primer vector to evaluate the gradient expression in equation III.85, candidate times, represented as dt_o and dt_f, are selected. New endpoints are identified by integrating the nonlinear equations of motion using the state vectors on the fixed paths that correspond to the endpoints of the transfer path as initial conditions

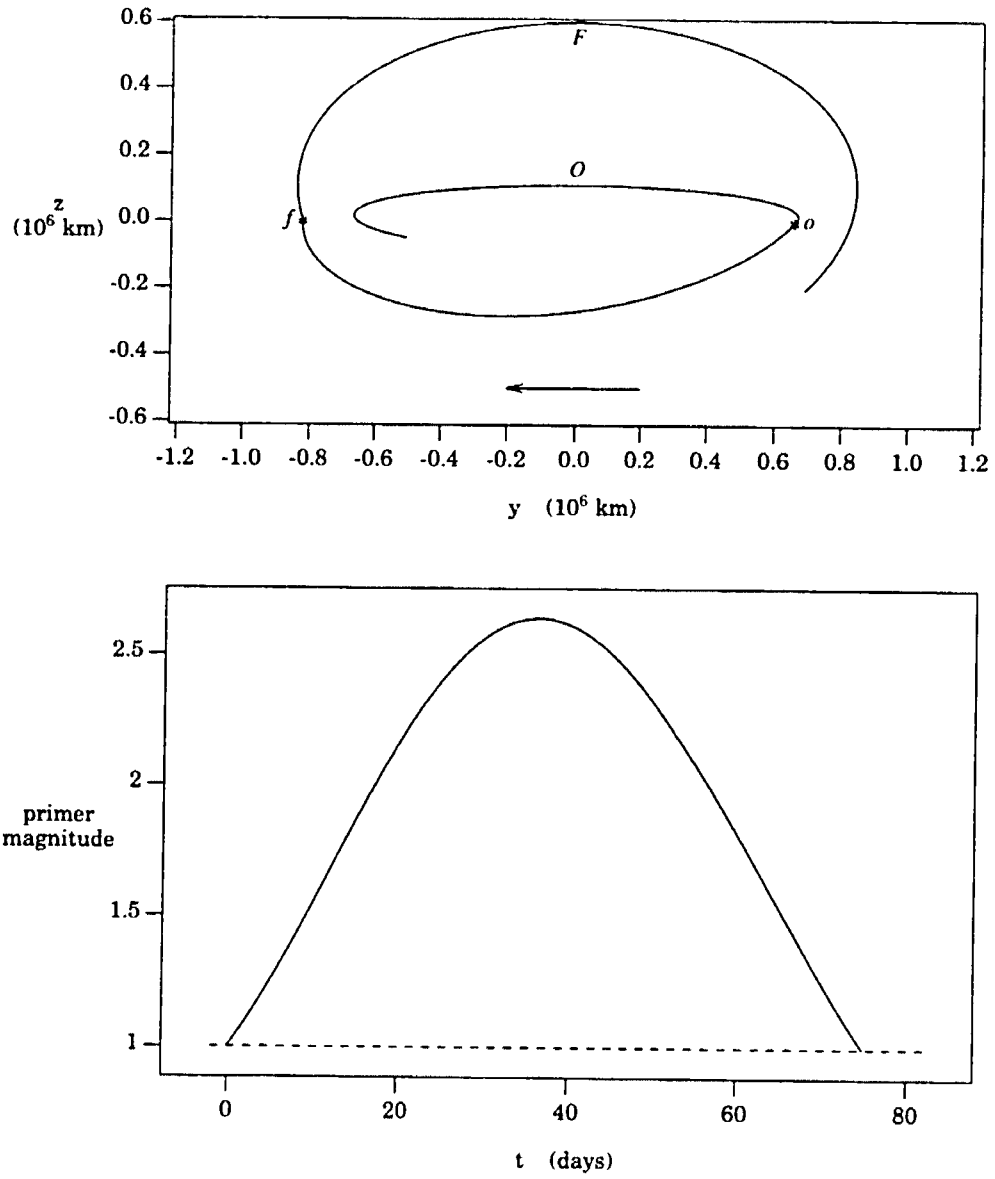

Figure III.3 Example: Improved Nominal Transfer and Primer History.

for the integrations. By integrating the nonlinear equations to identify the new points, as opposed to using a first-order approximation for the positions, the endpoints remain on the fixed paths. The time of flight associated with the new solution is, however, selected according to the linear relationship

$$t'_{f_p} = t_f - dt_o + dt_f \,. \qquad \text{[III.106]}$$

In the elliptic problem, this relationship guarantees that the periapsis times that correspond to the new departure and arrival points are consistent with the definition of the fixed paths. In the circular problem, however, since the time of periapsis passage is not a constraint, the time t'_{f_p} defined by this relationship is used only as the first guess for the optimal transfer time for the perturbed endpoints. Then, the variable-time optimization problem is solved for the optimal time corresponding to the perturbed path.

Using a numerical optimization routine to compute the optimal values of dt_o and dt_f, a transfer satisfying the necessary conditions for an optimal time-free problem is computed with $dt_o = 6.2$ days and $dt_f = -7.7$ days. The y − z projection of the new solution and the associated primer history are shown in Figure III.4. The primer slopes corresponding to the beginning and end of the transfer are zero (to within acceptable tolerances) indicating optimal endpoints. (Note that the time t=0 is defined to be the departure time on the transfer and does not represent the nominal departure time.) The initial ΔV is equal to 116.3 m/s; the final impulse magnitude is 106.6 m/s; therefore, the optimal two-impulse cost is 222.9 m/s. The optimal transfer time for the two-impulse case is 60.2 days. This time is not equal to the sum $t_f - dt_o + dt_f$ because the solutions to the variable-time optimization problems have been incorporated.

An optimization problem can be defined that eliminates the intermediate variable-time optimization procedure, where the problem is defined in terms of three variables, that is, dt_o, dt_f, and the transfer time of flight. This may reduce the total number of candidate solutions that are required by eliminating the need to solve the intermediate optimization problem at each iteration; however, as it was developed in this study, the use of a numerically computed gradient for the time of flight was not compatible with the use of an analytical gradient expression for the other two variables. Although the analytical gradient is derived using a first-order analysis and is, therefore, an approximation of the true gradient, the error in the numerically computed gradient is substantially larger. The elements of the gradient vector that are computed numerically generally suggest that large changes are required in the corresponding variables relative to the magnitude of the changes that are indicated for the variables associated with gradients that are computed analytically. This approach generally failed to converge to an optimal set of variables. Thus, the algorithm

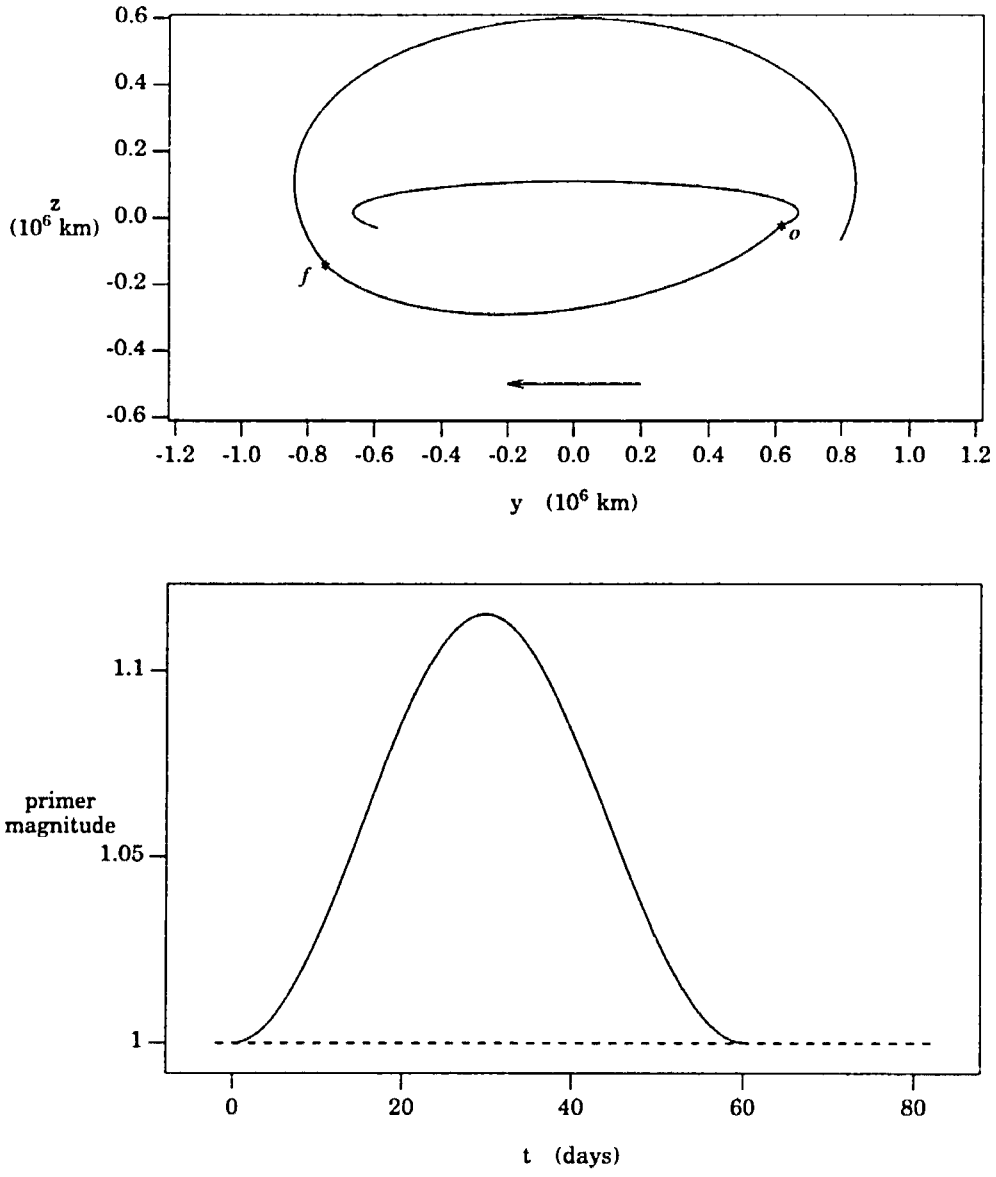

Figure III.4 Example: Optimal Two-Impulse Transfer and Primer History.

that solves the variable-time problem at each iteration is employed although it does incur a significant number of computations. A second alternative approach that eliminates the intermediate problem would define a constrained optimization problem in which the constraint on the Hamiltonian at the final time that results from the additional transversality condition is explicitly required. This method was not pursued in this work since analytical expressions for the gradient of the constraint with respect to the coast times are not available. The implementation of such a constrained problem would, therefore, again require the simultaneous incorporation of analytical and numerical gradients, which was shown to be unsuccessful in previous applications.

3. Additional Impulse Solutions

Although the primer history for the optimal two-impulse transfer indicates that the solution achieves the requirement for optimal endpoints (as derived for an impulsive transfer), the magnitude of the primer is greater than one during the transfer. Therefore, the cost can be further reduced by including an additional impulse at the time when the primer reaches its maximum ($\dot{p}$=0). In this example, the primer attains a maximum value of approximately 1.12 at a time of 30.3 days past the departure time (t = 0). Thus, to define the nominal three-impulse path, the magnitude of the additional impulse is determined by minimizing J_p as defined in equation III.96. Then, as discussed previously, a three-impulse path is constructed that connects the endpoints of the optimal two-impulse path with a fixed interior $\Delta\overline{V}$ applied at the time when the primer reaches its maximum on the two-impulse path. The nominal three-impulse path for this example is presented in Figure III.5. Stars indicate locations of the endpoints and interior impulses. The primer history computed for the nominal solution is also presented in the figure. The initial ΔV on the transfer is 112.5 m/s; the final ΔV is 103.6 m/s; and the interior ΔV equals the specified magnitude of 6.5 m/s. The 222.6 m/s cost of the nominal three-impulse transfer is less than the optimal two-impulse cost of 222.9 m/s; however, in the three-impulse nominal transfer, the slopes of the primer at the endpoints are not zero. Also, the slope of the primer is not zero at the interior impulse. Thus, the solution can be improved.

Given the nominal transfer path, the gradient expressions in equations III.85 and III.105 are used simultaneously to determine the optimal endpoints and the optimal location and time for an interior impulse. The optimal three-impulse solution that results from the procedure is shown in Figure III.6; the associated primer history is also presented. In the plot of the transfer path, arrows near the trajectory indicate the general magnitude and direction of the impulsive maneuvers at the impulse locations identified as points 'o', 'm', and 'f'. The $\Delta\overline{V}$'s, expressed in terms of barycenter rotating coordinates, are: $\Delta\overline{v}_o$ =

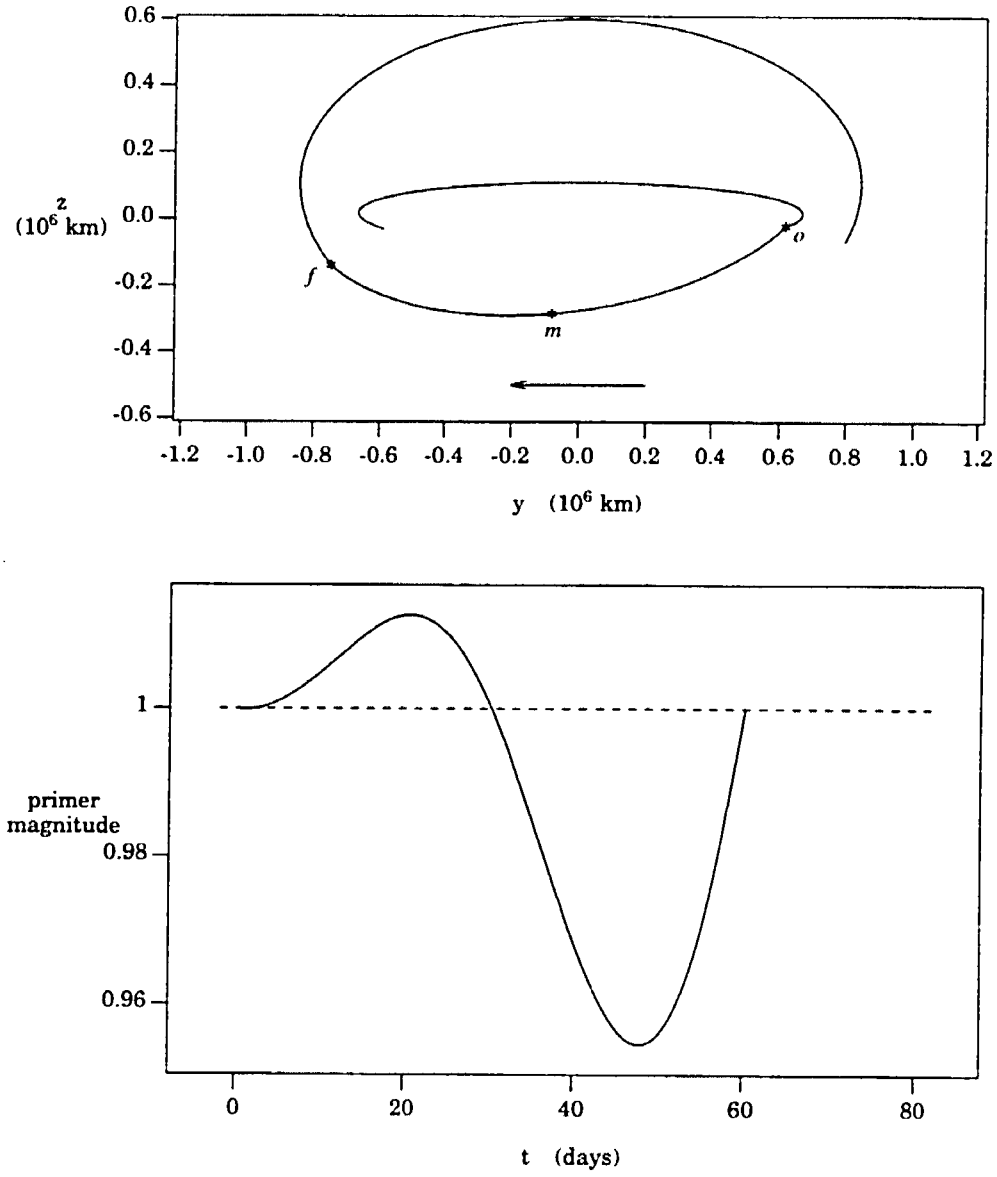

Figure III.5 Example: Nominal Three-Impulse Transfer and Primer History.

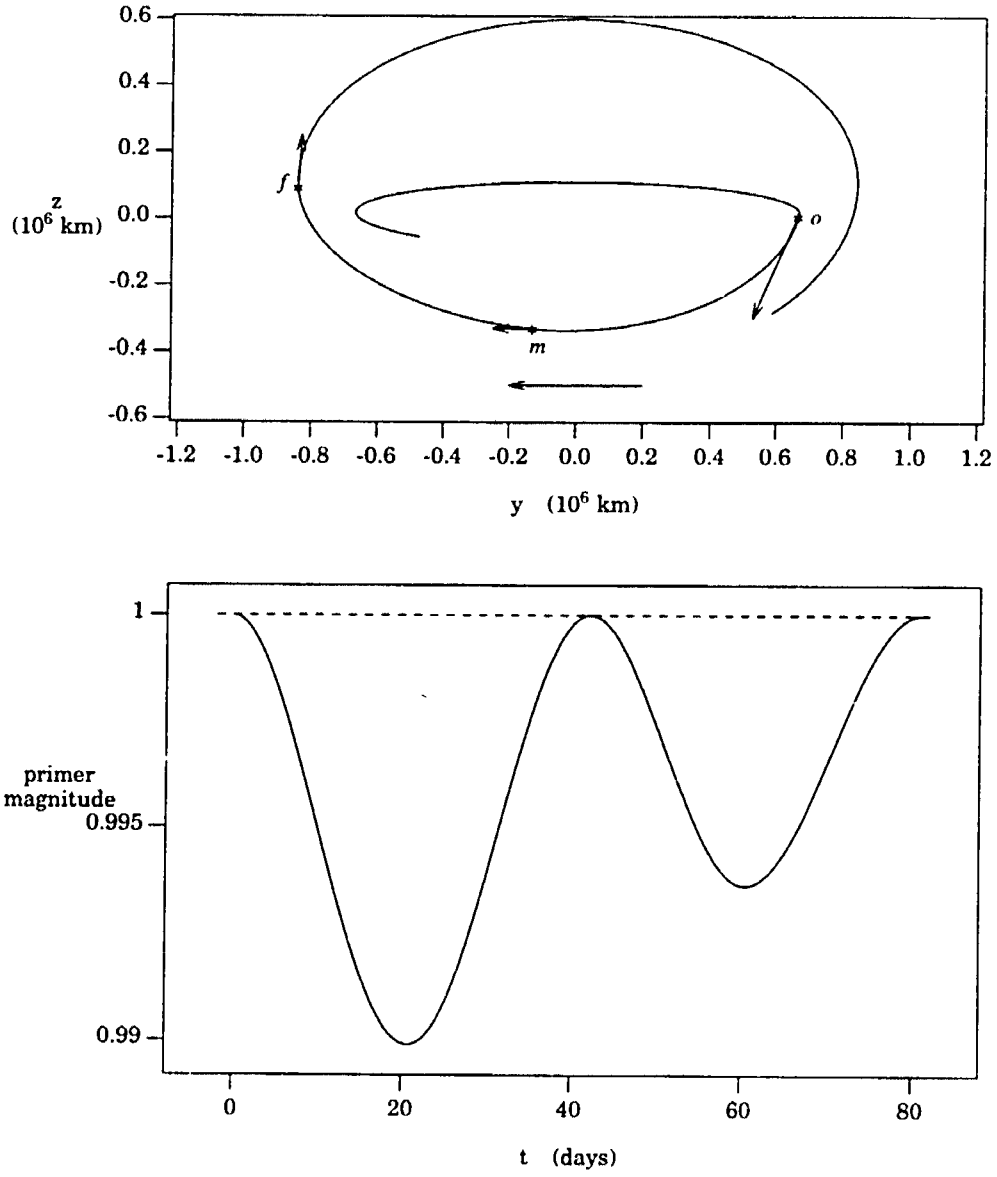

Figure III.6 Example: Optimal Three-Impulse Transfer and Primer History.

$\{23.7, -9.5, -114.3\}^T$ m/s; $\Delta\bar{v}_m = \{-0.1, -43.3, 6.5\}^T$ m/s; $\Delta\bar{v}_f = \{-19.4, 0.4, 54.4\}^T$ m/s. Thus, the cost is distributed as $\Delta V_o = 117.1$ m/s, $\Delta V_m = 43.8$ m/s, and $\Delta V_f = 57.8$ m/s, with a total cost of 218.7 m/s. In each case, the direction of the impulse is generally aligned with a vector that is tangent to the path at the position where the maneuver is applied. The optimal transfer time is 80.9 days with an interior impulse at 42.1 days past departure. The primer history associated with the transfer is plotted in the lower frame of the figure. The slopes of the primer at the endpoints are zero, and the derivative of the primer is continuous and equal to zero at the interior impulse time (within the tolerances deemed acceptable for all gradient conditions). In addition to the zero slope conditions, the primer associated with this path does not exceed one anywhere along the trajectory; therefore, this transfer satisfies all of the necessary conditions for an optimal impulsive solution and cannot be improved with the use of coast arcs or additional impulses. This is then denoted an optimal impulsive transfer. A similar algorithm is employed in all optimization problems in the circular case.

The necessary conditions require primer slopes that are equal to zero, primer magnitudes that are less than or equal to one, and continuity of the derivative of the primer across any interior impulses; however, non-zero, finite tolerances are employed in the assertion that each of the necessary conditions are met for all of the numerical solutions that are computed in this work. Although solutions that satisfy all of the necessary conditions for optimality to within defined numerical tolerances have been achieved using the algorithm that has been presented, the form of the expressions for the elements of the gradient vectors in equations III.85 and III.105 introduces a numerical issue that influences the specific tolerances that can be achieved. Recall, the component of the gradient of the cost with respect to the duration of a coast arc is a product of the derivative of the primer and the impulse magnitude. Since all computations are performed in terms of nondimensional variables, the nondimensional magnitude of the impulse is equal to the magnitude in meters/second divided by the characteristic length (in meters) and the mean motion (in inverse seconds). In the Sun-Earth/Moon barycenter system, the nondimensional ΔV is generally five orders of magnitude less than the dimensional value. Thus, in the time-free problem, the magnitude of an individual element of the the gradient vector is several orders of magnitude less than the slope of the primer. In the interior impulse problem, however, a component of the gradient vector is computed as the difference in the primer derivatives computed at the beginning and end of adjacent segments. Since the derivative should be zero at the optimal solution, the difference in the derivative should be small near the optimal solution; however, given a specified tolerance that defines an acceptably small derivative, the tolerance for the

difference in the derivatives is, at most, equal to the tolerance for the magnitude. This defines the smallest tolerance that can be established for the assertion that the gradient in the interior impulse problem is sufficiently small. Assuming that the value of the derivative can be computed to the same level of accuracy in the time-free and interior impulse problems, the value of $\dot{p}$ at the endpoints of a time-free solution can be assumed to be of the same order of magnitude as the components of $\dot{\bar{p}}$; however, the gradient in the time-free problem is several orders of magnitude less than the size of $\dot{\bar{p}}$. Thus, the gradient that can be achieved in a time-free problem is several orders of magnitude smaller than the value to be expected in the interior impulse problem. In this work, the magnitudes of the components of the time-free gradient vector are less than 1×10^{-8} in optimal time-free two-impulse transfers. The elements of the interior impulse gradient vector are, however, only required to achieve a magnitude that is less than 1×10^{-6}. Since the two optimization problems are solved simultaneously in the three-impulse solutions, all of the elements (six quantities) are required to satisfy the larger tolerance. Although endpoints that satisfy lower tolerances may be available, the optimal location and time of the interior impulse cannot be determined to within the accuracy required to achieve the lower value.

IV. OPTIMAL TRANSFER PATHS: CIRCULAR PROBLEM

Families of transfers between halo orbits in the circular restricted problem are formed from solutions that possess similar characteristics. Plots of the trajectories and of the transfer costs are employed to examine relationships that exist among members of a single family and to identify similarities among families. Both superior and inferior solutions are investigated. Also, transfers between southern halo orbits are compared with solutions that involve northern halos.

A. Superior Transfers: Positive z Families

Two types of superior transfers between northern halo orbits are initially considered. Solutions in one class exist such that the transfer path is primarily above the plane of primary motion (in the positive $\hat{z}$ direction). Motion below the plane (in the negative $\hat{z}$ direction) is representative of transfers in the second branch. In each class of solutions, impulsive transfers exist that satisfy the necessary conditions for a local minimum ΔV transfer between specified halo orbits to within acceptable numerical tolerances.

1. Positive z Family: 110,000 km A_z Departure Halo Orbit

Superior transfers that depart from a northern halo orbit with out-of-plane amplitude equal to 110,000 km and share similar characteristics are members of a 110,000 km A_z family. The family is represented by transfers to northern halo orbits with amplitudes equal to the following values: 160,000; 200,000; 240,000; 300,000; 400,000; 500,000; 600,000; 700,000; and 800,000 km. (All halo amplitudes refer to the out-of-plane, A_z, amplitude.) The departure orbit for each solution is the departure orbit displayed in Figure III.1. The arrival trajectory included in the figure represents the target orbit for one member of this family (the 600,000 km member).

To begin the search for optimal solutions, nominal trajectories are defined for each departure/arrival pair of halo orbits. The nominal departure position for each solution is the location along the 110,000 km A_z halo orbit where the x component of acceleration ($\ddot{x}$) is zero and the y component of position is negative. (The variables x, y, z represent

position coordinates relative to the libration point, L_1. In the circular problem, the x and x acceleration components are equivalent; however, this distinction is relevant for solutions computed in the elliptic problem.) The nominal arrival position is defined where $\ddot{x}$ is zero and y is positive on each of the arrival halo orbits. Thus, the departure and arrival locations are separated by approximately one-half revolution of a halo orbit in the $y-z$ projection. Consistent with the algorithm discussed previously, a transfer that connects the selected positions is computed for an arbitrary transfer time for each pair of halo orbits. Next, in each case, the best transfer between the nominal endpoints is computed as the solution to the variable-time optimization problem. The $y-z$ projections of the nominal paths are presented in Figure IV.1. Arcs of the 110,000 km and 800,000 km orbits are included in the figure to illustrate the orientation of the transfer relative to the halo orbits. The point designated as point o is the departure position along the 110,000 km orbit; each transfer includes this position. Point f denotes the arrival position for transfer to the 800,000 km halo orbit. In Figure IV.1, the transfer with the maximum excursion in the position z direction is the transfer to the 800,000 km halo orbit. As the maximum z excursions of the transfers decrease, the amplitudes of the target halo orbits also decrease.

Table IV.1 lists the total ΔV for each member of this family ranging from a cost of 20.97 m/s for transfer to the 160,000 km orbit to 352.60 m/s for transfer to the 800,000 km orbit. The heading 'TOF' indicates the time required to travel between the endpoints of

Final A_z	Nominal 2-Impulse		Optimal 2-Impulse	
	ΔV	TOF	ΔV	TOF
km	m/s	days	m/s	days
160000	20.97	72.38	20.74	77.73
200000	38.23	72.54	38.02	76.25
240000	56.00	72.71	55.88	74.94
300000	83.65	72.97	83.65	73.24
400000	132.52	73.26	132.18	71.00
500000	184.59	73.34	182.90	69.32
600000	239.17	73.25	235.16	68.08
700000	295.42	73.06	288.38	67.18
800000	352.60	72.83	342.12	66.57

Table IV.1 110,000 km Positive z Family: Transfer Costs.

the transfer. Table A.1 in the appendix includes the magnitudes of the departure impulse

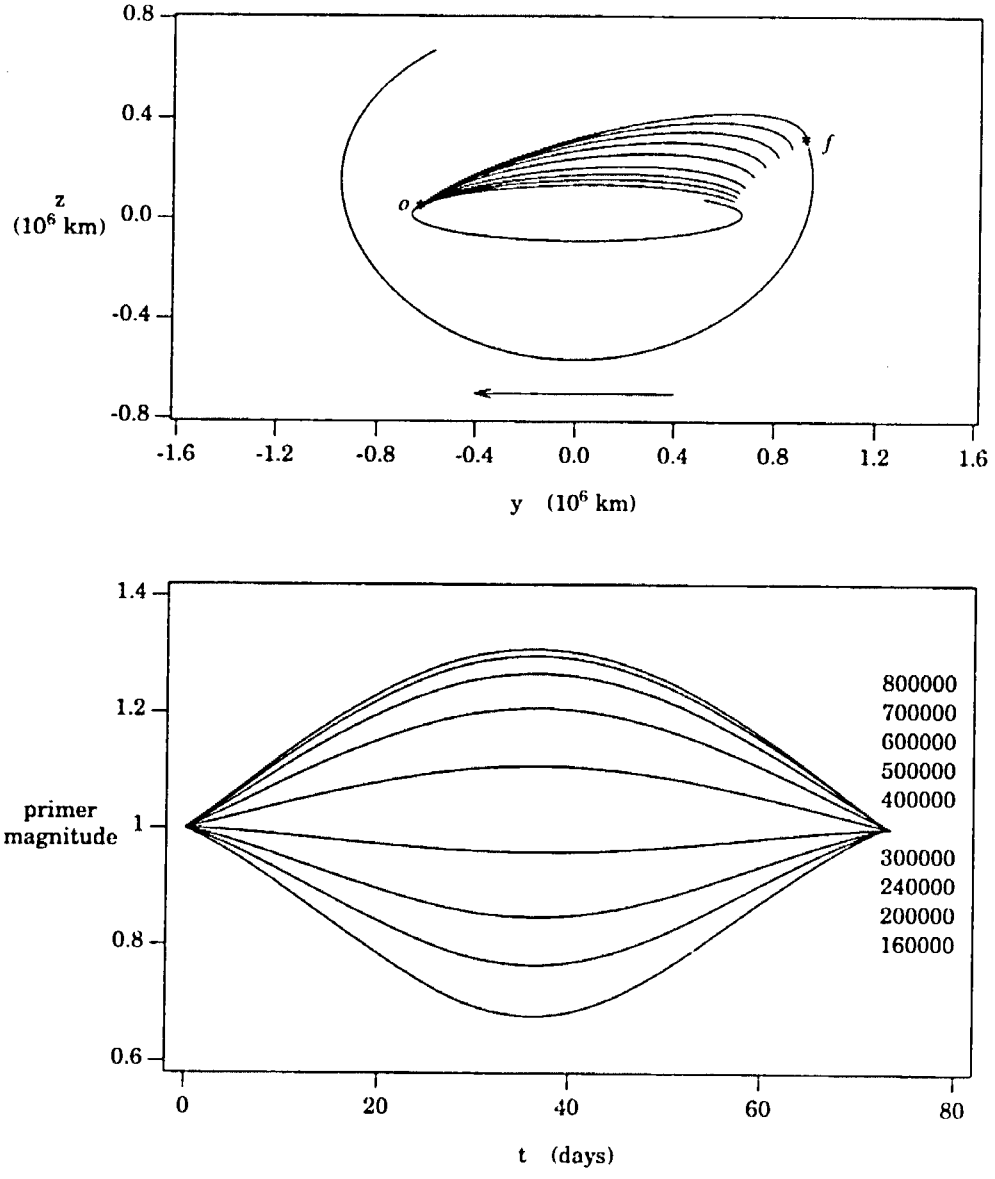

Figure IV.1 110,000 km Positive z Family: Nominal Two-Impulse Solutions.

(ΔV_1), the arrival impulse (ΔV_2), and the total cost ($\Delta V'$). Similar tables are used to report transfer costs for all solutions discussed in this document. The total $\Delta V'$ and the transfer times are presented in tables in the body of the text while the distribution of the cost is included in tables in the appendix. In all table entries, data is rounded to two decimal places.

The magnitudes of the primer vectors for this family are plotted in the lower frame of Figure IV.1. Although the primer histories for all members of the family are plotted in the same figure, the correlation of a particular primer with the associated transfer is denoted by a list of amplitudes of the destination halos in the primer plot. In all plots of primer histories, a list of amplitudes (in kilometers) is included that defines the correlation between a particular primer history and the transfer to which it is associated. For example, the primer associated with the transfer to the 800,000 km halo achieves the largest magnitude. (The correspondence between the primer history and a particular transfer can often be determined by comparing the transfer times listed in the table with the final time in the plot; however, a list of the amplitudes is included in the primer plots to assist in the identification if the individual times cannot be distinguished in the figure.) The slopes of the primer at the terminal times are non-zero for each of the solutions in this family; therefore, the costs can be reduced by employing coast arcs at both ends of each transfer. For transfers to large halo orbits (A_z greater than 300,000 km), the magnitude of the primer exceeds one, indicating that a transfer that employs the nominal endpoints used in the current solution, but includes an interior maneuver computed according to equation III.99 and applied at a position computed from equation III.95, will reduce the cost; however, in this study, coast arcs are employed to achieve the optimal time-free solution before additional maneuvers are considered.

The solutions to the time-free problem for this family are presented in Figure IV.2. Arcs of the 110,000 km halo and the 800,000 km halo are included in the figure. Point *o* indicates the optimal departure location for the 160,000 km solution (along the 110,000 km halo); point *f* corresponds to the optimal arrival point along the 800,000 km halo orbit. (Although each nominal solution employs the same departure position, each optimal transfer departs from a different location along the 110,000 km halo.) Similar notation is used for all superior transfers, where *o* refers to the departure point corresponding to the transfer to the halo of lowest A_z, and *f* refers to the arrival position for the largest target orbit. Transfers of increasing amplitude correspond to target halo orbits of increasing amplitude. The value of the out-of-plane component of position, z, along the optimal transfers are all generally positive; therefore, the solutions are members of a "positive z family." (Note that motion occurs in the positive $\dot{z}$ direction, but it is not confined to a constant plane; therefore, the

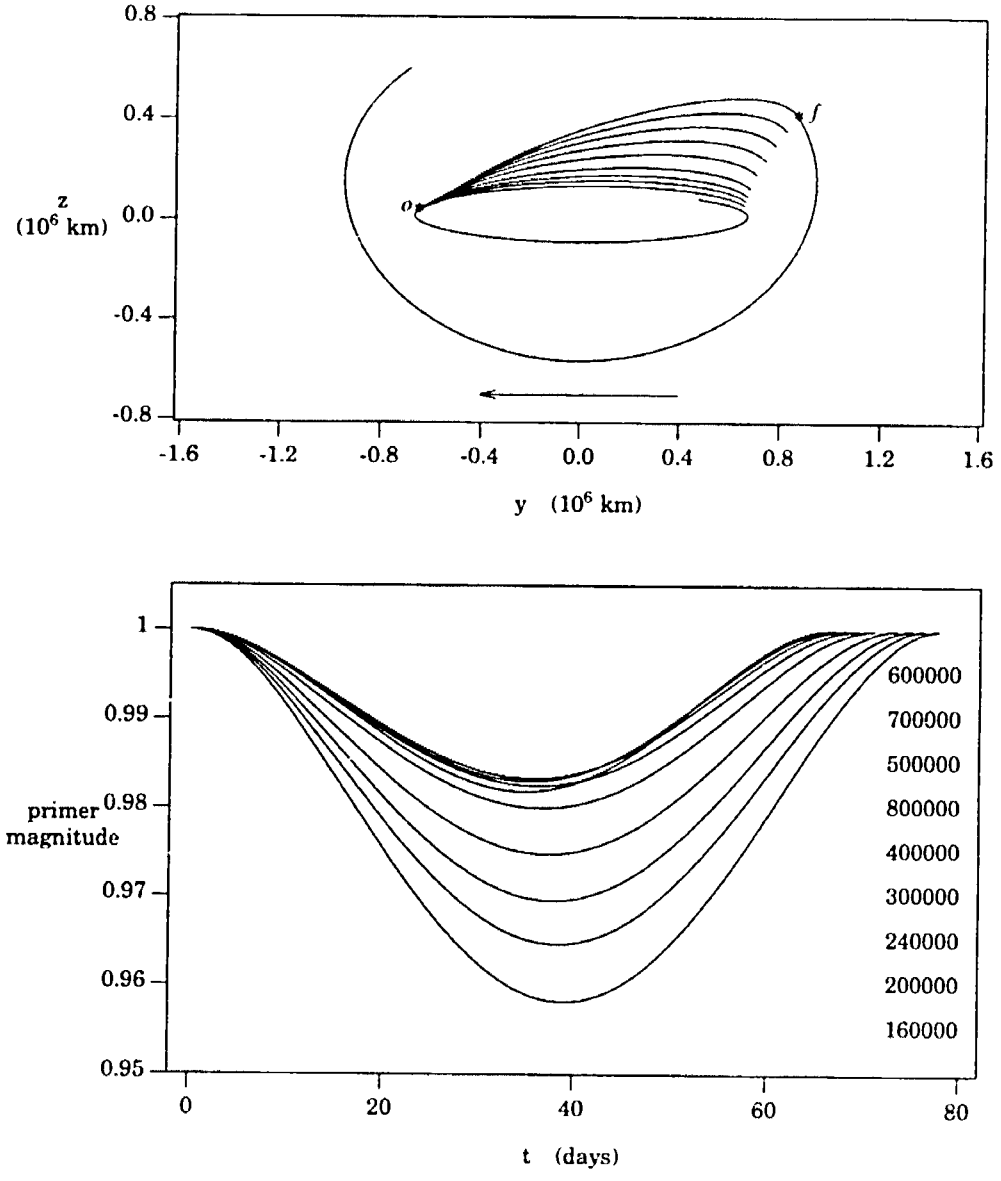

Figure IV.2 110,000 km Positive z Family: Optimal Two-Impulse Solutions.

phrase "positive $\hat{z}$ *plane*" is not appropriate.) The primer histories that are associated with the optimal transfers are plotted in the lower frame of the figure. (The time $t = 0$ in the primer plot is defined as the time of departure on the transfer and has no relationship to the nominal departure time.) The slopes of the primers in Figure IV.2 are zero at the endpoints to within an acceptable numerical tolerance; therefore, the solutions satisfy the necessary conditions for optimal time-free two-impulse solutions. In addition, the magnitude of each primer vector is less than one at all interior times. Thus, the solutions cannot be improved with additional impulses.

The transfer costs and the times of flight for the optimal solutions are included in Table IV.1. In the table, the time of flight refers to the transfer time between the endpoints and does not include the coast times on the halo orbits that are introduced in the time-free solutions. The optimal transfer costs computed for this family range from 20.74 m/s for transfer to the 160,000 km orbit to 342.12 m/s for transfer to the 800,000 km orbit. In each case, the optimal ΔV is within three percent of the nominal cost. Also, the optimal endpoints of the transfer are located less than five days from corresponding nominal positions. For example, the nominal and optimal departure locations are separated by only 2.7 days along the departure halo for transfer to the 160,000 km orbit. Thus, transfers with endpoints at locations where the x component of acceleration is zero, such as the nominal solutions used in this family (Figure IV.1), possess two useful properties. First, the endpoints can be identified on a halo orbit of any size. Second, the cost for a solution that employs such endpoints is close to the optimal cost for a neighboring time-free solution. The amplitudes of the target orbits are plotted in Figure IV.3 versus the optimal costs that are achieved. Triangles in the figure represent data points for the nominal solutions; dots indicate optimal solutions. Although the relationship among the optimal transfer costs is not linear, a linear approximation provides a reasonable prediction of the total ΔV that is required for transfers to halo orbits other than those considered here. For small differences between the departure and arrival halo orbit amplitudes, a ΔV of approximately 45 m/s per 100,000 km increase in the amplitude provides a predicted cost that is in the neighborhood of the actual optimal cost. A cost of 50 m/s per 100,000 km increase in A_z yields a better approximation for large amplitude differences.

Although the shape and the cost associated with each optimal solution are similar to those corresponding to the nominal path, nominal transfers that are substantially different from the optimal paths also yield optimal transfers that include only small variations from the optimal solutions identified in Figure IV.2. Minor differences in the solutions are possible due to numerical errors that result from the significant number of computations that are required to achieve an optimal solution from a distant nominal trajectory and the existence

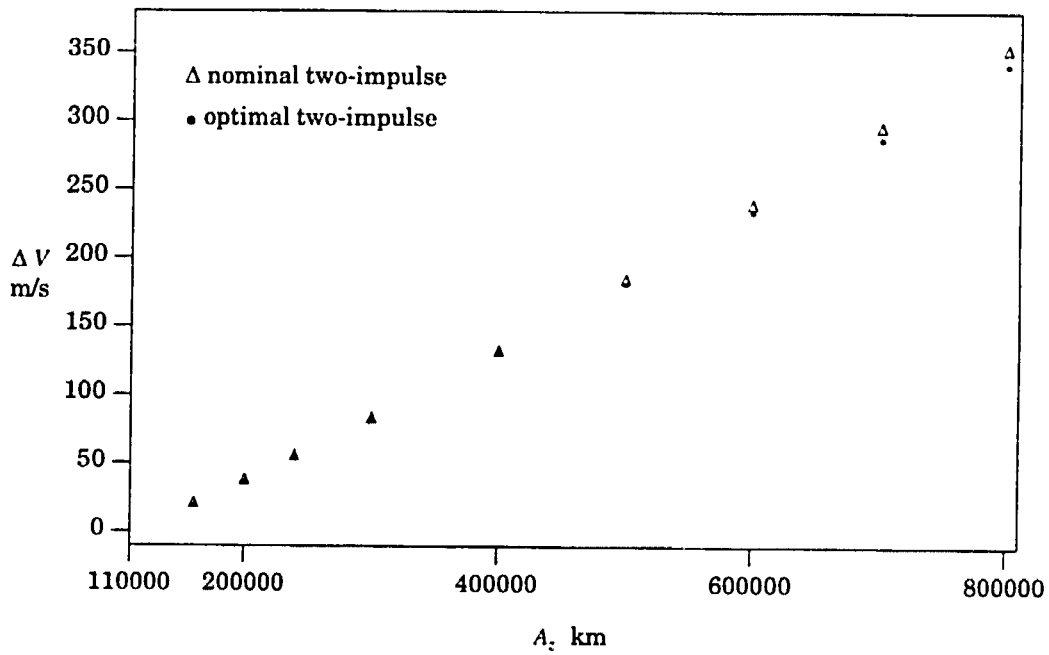

Figure IV.3 110,000 km Positive z Family: Arrival Amplitude — ΔV Relationship.

of several solutions that satisfy optimality given a finite numerical tolerance. One example of a transfer that is relatively far from the optimal solution for this family, but still yields essentially the same optimal solution in Figure IV.2 for the 600,000 km case, is presented in Figure IV.4. In this transfer, the departure and arrival positions are located at the positions of minimum and maximum z excursion, respectively. The cost for this solution is 692 m/s with a transfer time of 75 days. Although both the transfer in Figure IV.4 and the 600,000 km halo solution in Figure IV.1 are one-half revolution transfers between the same two halo orbits, the costs in each (non-optimal) case are significantly different. The cost for the optimal solution obtained using the distant nominal transfer as the initial guess is 235.16 m/s (consistent with Table IV.1). Thus, although the optimization algorithm converges to nearby optimal solutions using the nominal transfers presented in Figure IV.1, the algorithm can successfully reduce the cost by over sixty percent and move the endpoints more than one-quarter revolution in the search for an optimal solution.

2. Positive z Family: 200,000 km A_z Departure Halo Orbit

A family of optimal transfers that depart from a northern halo orbit with out-of-plane amplitude equal to 200,000 km is represented by arrival halo orbits with amplitudes equal to: 240,000; 300,000; 400,000; 500,000; 600,000; 700,000; and 800,000 km. Table IV.2 includes the nominal costs for this family computed using endpoints similar to those used in the sample transfers representing the 110,000 km positive z family (that is, locations where $\ddot{x}$ is zero). Optimal transfer paths that are achieved by solving the time-free problem

Final A_z	Nominal 2-Impulse		Optimal 2-Impulse	
	ΔV	TOF	ΔV	TOF
km	m/s	days	m/s	days
240000	17.87	72.91	17.86	72.28
300000	45.76	73.17	45.65	70.89
400000	95.16	73.52	94.21	69.02
500000	147.86	73.69	144.98	67.63
600000	203.12	73.69	197.29	66.62
700000	260.07	73.56	250.57	65.91
800000	317.91	73.38	304.37	65.44

Table IV.2 200,000 km Positive z Family: Transfer Costs.

for each member are presented in Figure IV.5 with the associated primer histories. The

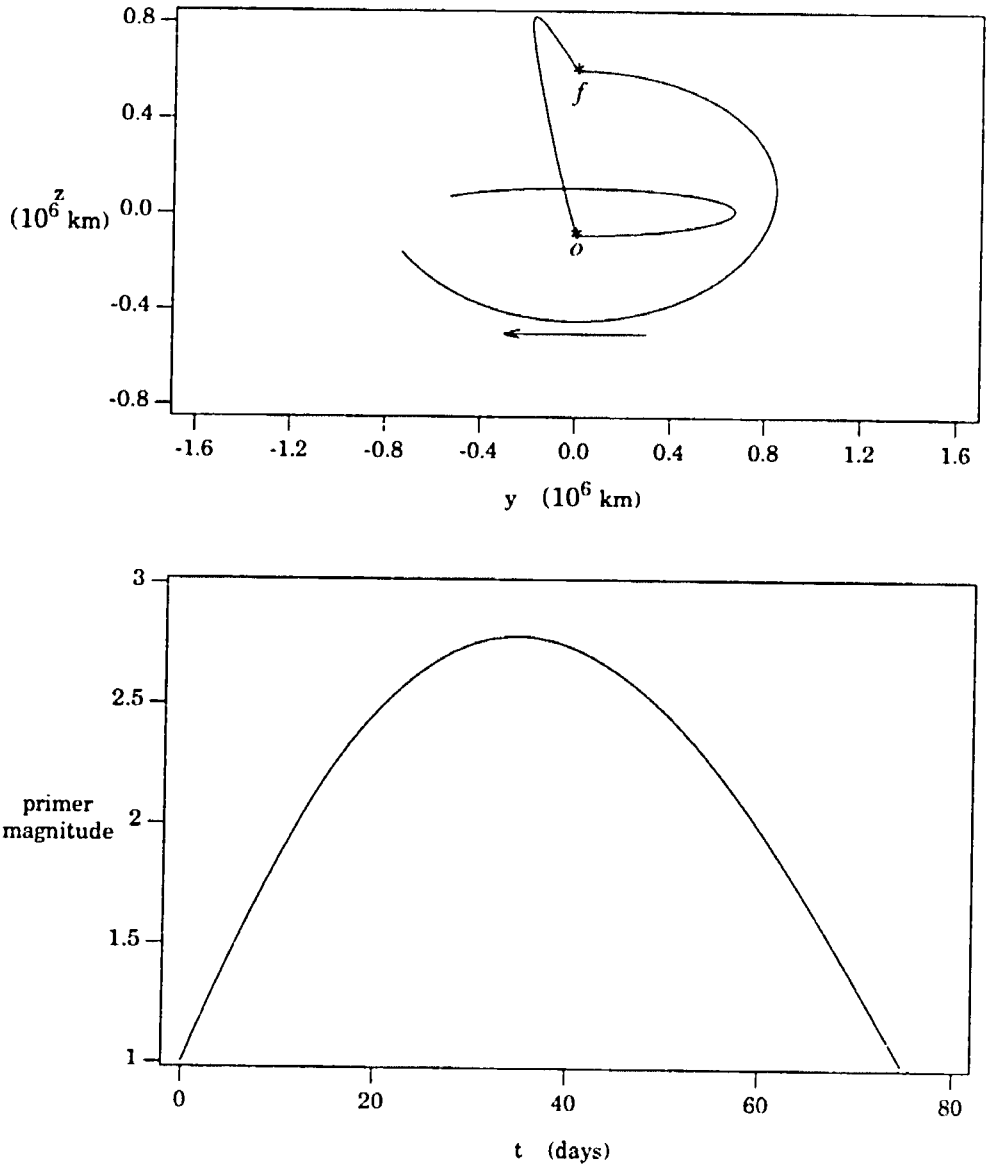

Figure IV.4 110,000 km to 600,000 km Transfer: Distant Nominal Solution.

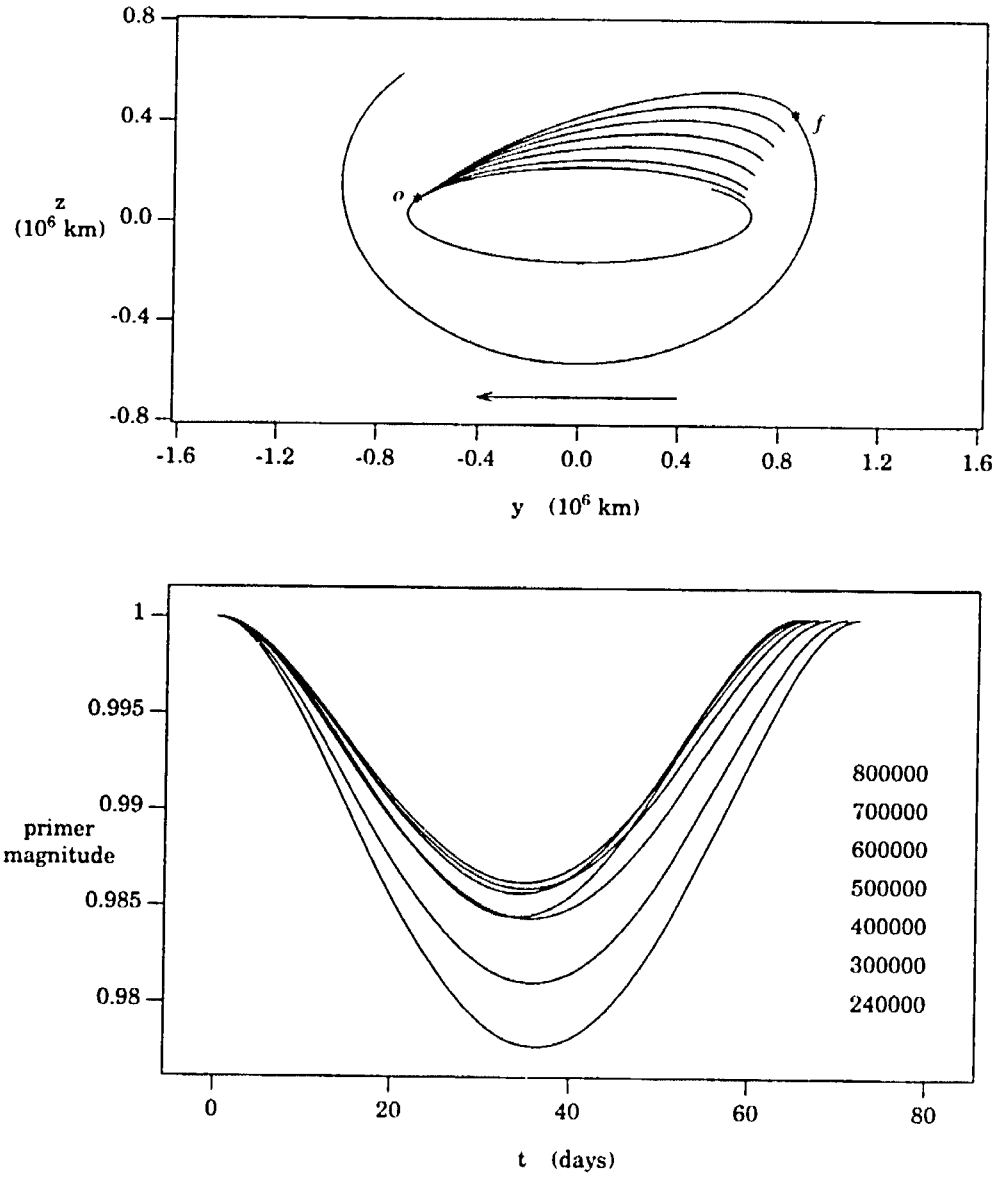

Figure IV.5 200,000 km Positive z Family: Optimal Two-Impulse Solutions.

transfer portion along each solution remains primarily in the positive $\hat{z}$ direction; therefore, the transfers are members of a positive z family. The characteristics of the family are similar to those of the 110,000 km A_z, positive z family of superior transfers: optimal solutions require only two impulses; optimal endpoints are close to the nominal locations; optimal costs represent modest reductions relative to the nominal ΔV's. Representative costs for the family are plotted relative to the amplitude of the arrival halo orbits in Figure IV.6. In agreement with the slope predicted in Figure IV.3, a change in the target amplitude of 100,000 km requires an increase in the ΔV of approximately 45 to 50 m/s.

B. Superior Transfers: Negative z Families

The existence of optimal impulsive transfers is verified by the solutions presented as members of positive z families; however, the necessary conditions for optimality only provide a test for a local minimum. Thus, additional solutions that satisfy the conditions are possible for any set of halo orbits. Given the presence of optimal transfers above the $x-y$ plane (in the positive $\hat{z}$ direction), transfers that exist primarily below the $x-y$ plane (in the negative $\hat{z}$ direction) are also considered.

1. Negative z Family: 110,000 km A_z Departure Halo Orbit

A family of optimal superior transfers that depart from a northern halo orbit with out-of-plane amplitude equal to 110,000 km is available where the out-of-plane component of position for the transfer path is negative along most of the trajectory path. Transfers to target halo orbits with amplitudes equal to: 160,000; 200,000; 240,000; 300,000; 400,000; 500,000; 600,000; and 700,000 km are representative members of the family. (The transfer to the 600,000 km halo discussed in Chapter III is a member of this family.) Nominal departure and arrival positions are selected at locations where z is zero: the departure position is located where z is zero and y is positive on the 110,000 km A_z northern halo orbit; the arrival points are the positions where z is zero and y is negative on each of the selected target orbits. The nominal two-impulse transfers and the associated primer histories are plotted in Figure IV.7. In each case, the slopes of the primer at the terminal times are non-zero; therefore, the costs can be reduced with the use of coast arcs. The nominal two-impulse costs are listed in Table IV.3. In most cases, the nominal costs for this family are larger than the nominal ΔV's in the 110,000 km A_z, positive z family (Table IV.1); however, this does not indicate that the optimal costs for this family are also larger than the those for the positive z solutions.

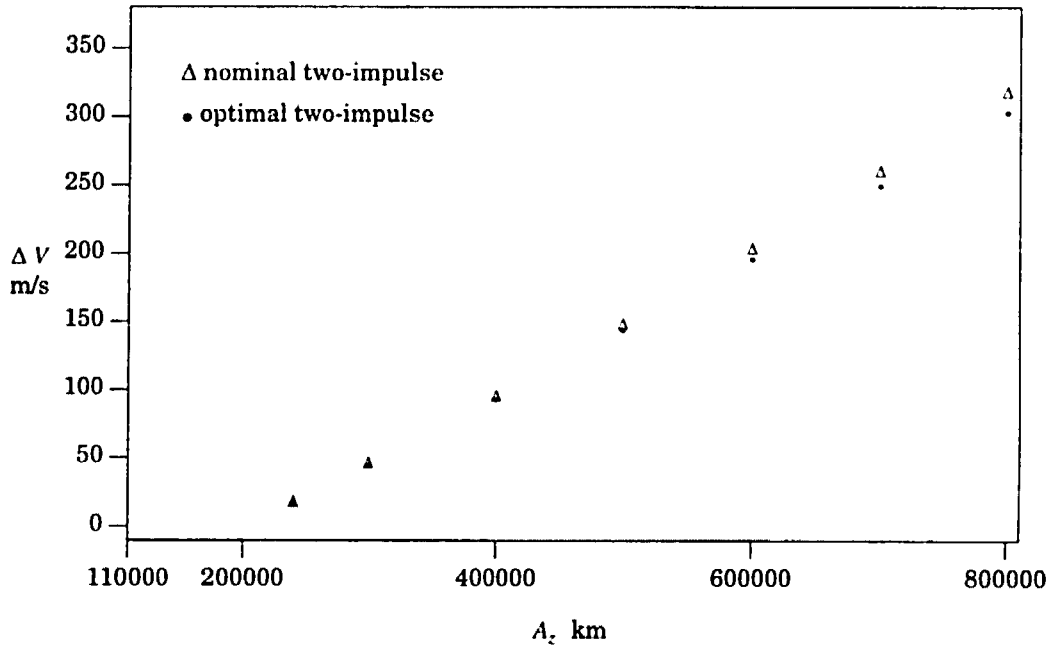

Figure IV.6 200,000 km Positive z Family: Arrival Amplitude — ΔV Relationship.

Final A_z	Nominal 2-Impulse		Optimal 2-Impulse		Nominal 3-Impulse		Optimal 3-Impulse	
	ΔV	TOF	ΔV	TOF	ΔV	TOF	ΔV	TOF
km	m/s	days	m/s	days	m/s	days	m/s	days
160000	20.70	76.68	20.02	69.26	20.02	69.26	20.02	71.98
200000	38.51	76.57	36.61	67.93	36.61	67.93	36.57	72.64
240000	57.10	76.45	53.68	66.74	53.67	66.74	53.57	73.31
300000	86.99	76.24	80.09	65.18	80.06	65.18	79.78	74.32
400000	140.81	75.81	126.01	63.06	125.92	63.06	125.00	76.07
500000	197.86	75.32	173.78	61.44	173.57	61.44	171.54	78.10
600000	256.12	74.80	222.87	60.18	222.50	60.18	218.72	80.94
700000	313.67	74.20	272.86	59.21	272.28	59.21	265.89	87.80

Table IV.3 110,000 km Negative z Family: Transfer Costs.

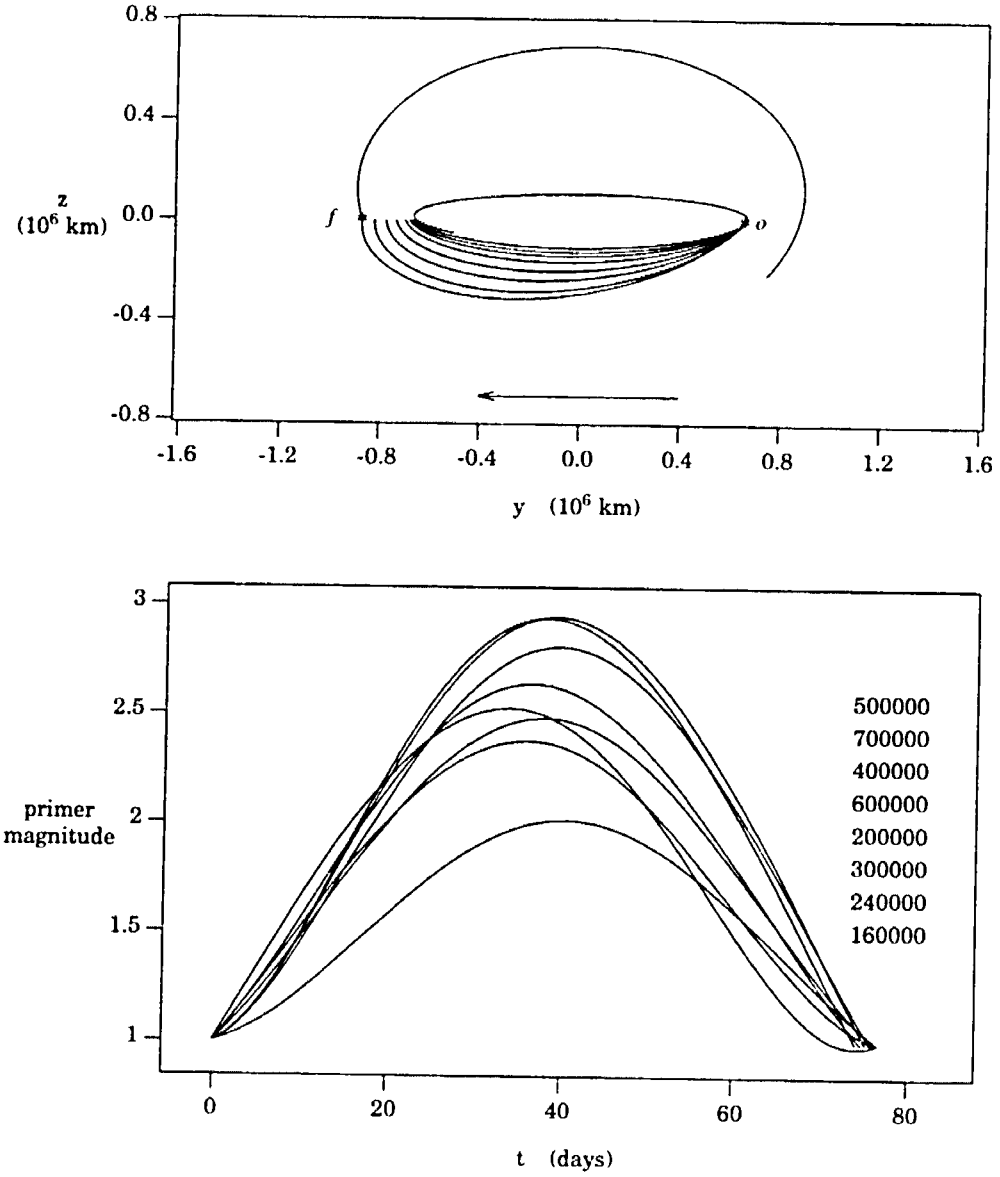

Figure IV.7 110,000 km Negative z Family: Nominal Two-Impulse Solutions.

Employing coast arcs in a time-free, two-impulse optimization problem for each case, optimal two-impulse solutions are achieved that remain generally below the $x-y$ plane, in the negative z direction. The trajectories are represented in Figure IV.8 with the corresponding primer histories. A relatively long coast arc at arrival is required to achieve optimality, particularly in transfers to large halo orbits. Thus, the selected nominal endpoints are not representative of the optimal locations. Also, for large amplitude differences, the optimization process reduces the cost to less than ninety percent of the nominal ΔV value. Alternative endpoints for negative z transfers, ones that yield nominal costs that are closer to the optimal (two-impulse) costs, and possess some distinguishing characteristics, are not available.

The costs in Table IV.3 corresponding to the optimal two-impulse trajectories are less than the optimal costs achieved in the corresponding positive z solutions (Table IV.1); however, further reductions are possible with the use of interior impulses. In each case, the slopes of the primer are zero at the terminal times on the trajectory, indicating an optimal time-free transfer, but the magnitude exceeds one along the path. Thus, an interior impulse is included in each solution at the time when the primer reaches its maximum. The nominal three-impulse solutions are plotted in Figure IV.9. Nominal costs for the three-impulse solutions are included in Table IV.3. Magnitudes of the individual impulses are provided in Table A.4 of the appendix, where ΔV_1 indicates the departure maneuver, ΔV_2 denotes the interior impulse magnitude, and the arrival cost is labeled ΔV_3. Note that the times of flight in Table IV.3 associated with the nominal three-impulse solutions are equal to the transfer times for the corresponding optimal two-impulse transfer. Each nominal three-impulse transfer employs the same terminal positions and total transfer time as the optimal two-impulse transfer, as discussed in the previous chapter. The nominal three-impulse primer histories are also included in Figure IV.9. The amplitudes listed in that frame identify the curves by indicating the relative positions of the minimum value of the primer at a point after the interior impulses. (The list of amplitudes is always included near the part of the primer plot to which it refers.) In each case, the primer violates the time-free requirement of zero slopes at the ends; therefore, coast arcs will reduce the costs. The optimal endpoints for the two-impulse solutions are not optimal for the three-impulse paths. Furthermore, at the time of the interior impulse on each solution, the derivative of the primer fails both the continuity requirement for an optimal interior maneuver and the zero slope condition. (The derivatives appear to be continuous on the scale of the plot; however, they do not satisfy the numerical tolerances that are required. The value of the slope at the endpoints, however, clearly is non-zero in each case.)

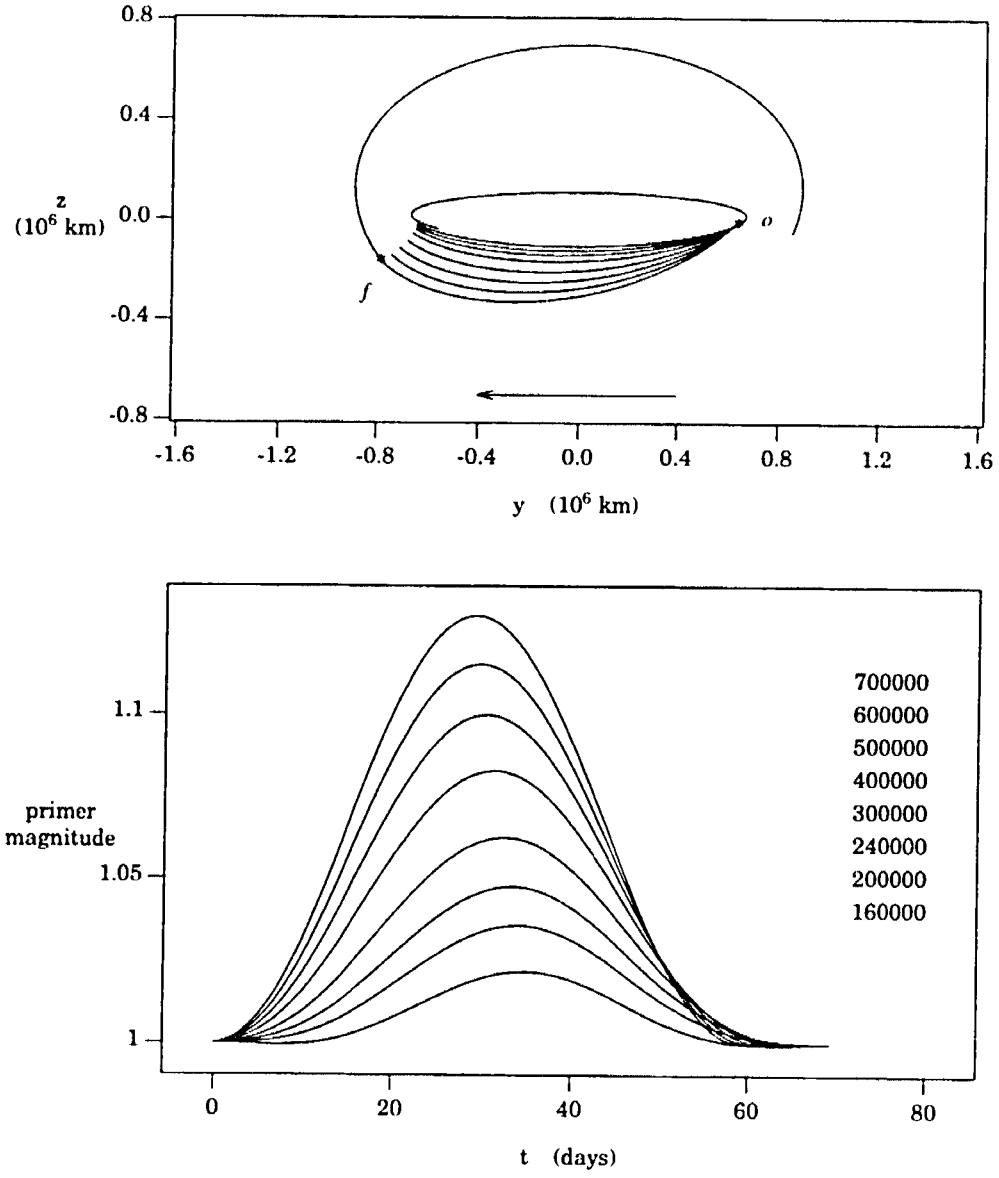

Figure IV.8 110,000 km Negative z Family: Optimal Two-Impulse Solutions.

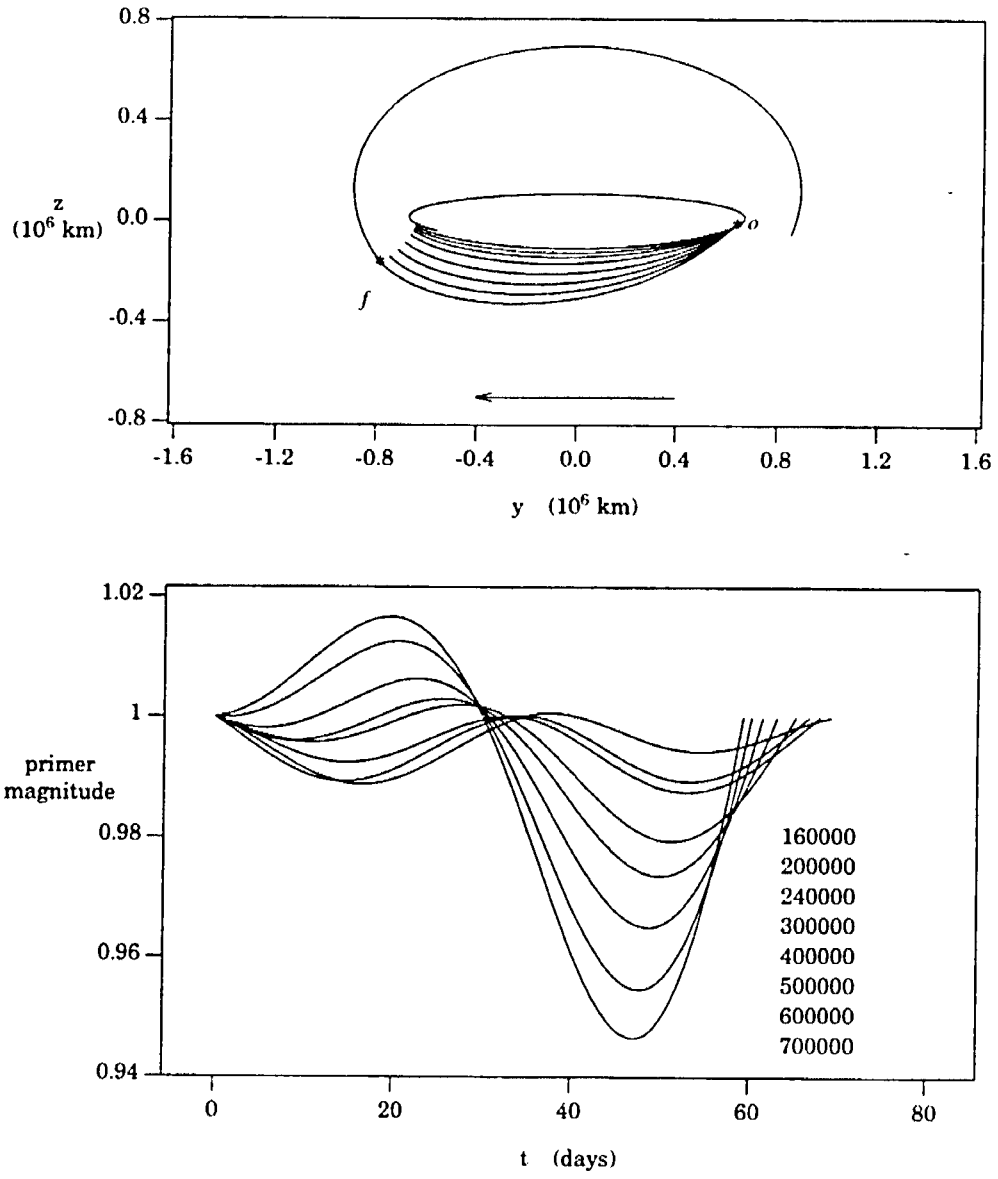

Figure IV.9 110,000 km Negative z Family: Nominal Three-Impulse Solutions.

To obtain an optimal three-impulse transfer, the location and time of the third (interior) impulse is optimized simultaneously with the coast arcs on each solution in an optimization problem that is defined by the six variables that represent these quantities. The goal in this step is a solution in which the slope of the primer is zero at each of the three impulses and is continuous across the interior impulse. The optimal solutions achieved for this family are presented in Figure IV.10. In the figure, the position identified as 'm_{160000}' indicates the location of the interior maneuver along the transfer to the 160,000 km halo orbit. The notation 'm_{700000}' indicates the position of the interior maneuver for transfer to the 700,000 km halo orbit. The optimality requirements are satisfied at each maneuver to within the numerical tolerances employed. Also, the magnitude of the primer is less than one at all non-impulse times. Thus, the solutions are optimal impulsive transfers; additional impulses will not reduce the cost. The time-free aspect of the optimization problem (that introduces coast arcs in the solutions) produces significant changes in the arrival locations relative to both the optimal two-impulse terminal positions and the nominal positions that were originally selected; however, the arcs represent delayed arrivals relative to the nominal positions as opposed to the early arrivals required in the two-impulse transfers. Thus, the optimization of the interior impulse simultaneously with the endpoints requires large changes in the transfer trajectories; however, the reduction in the cost that is achieved through the optimization process is small. The optimal three-impulse cost is within three percent of the value of the nominal three-impulse ΔV in each case; however, optimizing the interior impulse does cause a substantial redistribution of the cost (see Table A.4). As the arrival amplitude increases, the interior impulse increases from less than three percent of the total cost in the 160,000 km case to over twenty percent of the total ΔV for the 700,000 km solution. Thus, the interior impulse has a significant influence on the characteristics of the solution although it yields only a minor reduction in the total ΔV.

The transfer costs associated with this family are plotted in Figure IV.11. Triangles represent nominal two-impulse costs; stars indicate the optimal two-impulse solutions; optimal three-impulse costs are identified by dots. The costs associated with optimal solutions in this family are lower than the corresponding costs in the 110,000 km A_z, positive z family for the same pair of departure/arrival halo orbits. Furthermore, as the final amplitude increases, the difference in the costs between the two families increases. Reflective of the lower costs in this family compared with the positive z family, an approximate slope in the range of 43 to 48 m/s per 100,000 km change in the arrival amplitude yields a better prediction of the total ΔV than the 45 to 50 m/s range suggested by the positive z family. The stated ranges for each family are, however, only intended to indicate a reasonable prediction of the actual costs. Thus, the 2 m/s difference in the range of values for the slopes is not

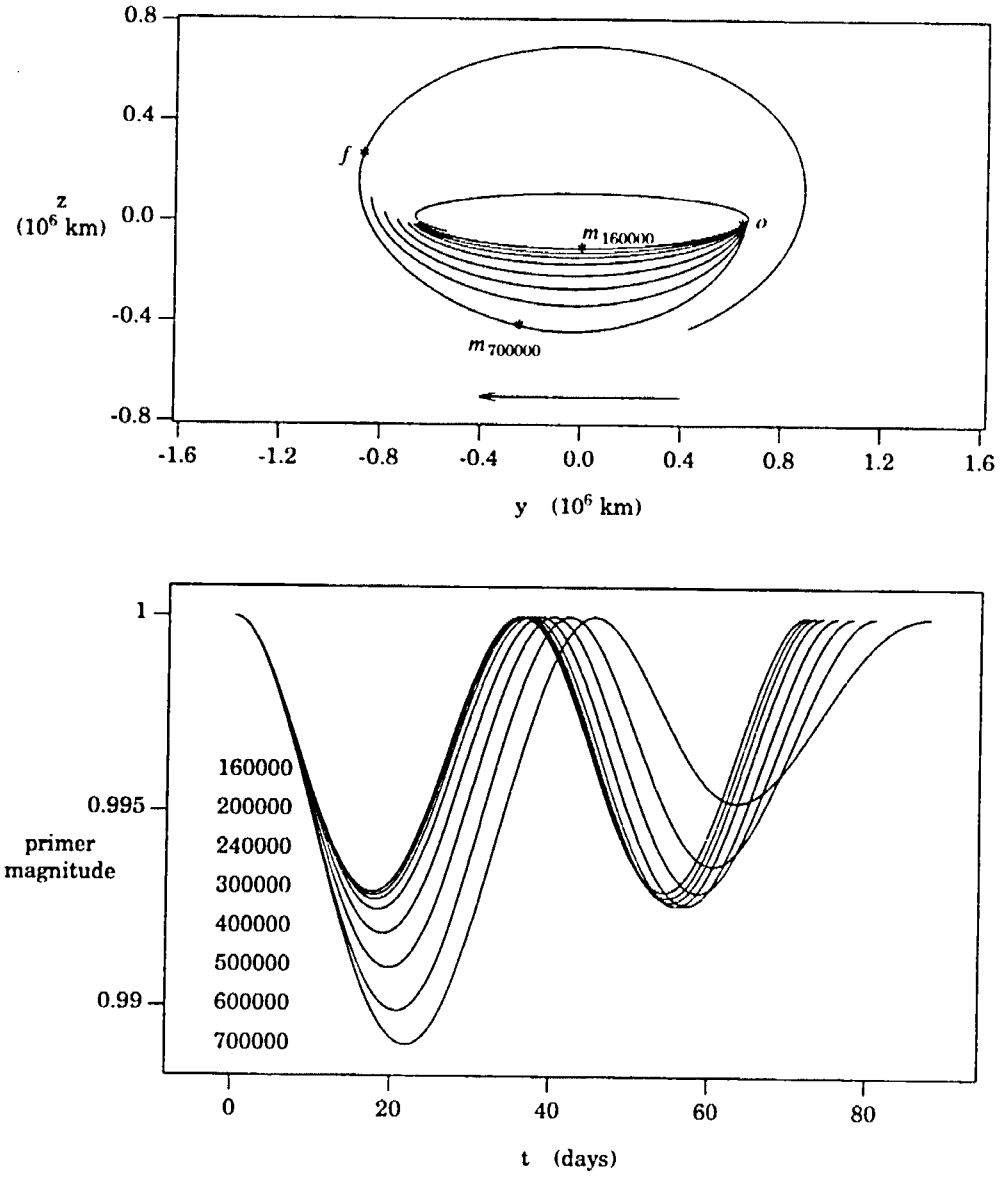

Figure IV.10 110,000 km Negative z Family: Optimal Three-Impulse Solutions.

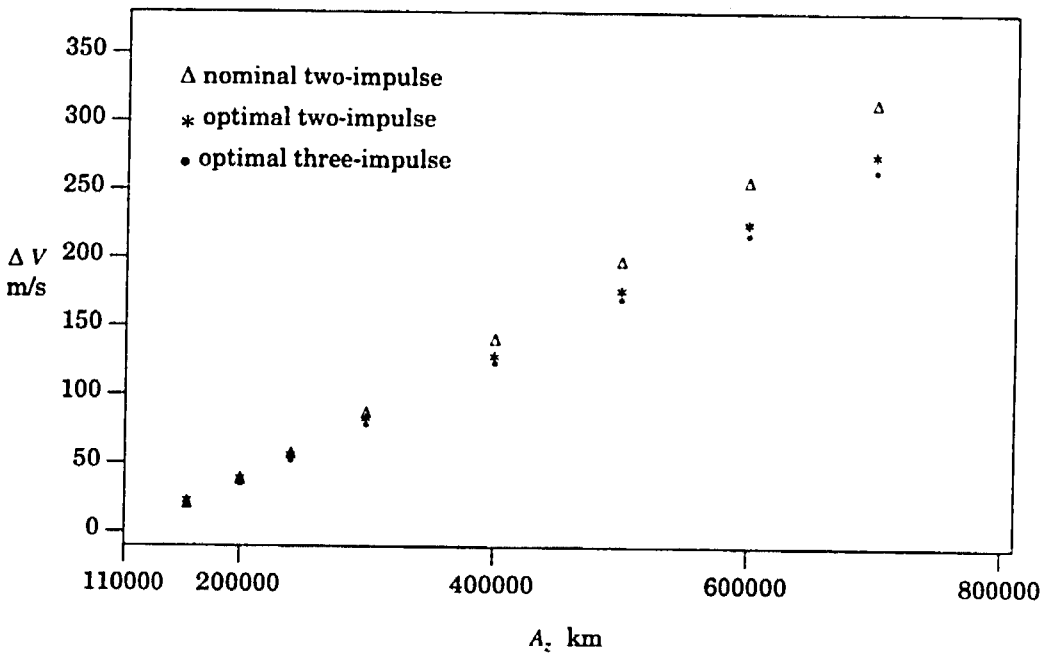

Figure IV.11 110,000 km Negative z Family: Arrival Amplitude — ΔV Relationship.

necessarily notable. It is noted, however, that both 110,000 km families possess generally linear relationships between the optimal costs and the target halo amplitudes.

2. Negative z Family: 200,000 km A_z Departure Halo Orbit

A comparison of the two positive z families presented earlier in this chapter indicates that families with similar characteristics may exist with different departure halo amplitudes. A similar conclusion for families that exist primarily below the x – y plane (in a negative z direction) is demonstrated by a family of superior transfers that depart from a 200,000 km A_z halo. Transfers to target orbits with z-amplitudes: 240,000; 300,000; 400,000; 500,000; 600,000; and 700,000 km are used to represent the family. The costs for nominal, two-impulse transfers are listed in Table IV.4 for solutions computed with a departure position where z is zero and y is positive and arrival at the location where z is zero and y is negative. The transfers resulting from the time-free problems for this family are similar to those

Final A_z	Nominal 2-Impulse		Optimal 2-Impulse		Nominal 3-Impulse		Optimal 3-Impulse	
	ΔV	TOF	ΔV	TOF	ΔV	TOF	ΔV	TOF
km	m/s	days	m/s	days	m/s	days	m/s	days
240000	18.84	76.26	17.08	64.41	17.08	64.41	17.00	74.71
300000	48.99	76.04	43.55	63.13	43.51	63.13	43.22	75.68
400000	103.31	75.61	89.57	61.38	89.46	61.38	88.45	77.34
500000	160.81	75.11	137.47	60.02	137.23	60.02	135.01	79.23
600000	219.37	74.56	186.70	58.99	186.28	58.99	182.22	81.73
700000	277.29	73.97	236.85	58.19	236.18	58.19	229.51	86.34

Table IV.4 200,000 km Negative z Family: Transfer Costs.

achieved in the 110,000 km, negative z family; the primers associated with the optimal two-impulse solutions have magnitudes greater than one, and early arrivals are required. Thus, in each case, a third impulse is included and optimized simultaneously with the endpoints in search of a three-impulse path that satisfies all optimality requirements.

The y – z projections of the optimal three-impulse solutions are plotted in Figure IV.12. As found in the 110,000 km negative z family, the addition of a third impulse to each solution shifts the arrival location to a position that indicates a late arrival (compared with the early arrival required for the two-impulse optimal transfers), but it reduces the cost less than three percent relative to the optimal two-impulse cost. Although the additional impulse has a small impact on the total cost, it substantially alters the distribution of the

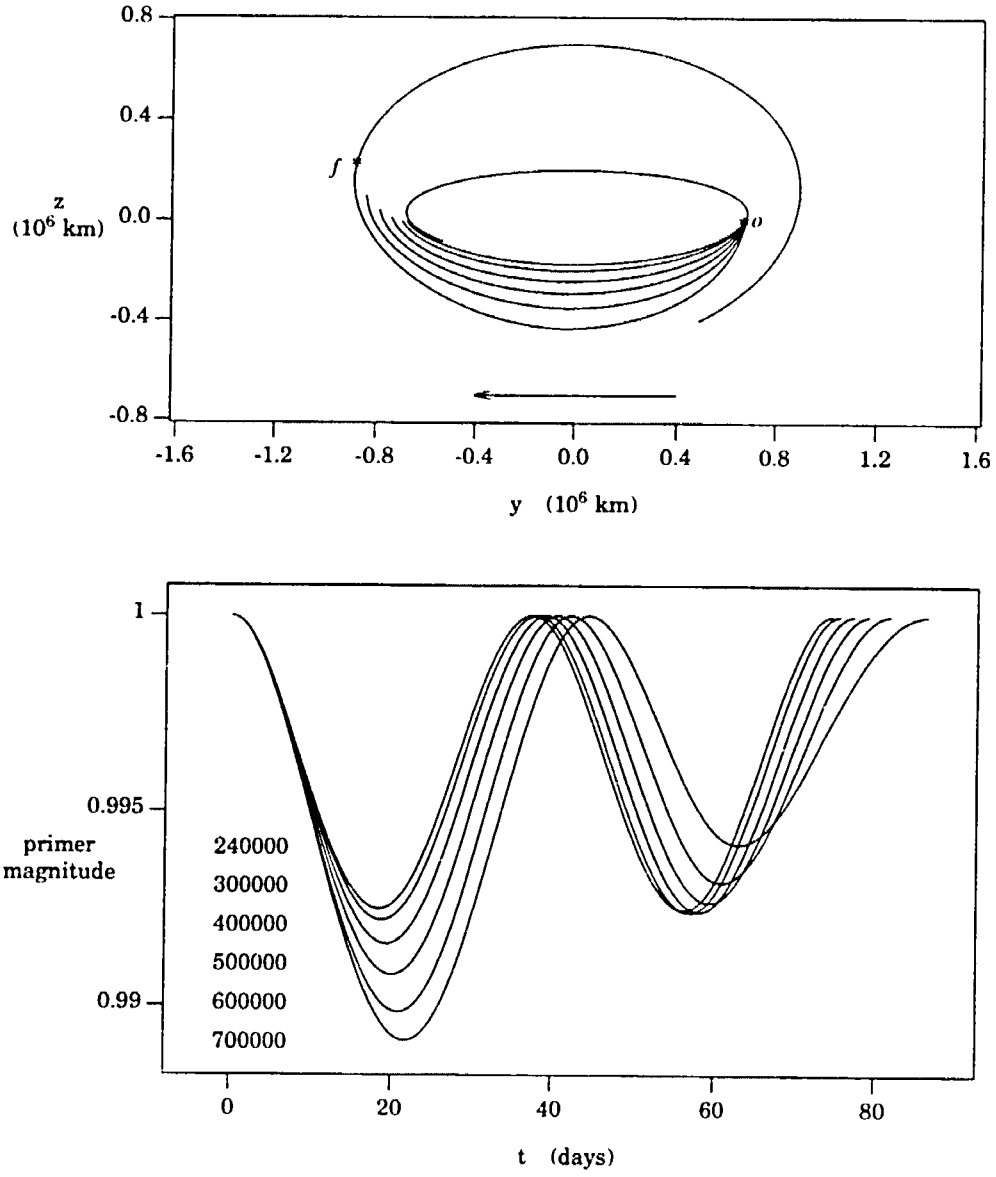

Figure IV.12 200,000 km Negative z Family: Optimal Three-Impulse Solutions.

total ΔV (see Tables A.5 and A.6). As the arrival amplitude increases, the influence of the interior impulse increases from eleven percent of the total ΔV in the 240,000 km solution to over twenty-four percent in the 700,000 km case. Representative costs for this family are plotted in Figure IV.13. The optimal costs for members of this family are less than the corresponding costs in the positive z family. At one end, the cost of the transfer to a 240,000 km halo is 4.8% less than the positive z transfer cost; for transfer to the largest halo, that is, A_z equal to 700,000 km, the optimal ΔV for a transfer below the x – y plane (negative z) is 8.4% less than the corresponding positive z solution; the differences in other cases are within the range defined by these bounds. The slope of the curve is consistent with that found in Figure IV.11.

3. Negative z Family: 240,000 km A_z Departure Halo Orbit

A third family of superior transfers associated with motion in a negative $\hat{z}$ direction is represented by transfers from an initial halo with out-of-plane amplitude equal to 240,000 km to final halos with amplitudes: 300,000; 400,000; 500,000; 600,000; and 700,000 km. Costs for nominal solutions with endpoints at locations where z is zero on the halo orbits are included in Table IV.5. Consistent with conclusions established for other superior transfers

Final A_z	Nominal 2-Impulse		Optimal 2-Impulse		Nominal 3-Impulse		Optimal 3-Impulse	
	ΔV	TOF	ΔV	TOF	ΔV	TOF	ΔV	TOF
km	m/s	days	m/s	days	m/s	days	m/s	days
300000	30.18	75.92	26.47	62.34	26.45	62.34	26.22	76.34
400000	84.61	75.48	72.52	60.73	72.41	60.73	71.46	77.89
500000	142.26	74.98	120.46	59.48	120.21	59.48	118.02	79.71
600000	200.94	74.42	169.74	58.52	169.30	58.52	165.25	82.07
700000	258.99	73.83	219.94	57.80	219.24	57.80	212.57	86.10

Table IV.5 240,000 km Negative z Family: Transfer Costs.

that exist primarily below the x – y plane, that is, in a negative $\hat{z}$ direction, solutions that achieve all conditions of optimality require three impulses. The optimal transfers are presented in Figure IV.14. The addition of the third impulse to the transfer produces only a small reduction in the cost (less than four percent of the optimal two-impulse cost), but optimizing the time and location of that maneuver, simultaneously with the endpoint locations, moves the arrival positions to locations that represent delayed arrivals on the halo orbits, compared with early arrivals that are required for optimal two-impulse solutions.

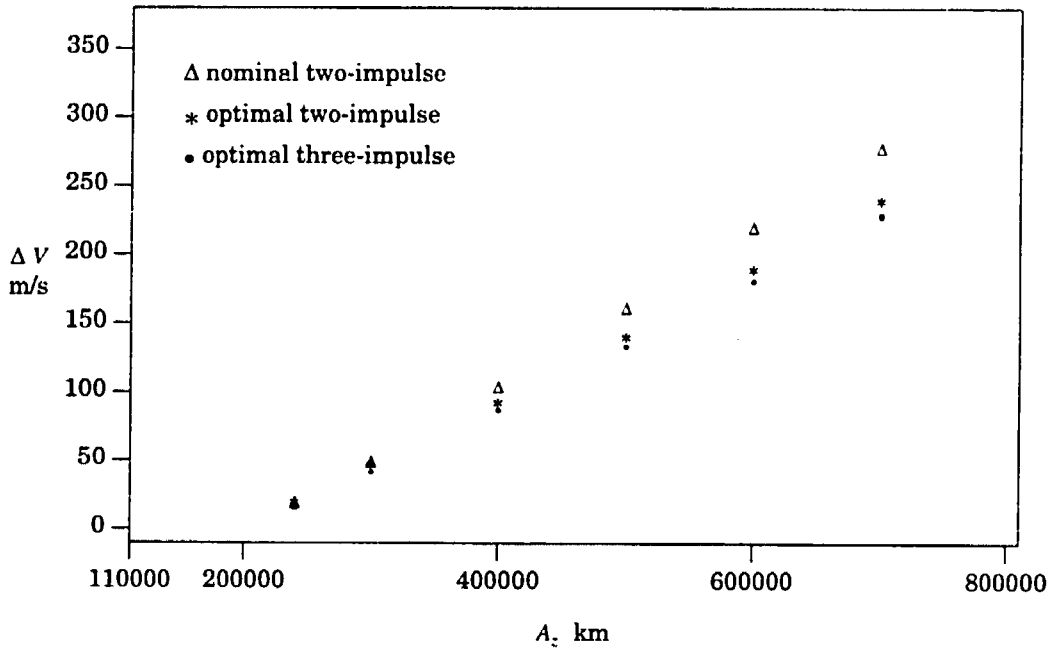

Figure IV.13 200,000 km Negative z Family: Arrival Amplitude — ΔV Relationship.

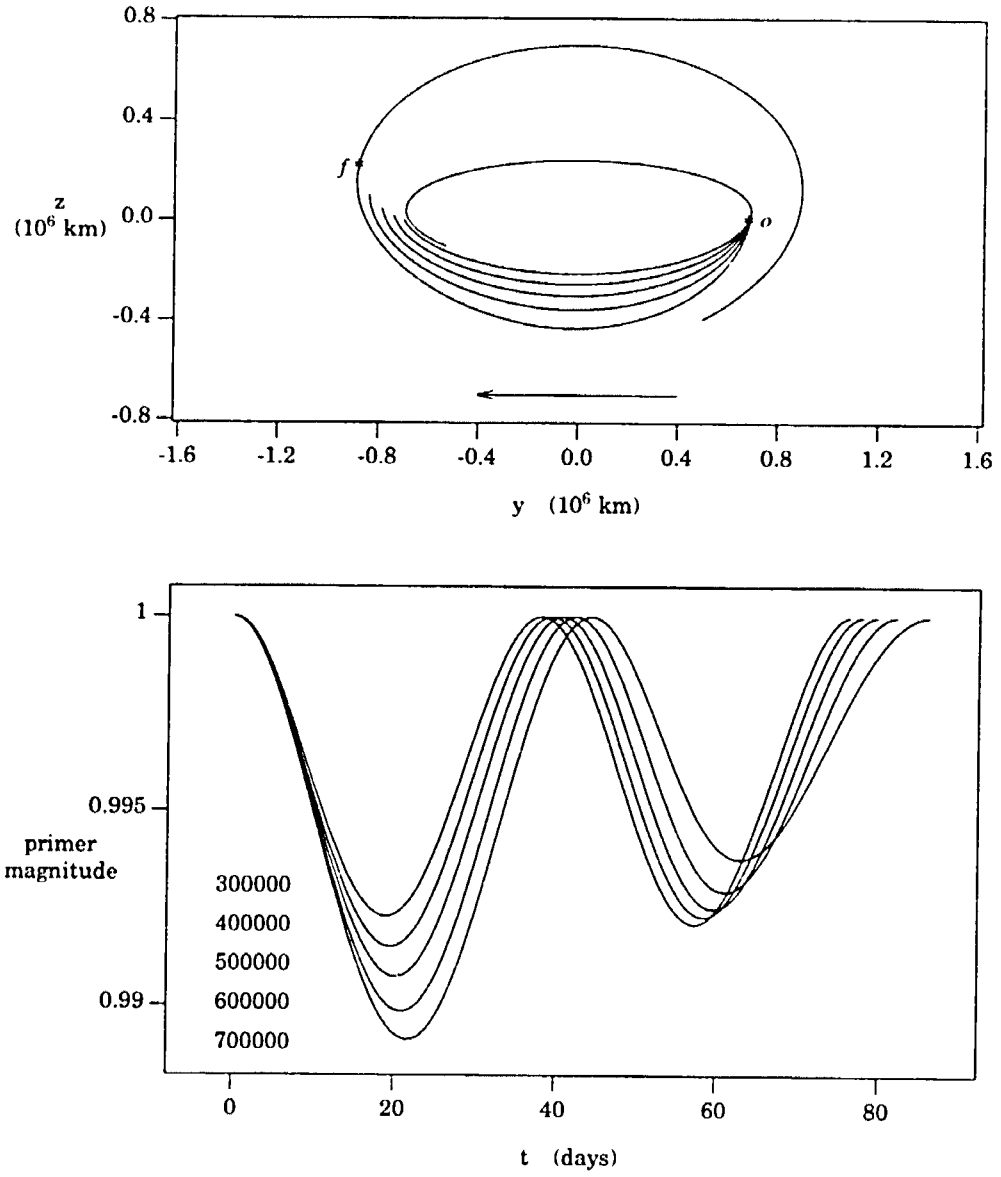

Figure IV.14 240,000 km Negative z Family: Optimal Three-Impulse Solutions.

The plot of the transfer costs versus the arrival amplitudes (Figure IV.15) also emphasizes that the trends established by other optimal solutions that include motion in a negative z direction are maintained.

For all sets of nominal endpoints that are considered in this study (including many combinations that are not discussed in this document), the optimization procedure converges to a solution that is equivalent to either a positive z solution or a negative z transfer, as represented by the two types of families discussed previously (to within defined numerical tolerances). If continuation is employed, however, additional solutions are possible that retain the general characteristics of these families but possess slightly altered shapes. Also, for superior transfers from halos with amplitudes equal to 110,000, 200,000, and 240,000 km, to an 800,000 km destination halo, continuation is necessary to achieve an optimal three-impulse solution that is below the x – y plane, that is, a negative z transfer. Optimal two-impulse solutions and nominal three-impulse transfers to the 800,000 km halo can be computed as direct transfers from the selected departure halo to the 800,000 km orbit; however, to achieve an optimal three-impulse solution, a transfer to a smaller halo is required to supply a first guess. The nominal three-impulse transfer computed using the primer vector to evaluate the appropriate interior maneuver, with endpoints at the locations determined in the optimal two-impulse solution, does not provide an adequate nominal solution for convergence to an optimal three-impulse transfer. Both the cost and shape of the solutions computed using continuation are influenced by the size of the halo orbit used to provide the improved nominal three-impulse path.

To illustrate the effects of a continuation procedure, two optimal three-impulse transfers from a 240,000 km halo to an 800,000 km halo are plotted in Figure IV.16. Both transfers are below the x – y plane, that is, negative z transfers. The solution labeled as '300000' uses the transfer to the 300,000 km halo (in Figure IV.14) to compute the first guess. The '600000' transfer is generated from the 600,000 km member of the 240,000 km A_z, negative z family (Figure IV.14). Both of the solutions are optimal impulsive transfers between the 240,000 and 800,000 km halos as shown by the two primer histories; however, the negative z excursions in both solutions in Figure IV.16 are less than that predicted by the trends in Figure IV.14. In all transfer families that have been previously presented, increasing the amplitude of the arrival halo increases the maximum z excursion of the transfer (in magnitude) (relative to transfers to smaller halo orbits); however, when this type of continuation is employed, the maximum z excursion associated with the transfer is generally less than that of the transfer used to produce the nominal solution. Also, the excursions of the solutions in the positive z direction in Figure IV.16 (the shifts in the arrival positions away from the location where z is zero) are less than that predicted by the trends

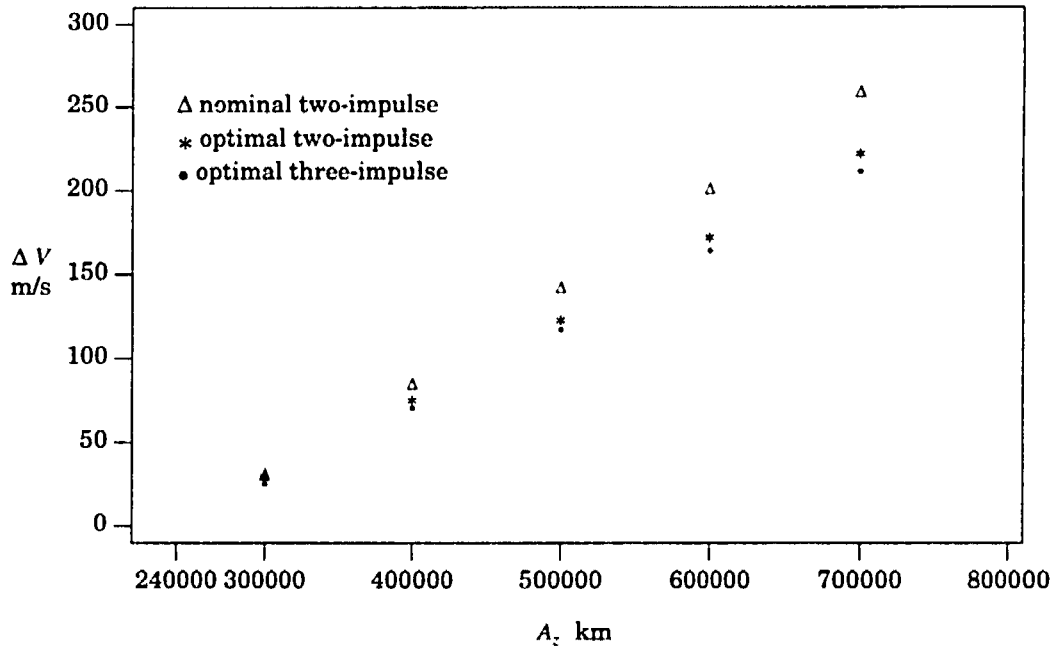

Figure IV.15 240,000 km Negative z Family: Arrival Amplitude — ΔV Relationship.

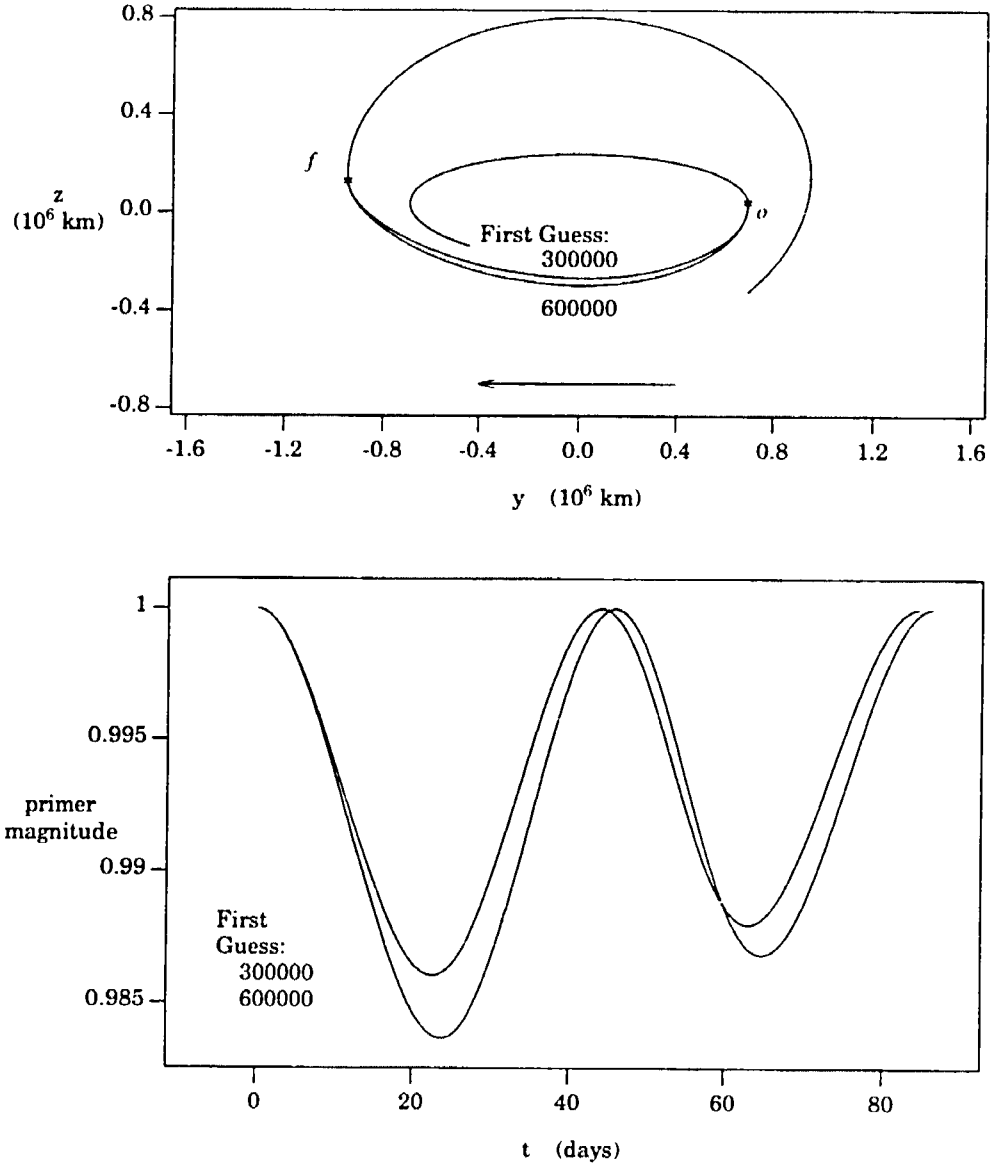

Figure IV.16 Optimal Transfers Computed Using Continuation.

associated with the arrival positions in Figure IV.14. Thus, the shapes of the solutions computed using continuation differ from the characteristics of family members computed with different procedures. The transfer cost is, however, consistent with that predicted by Figure IV.15. The cost for the '300000' solution is 263.15 m/s; the transfer cost in case '600000' is 262.55 m/s. Solutions computed using continuation that differ from those presented in the two types of families that have been discussed thus far are possible for all halo orbit combinations. Thus, many solutions exist that satisfy the necessary conditions for optimality for each pair of departure/arrival halo orbits; however, in all optimization problems that have been considered without the use of this type of continuation technique, the algorithm converges to one of the two classes of families that have been discussed. The necessity of continuation for the computation of optimal transfers to the 800,000 km halo (in the negative $\dot{z}$ direction) is believed to be the result of the large change in the arrival position that is required between the optimal two-impulse solution and the optimal three-impulse transfer and not necessarily the large difference in the amplitudes of the initial and final halos. It is possible to construct optimal three-impulse transfers to the 800,000 km halo without continuation if a nominal three-impulse path is defined with endpoints at the locations where z is zero (the endpoints used in the nominal two-impulse solutions). In this case, smaller coast arcs are required, and convergence is achieved. This contradicts the optimization steps that have been defined in this work (the results of the optimal two-impulse solutions are ignored), but it tends to support the conclusion that the difficulty is, in some respect, associated with the change in the endpoints.

C. Southern Halo Orbits

The previous discussion of superior transfers employs northern halo orbits for both the departure and arrival trajectories; however, transfers between southern halos of sizes similar to those considered in the northern families are available as mirror images of the northern solutions. A southern halo orbit can be computed from a corresponding northern halo by changing the sign of z and $\dot{z}$ in the state vector that defines the halo orbit. The symmetry of the equations of motion with respect to the z coordinate also permits a transfer path between southern halo orbits to be constructed from a transfer between northern halos.

To illustrate solutions for southern halos, a family of transfers is considered from a southern departure halo of A_z amplitude equal to 110,00 km to various southern halo orbits as the destination orbits. These target orbits are defined with A_z amplitudes equal to: 160,000; 200,000; 240,000; 300,000; 400,000; 500,000; 600,000; and 700,000 km. Optimal transfers between these pairs of halo orbits are presented in Figure IV.17. The solutions are

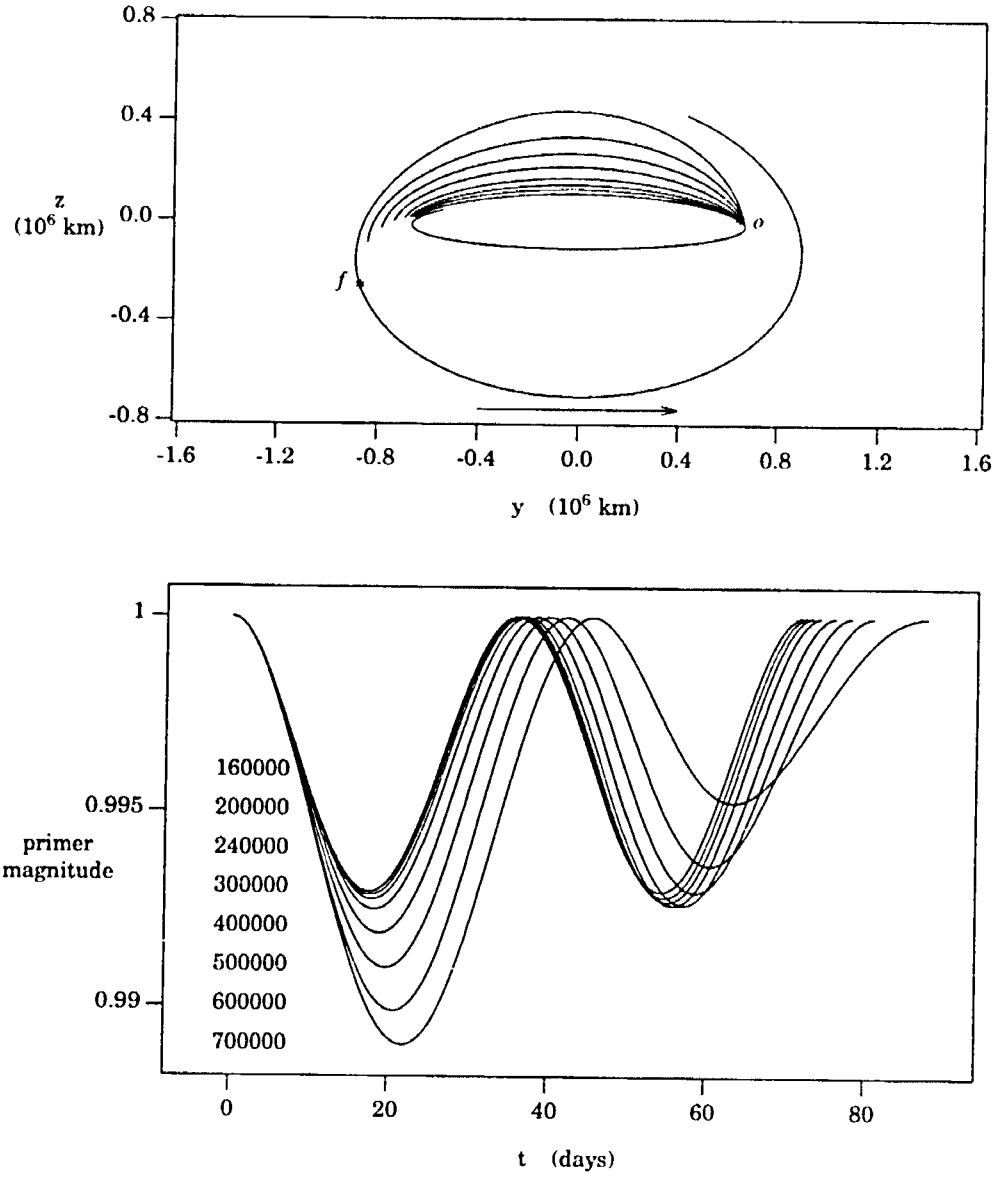

Figure IV.17 Family of Optimal Three-Impulse Superior Transfers Between Southern Halo Orbits.

symmetric about the $\hat{z}$-axis with respect to the northern trajectories presented in Figure IV.10. The magnitudes of the impulsive maneuvers are equal to those seen in Table IV.3; however, the out-of-plane component of the $\Delta\overline{V}$ vectors for the transfers between southern halos are the negative of the components of $(\Delta\overline{V} \cdot \hat{z})$ for their northern counterparts. The state transition matrix corresponding to a transfer between southern orbits is constructed by multiplying the entries that are associated with z and $\dot{z}$ (rows and columns three and six as developed in equation II.43) by negative one. Given this transformation and the sign changes in the $\Delta\overline{V}$'s, the solution for the mirror image primer is computed from equation III.67 as $\overline{p}_s = \{p_{1n}\ p_{2n}\ -p_{3n}\}^T$ where the primer vector for the northern halo solution is defined as $\overline{p}_n = \{p_{1n}\ p_{2n}\ p_{3n}\}^T$; therefore, the magnitude of the primer is unchanged. Thus, this discussion also identifies solutions between southern halo orbits, although it focuses on transfers between northern halos.

D. Inferior Transfers: Positive z Families

Given the two types of solutions that are available for superior transfers, similar classes of inferior transfers are sought. Optimal inferior transfers with motion generally above the $x-y$ plane (in a positive $\hat{z}$ direction) are available as time-free, two-impulse solutions. Optimal three-impulse transfers below the plane (negative $\hat{z}$) are also available. Northern halo orbits are used in the following examples; however, transfers between southern halo orbits can be constructed using the transformations discussed previously for superior solutions.

1. Positive z Family: 600,000 km A_z Departure Halo Orbit

A family of inferior transfers, represented by target halo orbits with amplitudes equal to: 110,000; 160,000; 200,000; 240,000; 300,000; 400,000; and 500,000 km, is constructed for a 600,000 km A_z departure halo orbit. The nominal departure position for each transfer is selected as the location along the 600,000 km departure halo orbit where the x component of acceleration is zero and y is negative. Locations where the x component of acceleration is zero and y is positive along each of the target halos are the nominal arrival positions. The $y-z$ projections of the nominal two-impulse transfers for this family are presented in Figure IV.18 with arcs of the 600,000 km departure halo and the 110,000 km arrival halo orbits also included. For inferior transfers, point o indicates the departure position for transfer to the largest destination halo orbit (the 500,000 km halo in this case); point f designates the arrival position on the smallest target halo orbit (the 110,000 km halo). The same nominal two-impulse departure position along the 600,000 km halo is employed in each of the nominal two-impulse solutions. The associated primer magnitude plots are

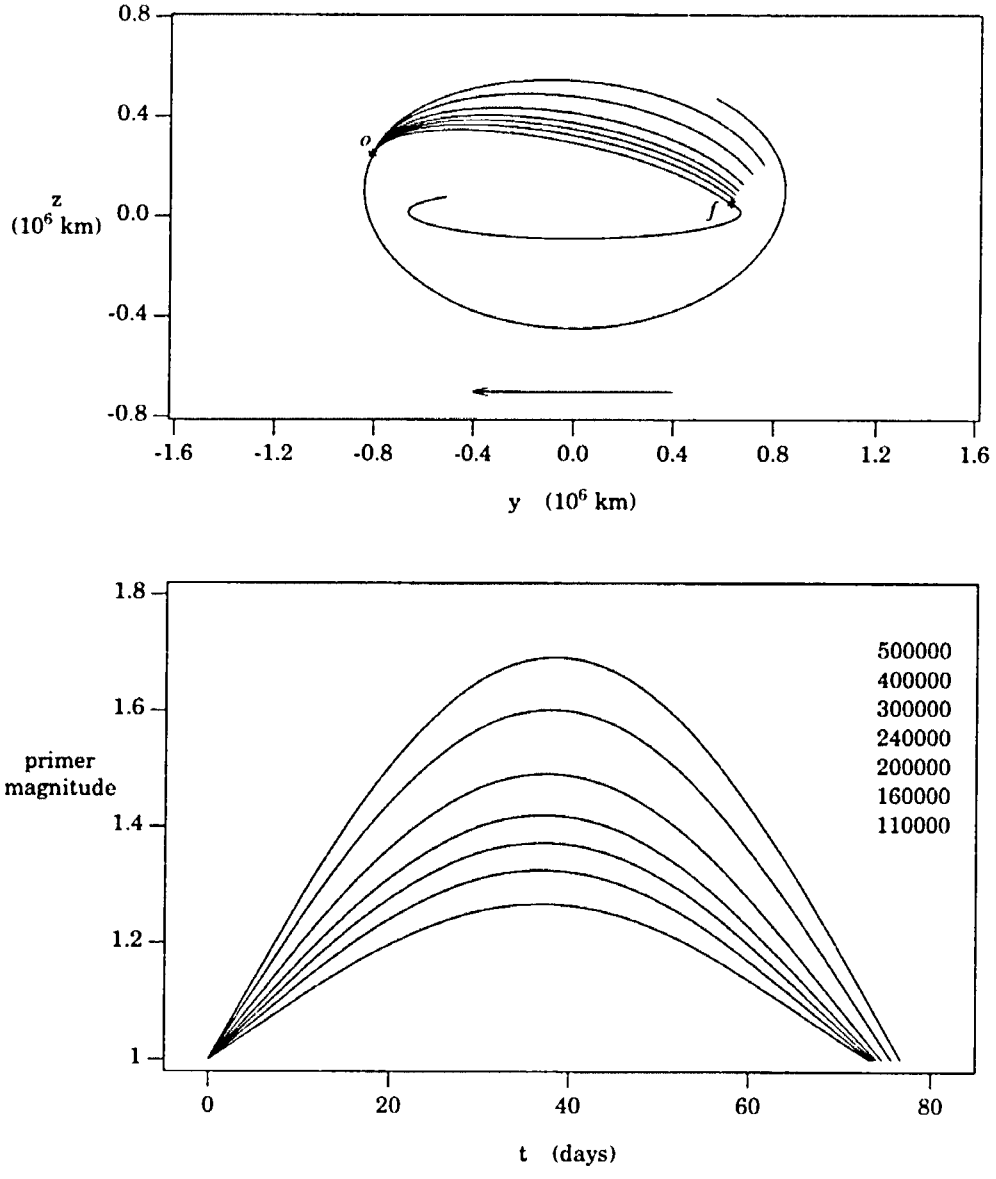

Figure IV.18 600,000 km Positive z Family: Nominal Two-Impulse Solutions.

included in the lower frame of the figure. In each case, the slopes of the primer are non-zero at the terminal times; therefore, coast arcs will reduce the cost.

Transfer costs for this family are given in Table IV.6. The entries in the first row of this

Final Halo A_z	Nominal 2-Impulse		Optimal 2-Impulse	
	ΔV	TOF	ΔV	TOF
km	m/s	days	m/s	days
110000	239.17	73.25	235.16	68.08
160000	219.58	73.44	214.52	67.23
200000	203.12	73.69	197.29	66.62
240000	185.95	74.00	179.47	66.08
300000	158.82	74.56	151.73	65.37
400000	109.96	75.61	103.18	64.44
500000	56.80	76.63	52.39	63.78

Table IV.6 600,000 km Positive z Family: Transfer Costs.

table (the 110,000 km case) are equivalent to entries in the row corresponding to a 600,000 km halo in Table IV.1. Entries in the third row (200,000 km A_z) are equivalent to data in the row for the 600,000 km solution in Table IV.2 for the 200,000 km A_z, positive z superior transfer family. This correspondence is indicative of similarities that exist among superior and inferior transfers that connect the same two halo orbits (in the circular problem). The terminal positions for a superior transfer can be transformed algebraically to those of an inferior solution between the same two halos using the symmetry of the halo orbits. If the departure state vector for a superior transfer is defined by $\overline{X}_o = \{x_o\ y_o\ z_o\ \dot{x}_o\ \dot{y}_o\ \dot{z}_o\}^T$, and the arrival state vector is $\overline{X}_f = \{x_f\ y_f\ z_f\ \dot{x}_f\ \dot{y}_f\ \dot{z}_f\}^T$, the corresponding initial state vector for an inferior solution is defined $\overline{X}_{oi} = \{x_f\ -y_f\ z_f\ -\dot{x}_f\ \dot{y}_f\ -\dot{z}_f\}^T$, and the state vector at arrival for the inferior transfer is $\overline{X}_{fi} = \{x_o\ -y_o\ z_o\ -\dot{x}_o\ \dot{y}_o\ -\dot{z}_o\}^T$. (The subscript i indicates that the state is associated with an inferior transfer.) The cost for the transformed solution is equivalent to the cost for the original path; however, the signs of the components of the $\Delta\overline{V}$ vectors reflect the changes in the state vectors. If the departure, interior, and arrival impulses for a superior three impulse transfer are defined as $\Delta\overline{V}_o = \{dv_{o1}\ dv_{o2}\ dv_{o3}\}^T$, $\Delta\overline{V}_m = \{dv_{m1}\ dv_{m2}\ dv_{m3}\}^T$, and $\Delta\overline{V}_f = \{dv_{f1}\ dv_{f2}\ dv_{f3}\}^T$, respectively, the departure, interior, and arrival maneuvers for the corresponding inferior solution are given by $\Delta\overline{V}_{oi} = \{dv_{f1}\ -dv_{f2}\ dv_{f3}\}^T$, $\Delta\overline{V}_{mi} = \{dv_{m1}\ -dv_{m2}\ dv_{m3}\}^T$, and $\Delta\overline{V}_{fi} = \{dv_{o1}\ -dv_{o2}\ dv_{o3}\}^T$. This type of transformation is only possible for transfers

between symmetric (and, therefore, periodic) orbits since the transformed position vector is not necessarily included in the new departure or target trajectory if the original orbit is not symmetric. Therefore, inferior transfers are considered in this work independently of the corresponding superior solutions to evaluate the application of the algorithm to the construction of inferior transfers. (Recall, the optimization algorithm does not rely on any specific characteristics of the halo orbits.) Small differences in inferior and superior solutions that are computed independently may exist due to the use of finite numerical tolerances in the test for optimality. For positive z families, the solutions are equivalent to within the two decimal places presented in the tables of this report; however, in negative z transfers that require larger changes relative to the nominal solutions and, therefore, more computations, minor variations between superior and corresponding inferior solutions are evident. Such differences are generally less than one percent of the quantity in which the difference occurs (and in most cases substantially less than one percent).

Optimal superior positive z transfers are time-free, two-impulse solutions to the optimization problem; therefore, corresponding optimal inferior transfers are also two-impulse trajectories. The optimal transfers for the 600,000 km A_z, positive z family are plotted in Figure IV.19 with the associated primer histories. Zero slopes in the primer history at the endpoints of each solution indicate optimal coast arcs. Also, the derivative of each primer is continuous across the interior impulse, and the magnitude of each primer is less than one at all interior times. Thus, the solutions satisfy all necessary conditions for optimality. The costs for this family are plotted in Figure IV.20 versus the target amplitude. A slope of approximately 45 to 50 m/s per $-100{,}000$ km change in amplitude is predicted, as expected given the symmetry of the solutions to existing results. In inferior transfer families, the 50 m/s value provides a better approximation for transfers to large halo orbits (consistent with the conclusion from analysis of the superior families), but, in terms of the change in amplitude, the 45 m/s per $-100{,}000$ km slope yields a better approximation for large changes from the departure halo. This conclusion agrees with the slope in Figure IV.3, for example, corresponding to superior families; that is, the 45 m/s value is appropriate for small target amplitudes while the 50 m/s approximation is a better slope for large target amplitudes.

2. Positive z Family: 700,000 km A_z Departure Halo Orbit

A second family of inferior transfers with a path predominantly above the $x-y$ plane (the positive $\hat{z}$ direction) is defined by a departure halo with out-of-plane amplitude equal to 700,000 km. In this case, the following target halo amplitudes are considered: 110,000; 200,000; 240,000; 300,000; 400,000; 500,000; and 600,000 km. The nominal transfer costs,

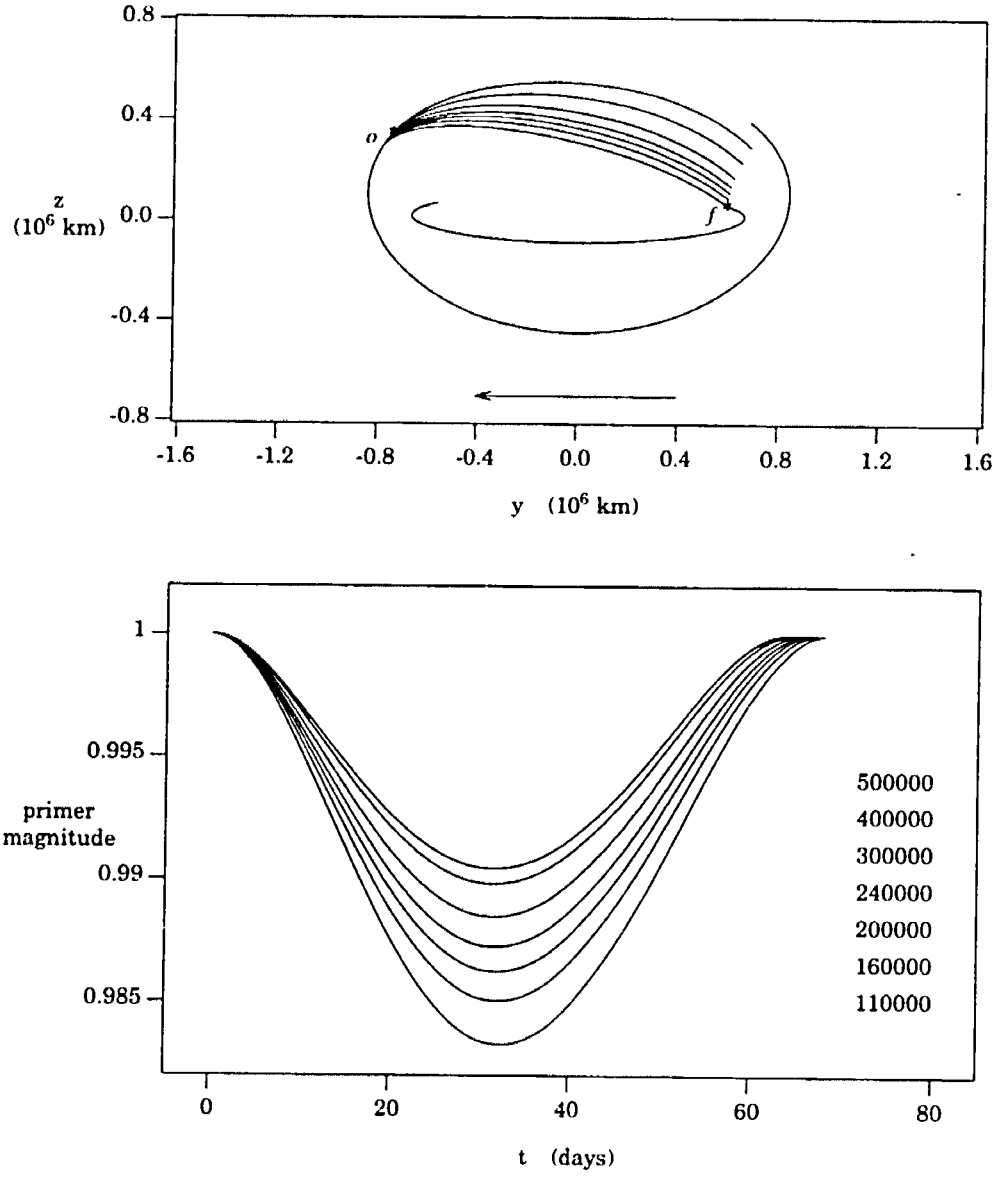

Figure IV.19 600,000 km Positive z Family: Optimal Two-Impulse Solutions.

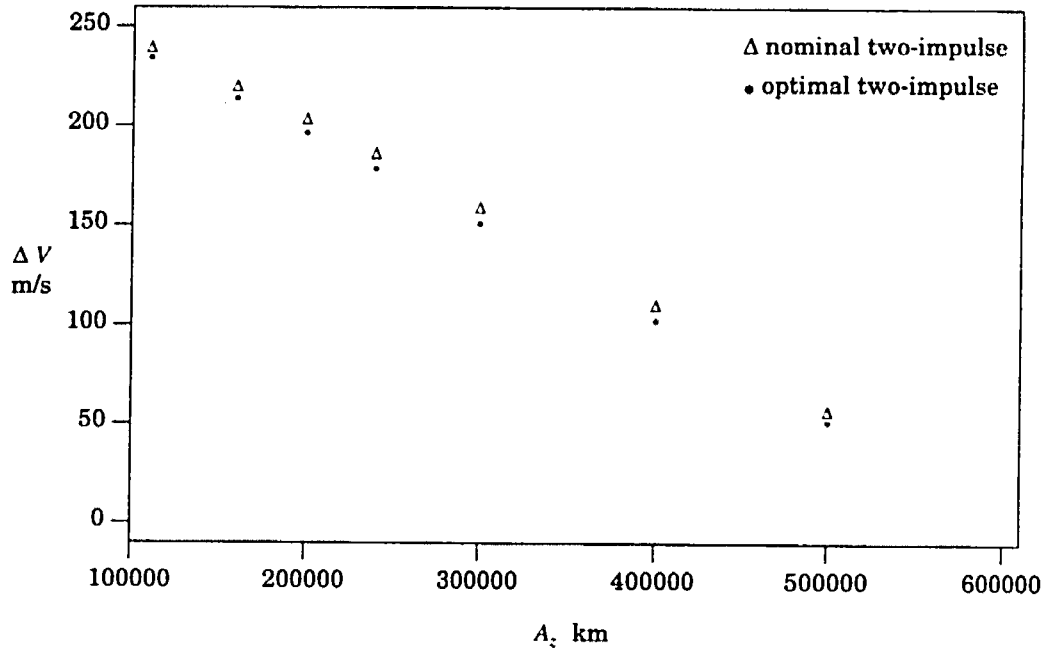

Figure IV.20 600,000 km Positive z Family: Arrival Amplitude — ΔV Relationship.

using endpoint locations defined as the positions where the x components of acceleration are zero, are included in Table IV.7. The rows in this table for transfer to the 110,000

Final Halo A_z	Nominal 2-Impulse		Optimal 2-Impulse	
	ΔV	TOF	ΔV	TOF
km	m/s	days	m/s	days
110000	295.42	73.06	288.38	67.18
160000	276.22	73.29	267.78	66.44
200000	260.07	73.56	250.57	65.91
240000	243.20	73.91	232.78	65.43
300000	216.54	74.53	205.06	64.82
400000	168.44	75.74	156.56	64.02
500000	115.91	76.98	105.78	63.46
600000	59.48	78.07	53.41	63.12

Table IV.7 700,000 km Positive z Family: Transfer Costs.

km and 200,000 km halos are equivalent to the rows for transfer to a 700,000 km halo in Tables IV.3 and IV.6, respectively, consistent with the symmetry that exists for superior and inferior transfers between halo orbits in the circular problem. The solutions for this family are plotted in Figure IV.21. Consistent with other superior and inferior transfer families with paths above the $x-y$ plane (positive $\dot{z}$), optimal impulsive solutions exist that include only two-impulses. The costs in Figure IV.22 are plotted versus the amplitude of the arrival halo orbits. The slope of the curve is approximately equal to that of other positive z transfer families.

3. Positive z Family: 800,000 km A_z Departure Halo Orbit

Various arrival halo orbits are used to construct another family of inferior transfers with paths of motion that are generally above the $x-y$ plane (positive $\dot{z}$). The departure orbit is defined with an amplitude equal to 800,000 km; the destination halos are generated with the following amplitudes: 110,000; 160,000; 200,000; 240,000; 300,000; 400,000; 500,000; 600,000; and 700,000 km. In this family, the transfers to the 110,000 km and 200,000 km halos are similar to the superior transfers to an 800,000 km halo from the 110,000 and 200,000 km halos in the positive z families. The nominal and optimal transfer costs for members in this family are listed in Table IV.8 for nominal transfers computed with terminal positions where the x components of acceleration are zero. Consistent with the trends that

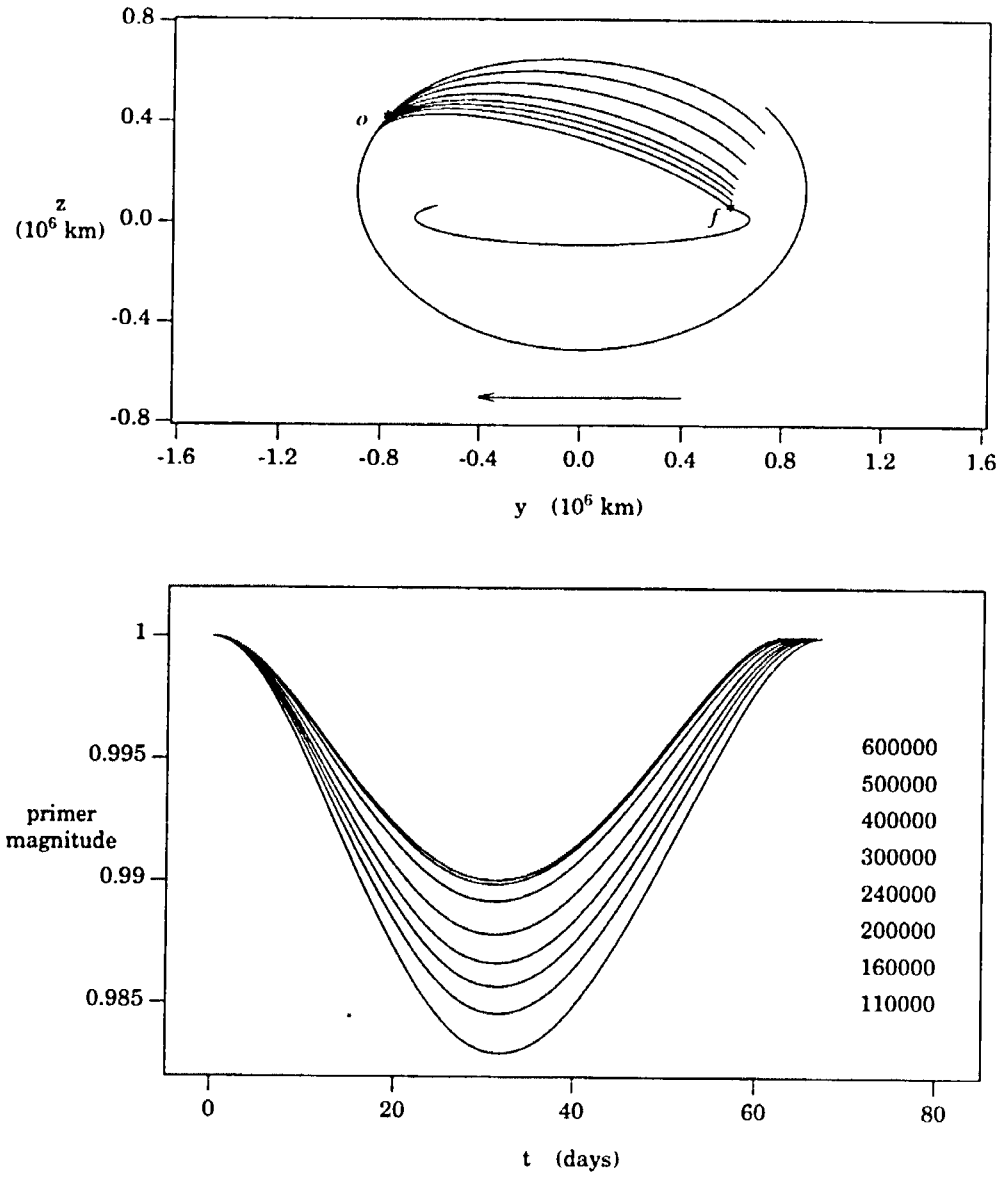

Figure IV.21 700,000 km Positive z Family: Optimal Two-Impulse Solutions.

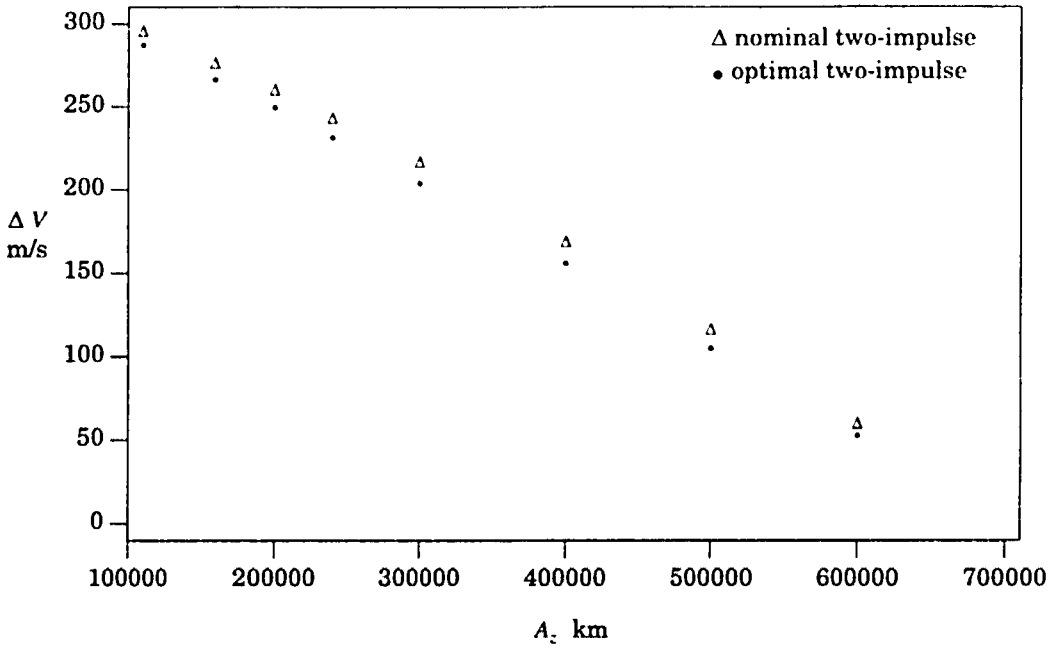

Figure IV.22 700,000 km Positive z Family: Arrival Amplitude — ΔV Relationship.

Final Halo A_z	Nominal 2-Impulse		Optimal 2-Impulse	
	ΔV	TOF	ΔV	TOF
km	m/s	days	m/s	days
110000	352.60	72.83	342.12	66.57
160000	333.77	73.08	321.55	65.91
200000	317.91	73.38	304.37	65.44
240000	301.36	73.74	286.60	65.02
300000	275.19	74.41	258.92	64.48
400000	227.97	75.74	210.46	63.79
500000	176.31	77.14	159.72	63.32
600000	120.57	78.45	107.37	63.05
700000	61.47	79.56	53.98	62.94

Table IV.8 800,000 km Positive z Family: Transfer Costs.

exist in other positive z families, optimal solutions are achieved with two impulses. Also, solutions are obtained without the use of continuation for each member of the family. The shapes of the optimal solutions in this family, plotted in Figure IV.23, are consistent with other inferior solutions that exist above the fundamental plane, that is, in a positive $\hat{z}$ direction. Also, the approximately linear relationship between the total ΔV and the change in the amplitude, indicated in Figure IV.24, maintains the same slope found in other positive z transfer families, that is, 45 to 50 m/s per $-100{,}000$ km.

E. Inferior Transfers: Negative z Families

Given the relationships that exist between superior and inferior transfers that connect pairs of halo orbits, the existence of inferior transfers with paths below the x – y plane (in a negative $\hat{z}$ direction) is expected. Such transfers are available as transformations of superior transfers or as solutions to the optimization algorithm given a nominal transfer that exists as a negative $\hat{z}$ solution.

1. Negative z Family: 500,000 km A_z Departure Halo Orbit

Members of a family of inferior transfers that depart from a 500,000 km halo orbit and arrive at halos with amplitudes equal to the following are considered: 110,000; 200,000; 240,000; 300,000; and 400,000 km. Consistent with the calculation of superior transfers computed in the negative $\hat{z}$ direction, nominal endpoints are selected at locations where z is zero. The nominal departure point is the position where z is zero and y is positive on the 500,000 km departure halo. At the nominal arrival position on each final halo orbit, z is zero and y is negative. The nominal transfers, and arcs corresponding to the 110,000 km halo orbit and the 500,000 km halo orbit, are plotted in Figure IV.25. The primer histories are also included in the figure. The transfer costs for the family are seen in Table IV.9. The costs and times listed in the first row of this table are equivalent to the entries in the 500,000 km row of Table IV.3 for the 110,000 km positive z family with the exception of the nominal three-impulse cost and the optimal three-impulse time. In Table IV.3, the nominal three-impulse cost is 173.57 m/s compared with a cost of 173.83 in Table IV.9; the optimal three-impulse time in Table IV.3 is 78.10 days compared with a time of 78.11 days in Table IV.9. Differences in the optimal solutions are the result of the numerous computations that are required to achieve optimal transfers in negative z families. Recall, in superior transfers that take place generally below the x – y plane (negative $\hat{z}$), the endpoints of the optimal transfer in each step are significantly different from the nominal terminal locations. Given the use of finite tolerances for the evaluation of optimality and the large shifts in

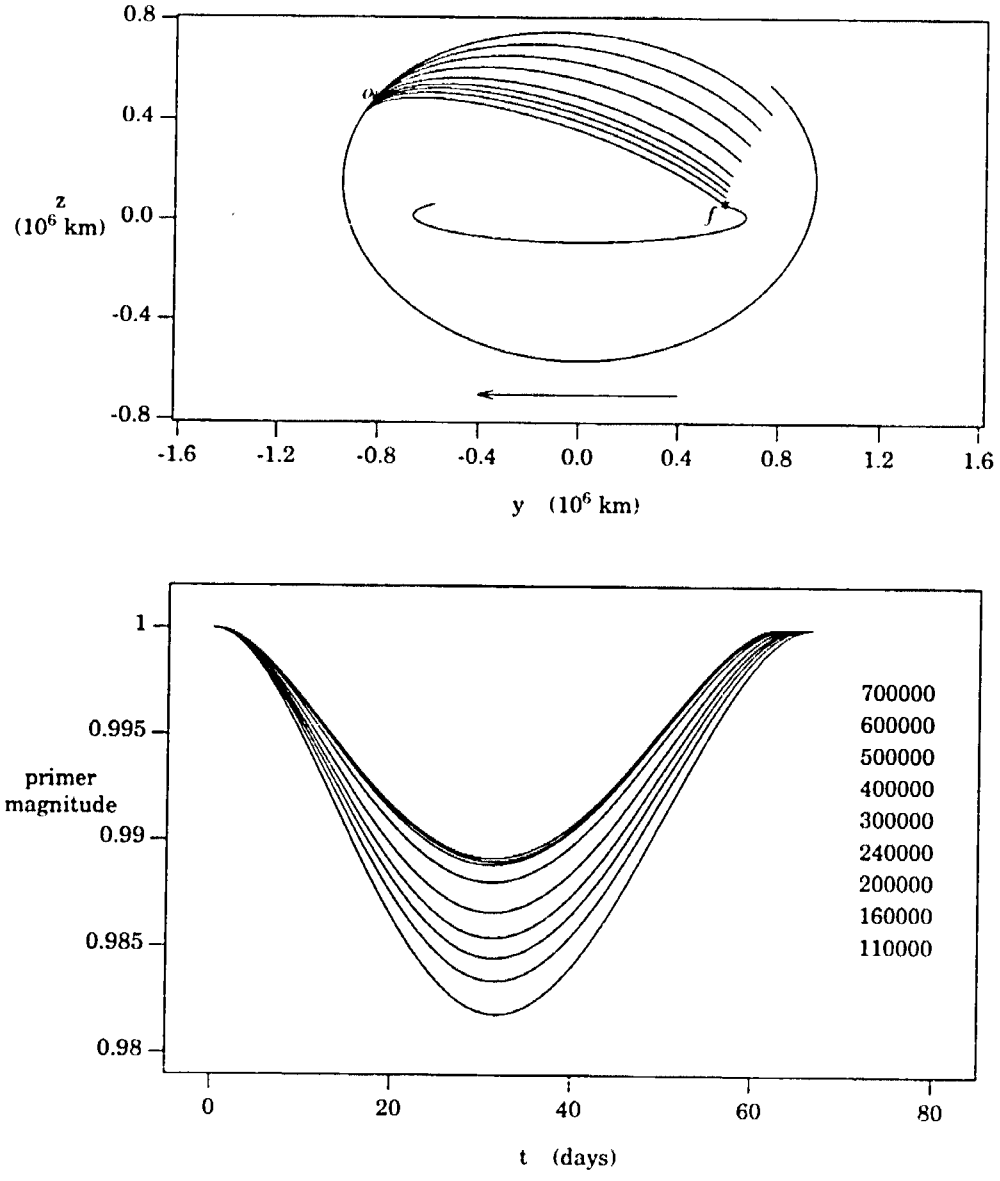

Figure IV.23 800,000 km Positive z Family: Optimal Two-Impulse Solutions.

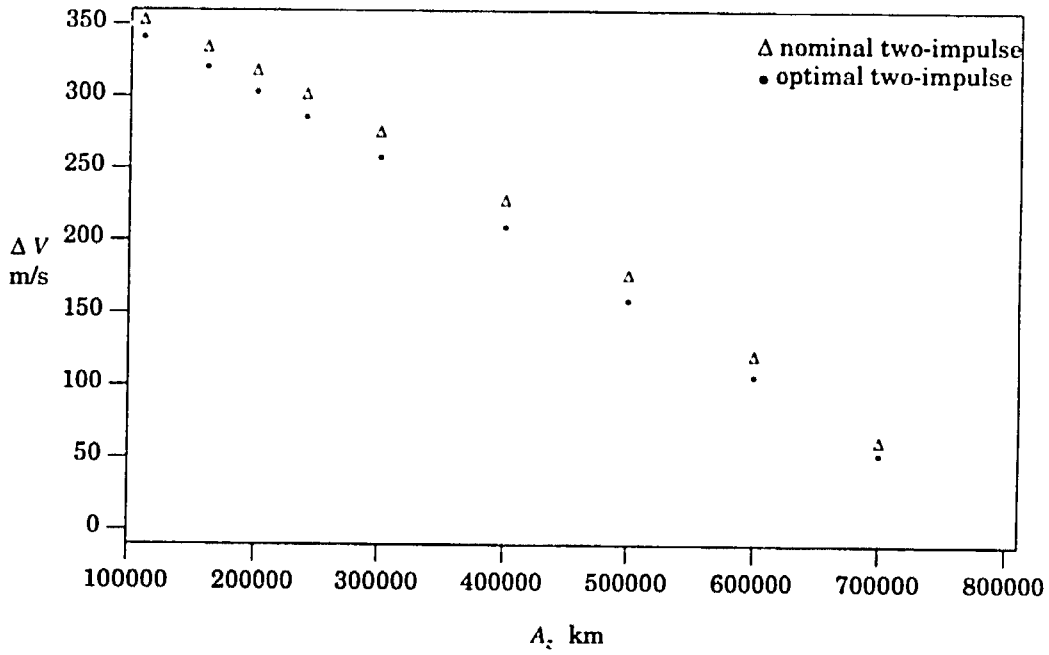

Figure IV.24 800,000 km Positive z Family: Arrival Amplitude — ΔV Relationship.

Final A_z	Nominal 2-Impulse		Optimal 2-Impulse		Nominal 3-Impulse		Optimal 3-Impulse	
	ΔV	TOF	ΔV	TOF	ΔV	TOF	ΔV	TOF
km	m/s	days	m/s	days	m/s	days	m/s	days
110000	197.86	75.32	173.78	61.44	173.83	61.44	171.54	78.11
160000	178.12	75.22	153.95	60.62	154.00	60.62	151.55	78.73
200000	160.81	75.11	137.47	60.02	137.51	60.02	135.01	79.23
240000	142.25	74.98	120.46	59.48	120.50	59.48	118.02	79.71
300000	112.29	74.74	94.05	58.75	94.08	58.75	91.81	80.43
400000	57.91	74.24	48.01	57.76	48.03	57.76	46.57	81.61

Table IV.9 500,000 km Negative z Family: Transfer Costs.

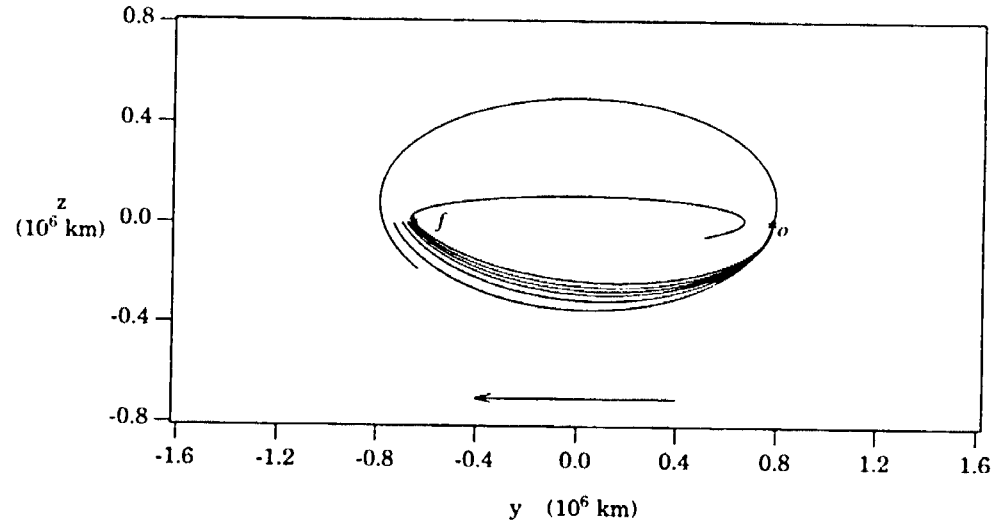

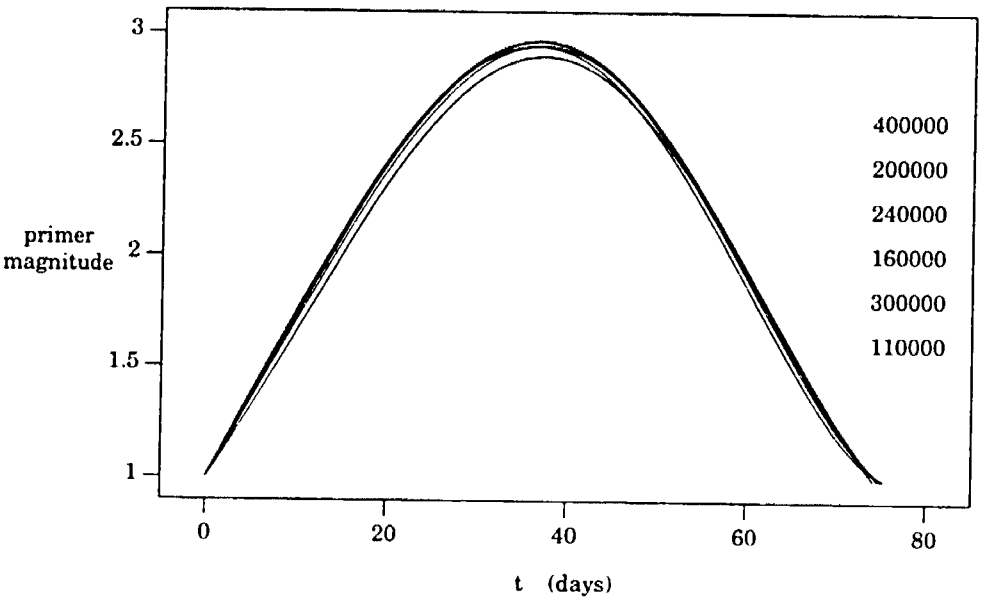

Figure IV.25 500,000 km Positive z Family: Nominal Two-Impulse Solutions.

the endpoints that are required, small variations among the optimal solutions are possible. Larger variations that exist between corresponding nominal three-impulse costs in the two types of families are primarily the result of the application of alternate assumptions in the algorithm. A comparison of the optimal two-impulse costs and the nominal three-impulse ΔV magnitudes listed in Table IV.9 indicates that each three-impulse ΔV is slightly larger than the corresponding two-impulse cost, although the purpose of the additional impulse is to reduce the total cost. As discussed in the development of the algorithm (section III.D.3), all assumptions employed in the derivation of the equations III.95 and III.99 (that define the position at which to apply a third impulse, and the magnitude and position of the maneuver) cannot be imposed simultaneously when the terminal positions of the transfer are constrained. In the families discussed previously, the nominal three-impulse path is constructed by calculating a value of $\Delta\overline{V}$ at the interior time and constraining the $\Delta\overline{V}$, while shifting the location of the impulse as required to achieve position continuity at the interior position. In the inferior transfer families, the nominal solutions are computed by constraining the location of the interior impulse and varying the $\Delta\overline{V}$. In general, fixing the $\Delta\overline{V}$ value yields a slightly lower cost than solutions that constrain the proposed interior position; therefore, the nominal (three-impulse) costs computed for inferior transfer families are higher than the costs that may be possible if the $\Delta\overline{V}$ were fixed. Nominal solutions were computed with fixed interior positions (rather than fixed interior $\Delta\overline{V}$'s) to test the impact of this assumption on the result of the subsequent optimization process. Although slightly higher transfer costs are achieved in nominal three-impulse solutions when the interior position requirement is imposed, the results of the optimization are generally consistent with optimal solutions computed using a nominal solution generated using a fixed interior $\Delta\overline{V}$.

The optimal inferior transfers representing this family and the associated primer histories are plotted in Figure IV.26. The solutions satisfy the requirements of the time-free problem, as indicated by zero primer slopes at the ends of the transfers. At the interior impulse time, the derivative of the primer is zero, and the derivative is continuous within defined standards; therefore, the time and location of the interior impulse are optimal. Finally, the magnitude of the primer is less than one at all non-impulse times. Thus, the solutions satisfy all necessary conditions for optimal time-free solutions. The costs for the family are plotted in Figure IV.27. Consistent with the conclusions reached in other families, Figure IV.27 predicts an approximately linear relationship between the target amplitude and the total ΔV.

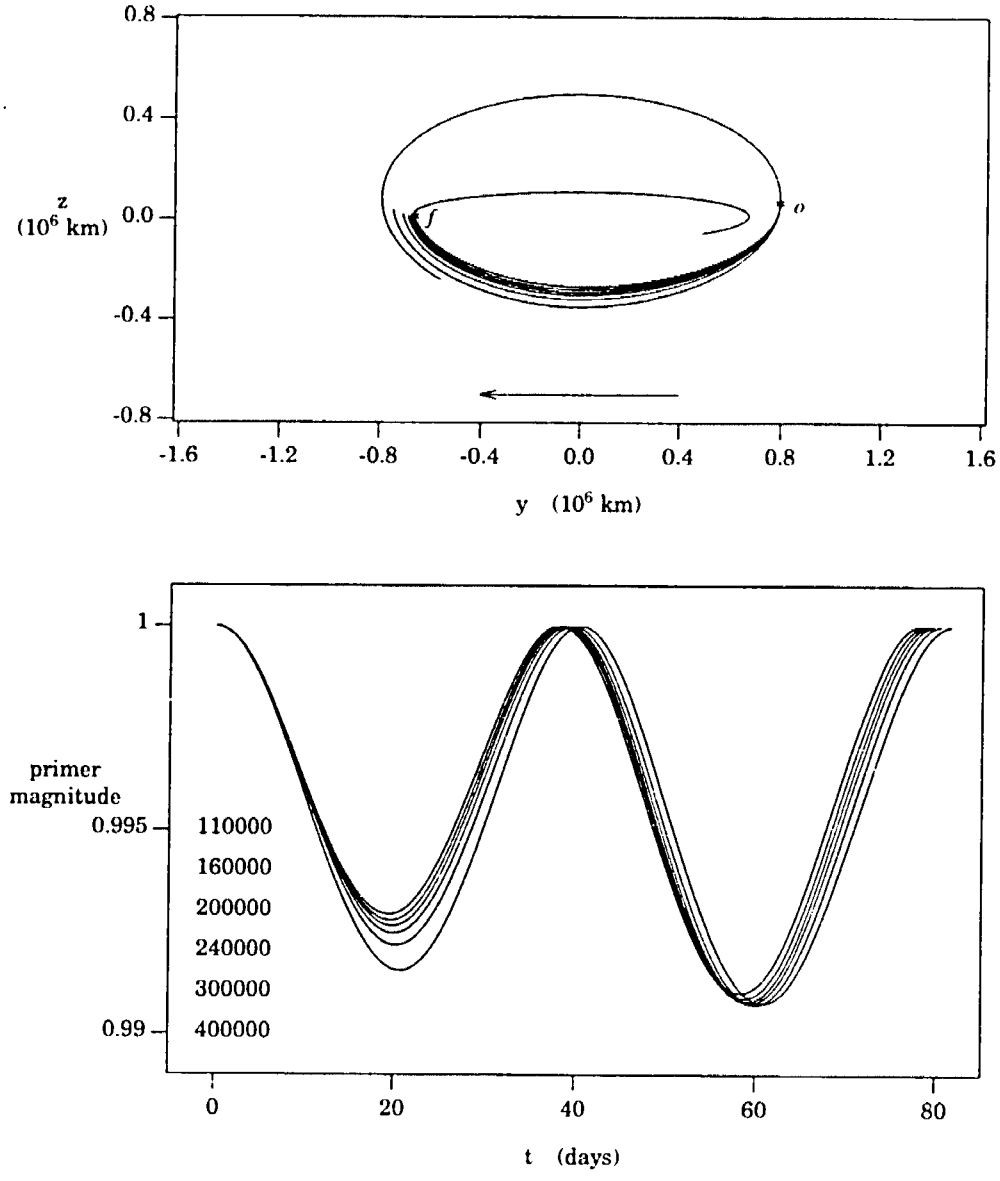

Figure IV.26 500,000 km Negative z Family: Optimal Three-Impulse Solutions.

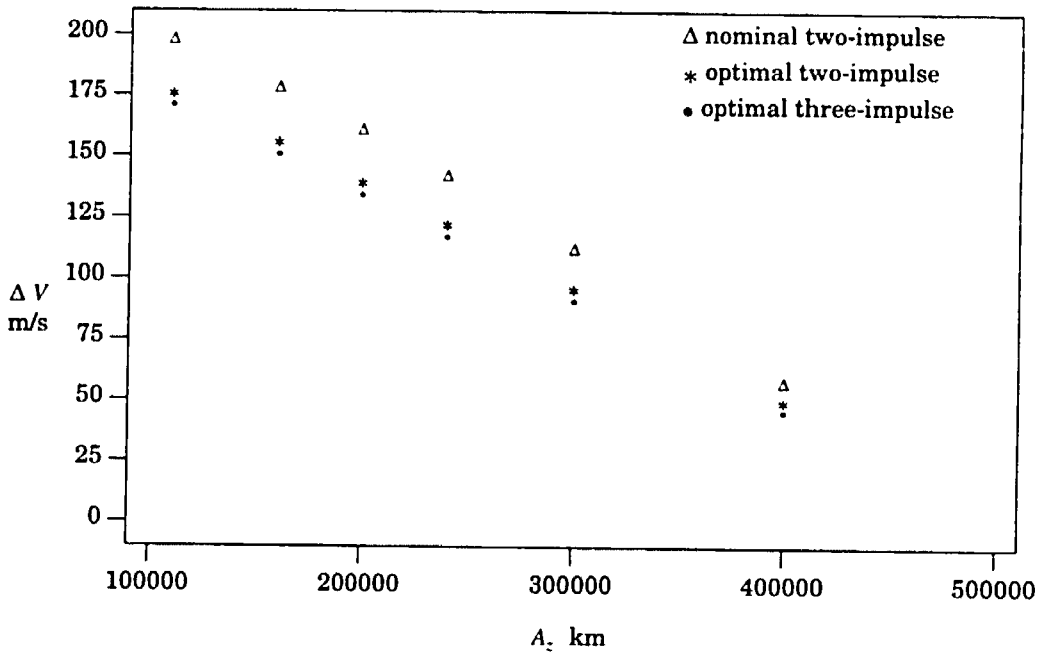

Figure IV.27 500,000 km Negative z Family: Arrival Amplitude — ΔV Relationship.

2. Negative z Family: 600,000 km A_z Departure Halo Orbit

A second family of optimal inferior solutions in the negative $\hat{z}$ direction is defined incorporating a 600,000 km A_z departure halo. Table IV.10 lists the transfer costs for the following target amplitudes: 110,000; 160,000; 200,000; 240,000; 300,000; 400,000; and 500,000 km. The optimal three-impulse transfers for this family are plotted in Figure IV.28

Final A_z	Nominal 2-Impulse		Optimal 2-Impulse		Nominal 3-Impulse		Optimal 3-Impulse	
	ΔV	TOF	ΔV	TOF	ΔV	TOF	ΔV	TOF
km	m/s	days	m/s	days	m/s	days	m/s	days
110000	256.05	74.78	222.87	60.18	222.97	60.18	218.72	80.95
160000	236.52	74.68	203.14	59.48	203.23	59.48	198.75	81.38
200000	219.37	74.57	186.70	58.98	186.80	58.98	182.22	81.73
240000	200.94	74.42	169.74	58.52	169.83	58.52	165.25	82.08
300000	171.16	74.17	143.39	57.91	143.47	57.91	139.05	82.59
400000	117.02	73.65	97.40	57.08	97.46	57.08	93.83	83.43
500000	59.22	73.01	49.41	56.47	49.43	56.47	47.27	84.35

Table IV.10 600,000 km Negative z Family: Transfer Costs.

with the corresponding primers. The transfers to orbits of amplitude 110,000, 200,000 and 240,000 km are symmetric about the $\hat{z}$ axis to those computed in the 110,000, 200,000, and 240,000 km negative z, superior transfer families, for transfer to the 600,000 km orbit. The corresponding table entries also indicate similarities in the solutions with only minor differences in related data. In agreement with the results found in other negative z families, the costs, plotted in Figure IV.29, predict a change in ΔV in the range of 43 to 48 m/s per 100,000 km decrease in the amplitude of the target orbit.

3. Negative z Family: 700,000 km A_z Departure Halo Orbit

The data for a negative z inferior transfer family, defined by a departure halo orbit of amplitude equal to 700,000 km, is presented in Table IV.11. The nominal solutions are constructed from endpoints located where z is zero, consistent with the definitions employed in other negative z inferior transfers. Rows corresponding to the 110,00 and 200,000 km halo orbits are consistent with corresponding entries in Tables IV.3 and IV.4 for transfer to a 700,000 km halo orbit, with small differences due to alternate assumptions in the computation of the nominal three-impulse paths and other numerical issues. The optimal solutions for this family are plotted in Figure IV.30; Figure IV.31 represents the relationship

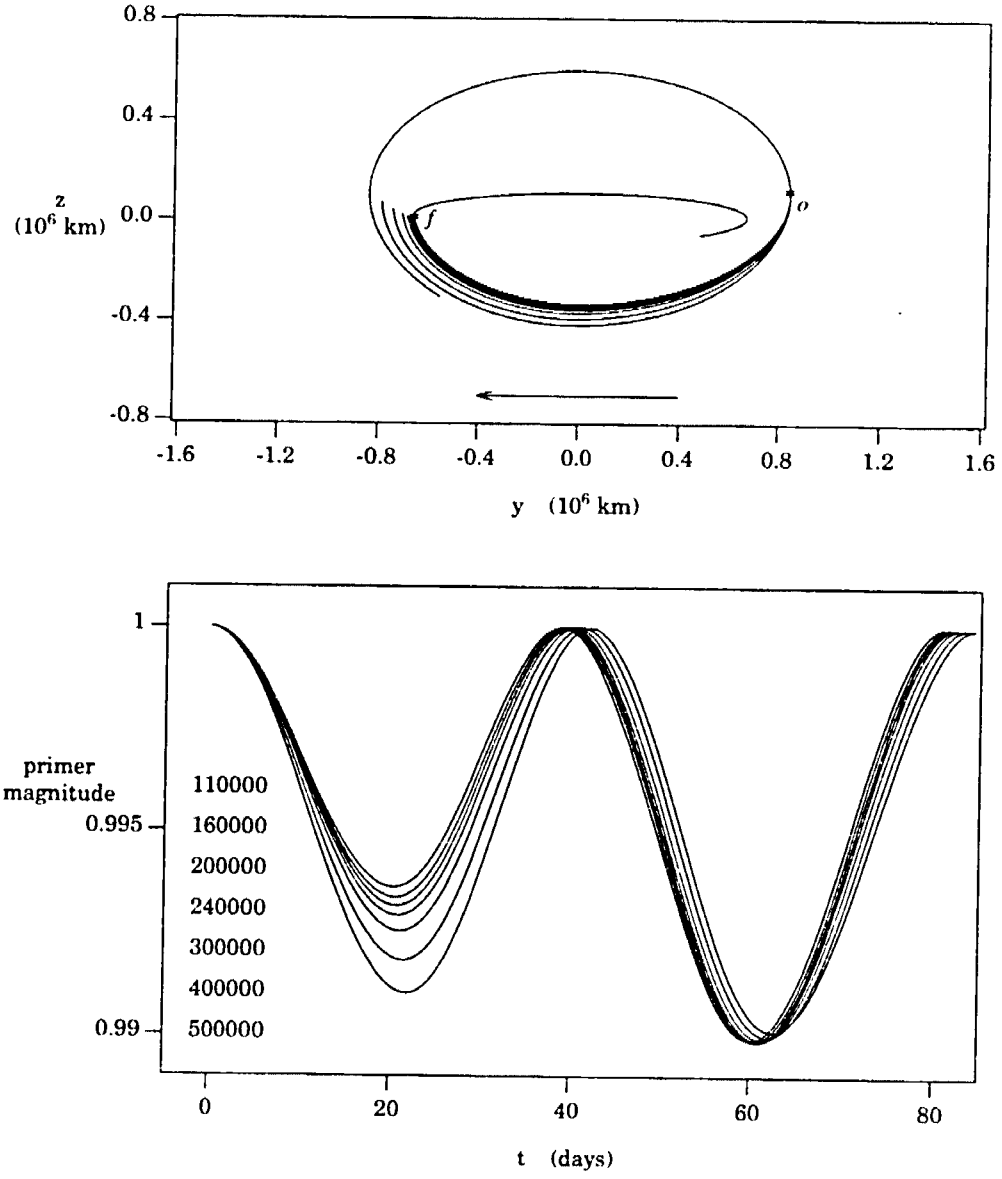

Figure IV.28 600,000 km Negative z Family: Optimal Three-Impulse Solutions.

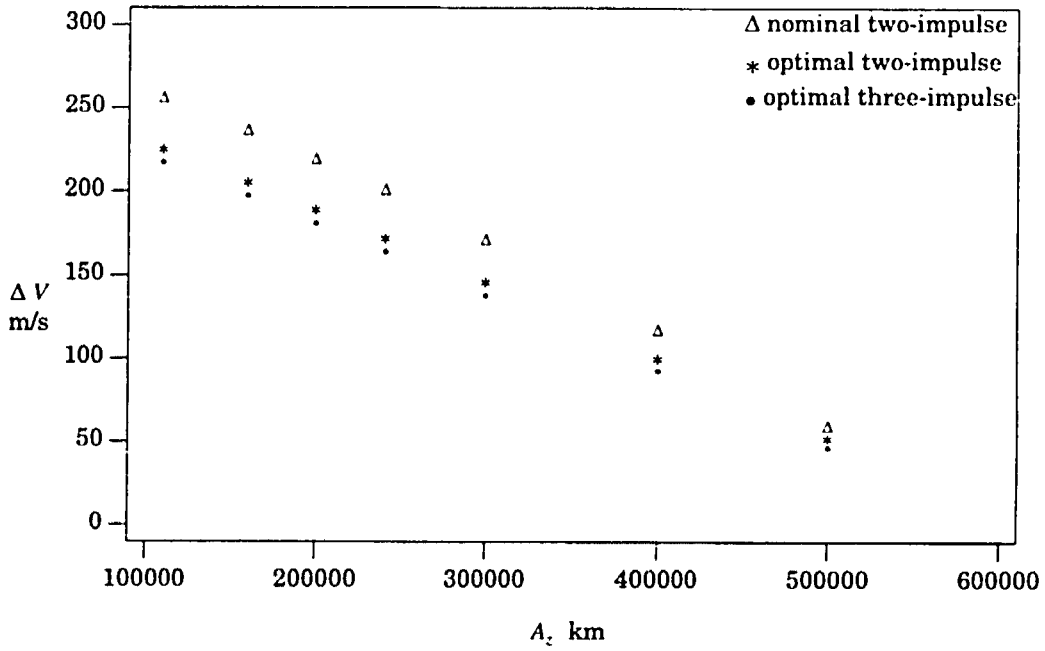

Figure IV.29 600,000 km Negative z Family: Arrival Amplitude — ΔV Relationship.

Final A_z	Nominal 2-Impulse		Optimal 2-Impulse		Nominal 3-Impulse		Optimal 3-Impulse	
	ΔV	TOF	ΔV	TOF	ΔV	TOF	ΔV	TOF
km	m/s	days	m/s	days	m/s	days	m/s	days
110000	313.67	74.20	272.86	59.21	273.03	59.21	265.89	87.81
160000	294.31	74.09	253.22	58.62	253.39	58.62	246.00	86.74
200000	277.29	73.98	236.85	58.19	237.02	58.19	229.51	86.32
240000	258.99	73.83	219.94	57.80	220.10	57.80	212.57	86.08
300000	229.40	73.56	193.65	57.29	193.80	57.29	186.41	85.95
400000	175.88	73.05	147.72	56.60	147.85	56.60	141.25	86.00
500000	118.05	72.33	99.76	56.10	99.84	56.10	94.73	86.33
600000	58.98	71.59	50.36	55.77	50.39	55.77	47.47	87.01

Table IV.11 700,000 km Negative z Family: Transfer Costs.

between the cost and the amplitude of the target halo orbit. This example emphasizes several trends realized in other negative z inferior solutions: three impulses are required to achieve optimality; the transfer predominantly exists below the plane of primary motion, that is, in the negative $\dot{z}$ direction; and a change in cost of approximately 43 to 48 m/s is required for each −100,000 km change in the arrival amplitude.

4. Application

To demonstrate one application of the transfers that have been presented in this work, a transfer from a circular Earth parking orbit of altitude 185 km to an L_1 halo orbit with an amplitude of 110,000 km is considered. The insertion cost at the halo orbit for a direct transfer between the two orbits is approximately 180 m/s[32]. In recent work, Barden has examined the transfer problem between the Earth and libration point orbits in search of a solution for which the insertion cost at the halo is zero, a "free" transfer[32]. Such solutions were shown to exist, but they arrive at halo orbits with relatively large out-of-plane amplitudes. Combining a solution of this type with an inferior transfer, such as one presented in this work, could potentially yield an Earth-to-halo transfer cost that is less than that required for transfer directly to halo orbits that are smaller than those available with free solutions. As an example, consider the specific transfer problem from an Earth parking orbit and the 110,000 km A_z halo orbit. A free transfer to a halo of this size is not available; however, a free insertion does exist for a halo with A_z equal to approximately 440,000 km. Thus, the complete path (Earth to 110,000 km halo orbit) is computed as three segments. First the free transfer between the Earth and the 440,000 km halo orbit is computed. Next, an optimal inferior transfer between the 440,000 km halo and the 110,000 km halo is generated. Finally, a coast arc along the 440,000 km halo orbit is determined that connects the arrival point for the first segment to the departure position for the inferior transfer.

Using the slope computed for the transfer families that have been presented here, a reduction in the amplitude of roughly 330,000 km should require a ΔV of approximately 142 m/s. This prediction is computed using the 43 m/s per 100,00 km slope predicted for inferior transfer families that are computed below the $x - y$ plane, in the negative $\dot{z}$ direction. (Note that it is not necessary to travel in the negative $\dot{z}$ direction; however, since the transfer costs for solutions in that direction are generally slightly smaller than corresponding positive z transfers, the negative direction is selected.) Thus, the three-step transfer should require a smaller total ΔV than the direct solution. To verify that assumption, an inferior transfer from the 440,000 km halo to the 110,000 km orbit is computed. The cost corresponding to

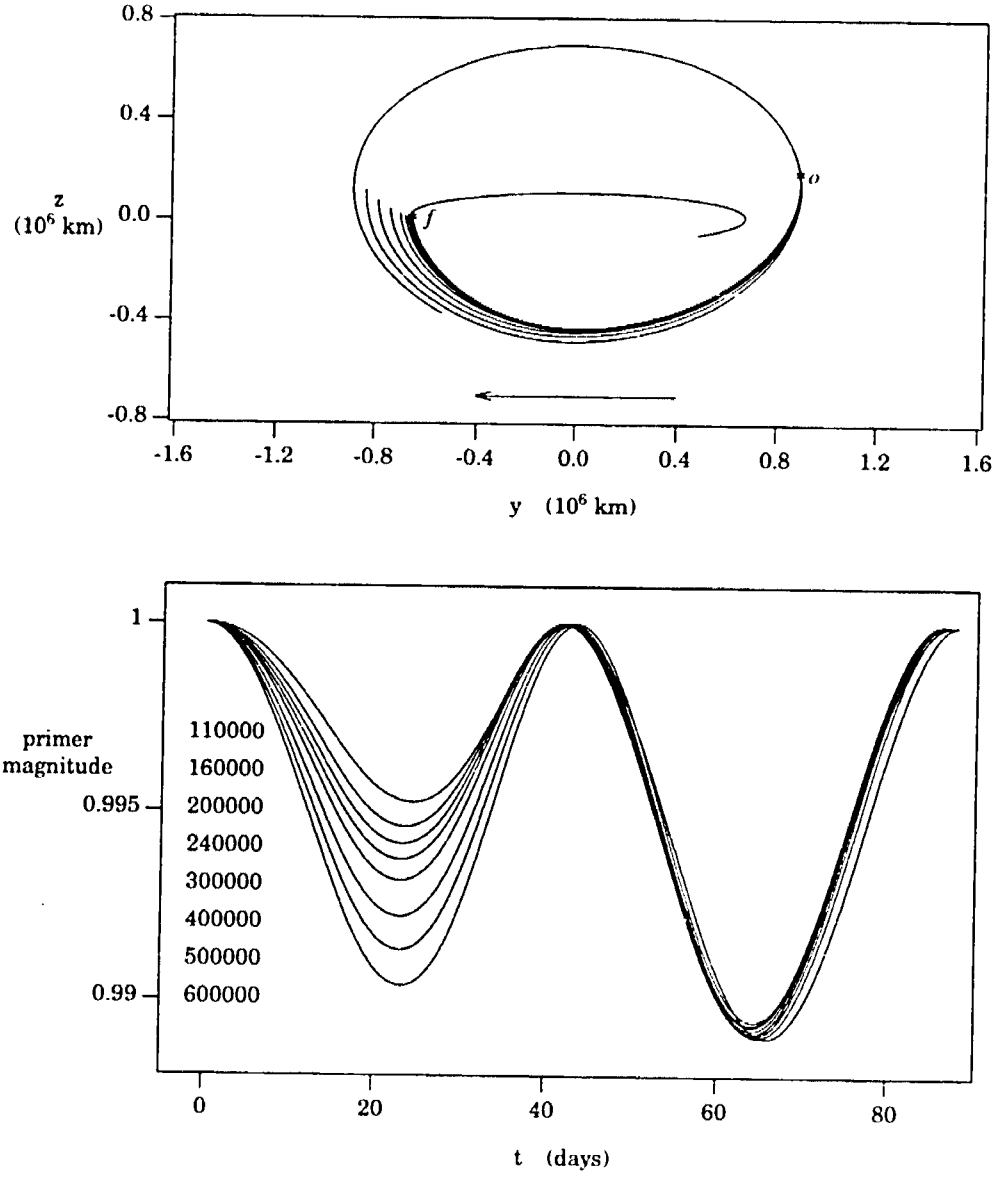

Figure IV.30 700,000 km Negative z Family: Optimal Three-Impulse Solutions.

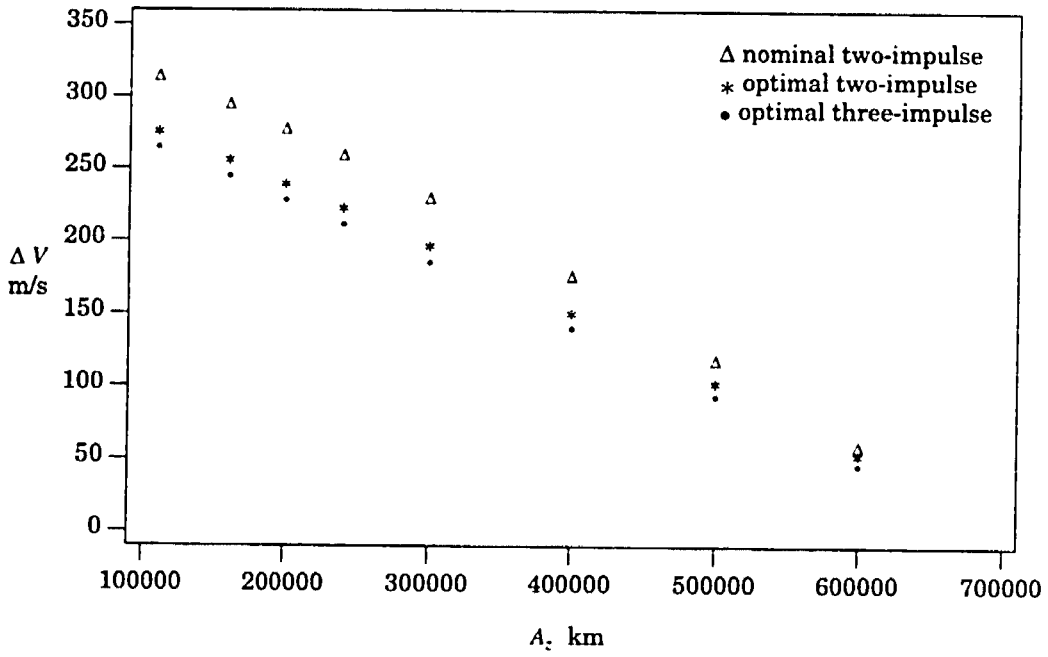

Figure IV.31 700,000 km Negative z Family: Arrival Amplitude — ΔV Relationship.

this solution is 143.50 m/s; therefore, the total cost for the three-step solution is less than the 180 m/s direct transfer cost.

The three segments of the transfer are plotted in Figure IV.32. The label 'E' denotes the departure position at the Earth; 'i' indicates the arrival at the 440,000 km halo; 'o' is the departure position from the 440,000 km halo on the inferior transfer; 'f' denotes the arrival position the the desired final halo orbit of amplitude 110,000 km. The transfer time from the Earth to the 440,000 km halo is 211 days. The time of flight from the 440,000 km halo to the 110,000 km orbit is 76 days. However, the total transfer time between the Earth and the target (110,000 km) orbit also includes the coast time along the 440,000 km halo, that is, the time between the insertion position after the transfer out from the Earth and the optimal departure position for the inferior transfer between the halos. Thus, the total transfer time is approximately 329 days.

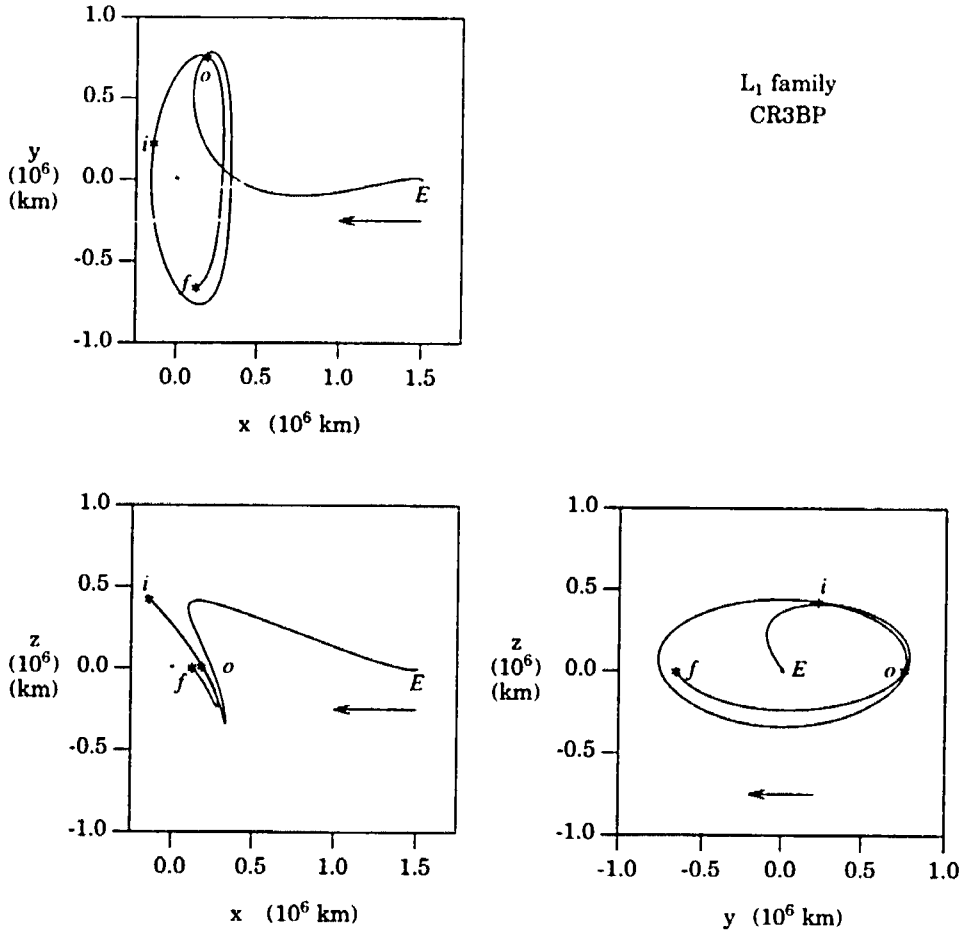

Figure IV.32 Earth to Halo Orbit, Three-Step Transfer.

V. OPTIMAL TRANSFER PATHS: ELLIPTIC PROBLEM

In the circular restricted three-body problem, a transfer between two specified orbits is constructed by computing a trajectory that passes through one position along each orbit. Thus, finding a transfer between the orbits is identical to finding a transfer between the positions. Algorithms designed to compute transfers in the elliptic restricted problem must also incorporate constraints on time that are associated with the positions along the orbits; that is, a trajectory that connects two *positions* that are included in the selected orbits does not connect the two *orbits* if the times of departure and arrival at the positions is not consistent with their definition as positions along the orbits. The optimization algorithm developed for use in the circular problem is modified to accommodate the additional time constraints. By considering the impact of the timing issues on the optimization process, families of transfers, computed in the elliptic problem, can be constructed that possess characteristics that are similar to their circular problem counterparts.

A. Preliminary Definitions

The construction of trajectories in the elliptic restricted problem requires the selection of appropriate initial position and velocity vectors and specification of a quantity that represents the location of the primaries at the time associated with the state vector. Thus, the definition of both the halo orbits and the transfer path between the orbits must consider this additional time requirement.

1. Construction of Near-Halo Orbits

Periodic halo orbits with amplitudes in the range of interest are not available in the Sun-Earth elliptic restricted problem (or the Sun-Earth/Moon barycenter system); therefore, trajectories that maintain the general shape of a halo orbit, but are not precisely periodic, are employed. Such trajectories are denoted as near-halo orbits. The near-halo orbits are computed using a multi-state differential corrections algorithm developed by Howell and Pernicka for the computation of general trajectories in the restricted three-body problem[22]. State vectors defined at intervals approximately one-quarter revolution in length, along a

periodic halo orbit (that is, computed in the circular problem), are identified as target states for input to the algorithm. One of the states is selected as the position that corresponds to the maximum z excursion along the halo orbit. The time of periapsis passage of the primaries that is associated with this position is defined to be zero. (Thus, the primaries are assumed to be at periapsis when the vehicle is at the maximum z position along the halo orbit.) Then, given the set of target state vectors, the algorithm adjusts the target points to produce a trajectory that is continuous in both position and velocity but does not necessarily include any of the original targeted positions. To accomplish this objective, the algorithm numerically integrates the differential equations that are associated with the elliptic problem using the six-dimensional original target states as the initial conditions. Then, appropriate differential corrections routines are employed to compute the modification of the states that yields position and velocity continuity at each of the patch points. Since the position associated with the maximum z excursion along the halo orbit is also modified in the procedure, the position associated with the zero periapsis time along the near-halo orbit is not coincident with the position of maximum z excursion along the path. Thus, the near-halo orbit is constructed so that the time of periapsis passage is zero at a location near, but not exactly at, the position of maximum z excursion. (That is, the primaries are not exactly at periapsis when the vehicle is at the position corresponding to the maximum z excursion along the *near*-halo orbit.) This criterion is used to define both the initial and final orbits. The definition of the times of periapsis associated with the departure and arrival orbits is an important step in the process of determining optimal transfers between the orbits, since the definition of these times is incorporated in the selection of the times of flight that may be considered for the transfer paths.

Although the Howell/Pernicka algorithm produces several state vectors along the near-halo path for computational purposes, a single state vector defines a unique near-halo orbit (as a single initial state vector defines a halo orbit in the circular problem). Thus, one state is selected to represent the trajectory for use in the optimization routine. Then, numerical integration, forward or backward in time, from that initial state produces new terminal states along the orbit for use in time-free optimization problems. Thus, the techniques employed in the circular problem are also applicable in the elliptic problem, given the initial conditions that define the desired departure/arrival halo orbits.

2. Optimization Algorithm

Given the dependence of the near-halo orbits on time, a transfer between the orbits must intersect the orbits at times that are consistent with the periapsis times that are employed in the construction of the near-halos. This provides a constraint on transfers computed

in the elliptic problem that does not exist in circular problem solutions. Given selected terminal positions, the transfer time for a solution between those positions is *specified* as the difference in the times of passage through each respective point. Thus, the variable-time optimization step in the algorithm is eliminated. Although lower cost transfers between the specified positions may be available, such trajectories do not yield transfers between the selected orbits. The time associated with an interior position is not required to satisfy any additional constraints since that position is not assumed to exist along a specific orbit. No other modification of the algorithm is required.

B. Optimal Impulsive Transfers

Two types of superior transfers between halo orbits are presented to illustrate the application of the optimization algorithm in the elliptic problem. The near-halo orbits that are used in both cases are identified by the amplitudes associated with the periodic halo orbits (computed in the circular problem) that provide the target points for the Howell/Pernicka algorithm; therefore, the actual maximum z excursions of the near-halo orbits are not exactly equal to the amplitudes that are used to identify the paths. The approximate maximum z excursion, in a positive direction, for one revolution of each near-halo is listed in Table V.1 with the amplitude of the halo orbit that was used to define the target points. In

Halo Orbit Amplitude	Near-Halo Orbit Maximum z excursion
km	km
110,000	111,390
160,000	163,930
200,000	203,644
240,000	244,345
300,000	305,355
400,000	408,303
500,000	508,055
600,000	611,270

Table V.1 Orbital Amplitudes in the Circular and Elliptic Problems.

each case, the amplitude of the halo orbit provides a reasonable representation of the size of the near-halo trajectory.

1. Positive z Family: 110,000 km A_z Departure Near-Halo Orbit

A family of superior transfers that depart from a 110,000 km near-halo orbit and move above the x − y plane (in a positive z direction) is represented by solutions for the following near-halo orbit amplitudes: 160,000; 200,000; 240,000; 300,000; 400,000; 500,000; and 600,000 km. The nominal endpoint location is selected such that the x component of acceleration is zero and the y position component is negative; at the nominal arrival point, $\ddot{x}$ is again zero and y is positive. Note that, in the elliptic problem, the x and x components of acceleration are not equal. Furthermore, the locations where each of these quantities is zero are significantly different; however, the location where the libration point centered component of acceleration ($\ddot{x}$) in the $\hat{x}$ direction is zero can be identified.

The location where $\ddot{x}$ is zero is determined from knowledge of $\ddot{x}$ and $\ddot{x}_{L1}$, where x_{L1} represents the position of the L_1 libration point relative to the barycenter. As an equilibrium solution to the equations of motion (equations II.23 through II.25), the position and velocity of the libration point are governed by

$$\dot{x}_{L1} = -\frac{\ddot{\theta}}{2\dot{\theta}} x_{L1} . \qquad [V.1]$$

Differentiating this expression, and using equations II.13 and II.14, the acceleration of the libration point along the $\hat{x}$ axis can be expressed in the form

$$\ddot{x}_{L1} = \frac{x_{L1}}{R} \frac{(e cos E - e^2)}{R^3} . \qquad [V.2]$$

Then, $\ddot{x}$ is given by

$$\ddot{x} = \ddot{x} - \ddot{x}_{L1} . \qquad [V.3]$$

Thus, the terminal points for the transfer can be identified.

Nominal costs for solutions employing endpoints where $\ddot{x}$ is zero are included in Table V.2. The nominal transfer costs are generally close to those computed for similar transfers computed in the 110,000 km A_z, positive z family for the circular problem; however, the transfer times between the two families differ by three to four days. These results are a consequence of the timing condition that is used to define the target orbits. Recall, both the departure and the arrival near-halo orbits are defined such that the primaries are at periapsis near the location of maximum z excursion. The actual periapsis time relative to the time of maximum z excursion influences the shape of the orbits; however, it has little impact on the relative orientation of the trajectories. The use of the same time of periapsis passage for the primaries in the definition of both orbits is, however, relevant to this result. By constructing each near-halo such that a maximum z excursion point along the trajectory corresponds to the time when the primaries are near periapsis, the time required for transfer between

Final Halo A_z	Nominal 2-Impulse		Optimal 2-Impulse	
	ΔV	TOF	ΔV	TOF
km	m/s	days	m/s	days
160000	22.82	75.22	22.69	76.73
200000	39.45	75.36	39.37	76.60
240000	56.96	75.51	56.93	75.77
300000	84.49	75.80	84.41	74.35
400000	132.91	75.91	132.28	72.61
500000	186.29	76.96	182.92	70.55
600000	241.23	77.21	234.89	69.50

Table V.2 110,000 km Positive z Family: Transfer Costs — Elliptic Problem.

the two near-halo trajectories is generally close to the nominal transfer time computed in the variable-time optimization step in the circular problem. Solutions in which the elliptic problem transfer time is closer to that achieved in the circular problem can be constructed by considering the circular problem transfer time in generating the target near-halo orbit, that is, using the desired transfer time to define the periapsis location of the primaries at a point of maximum z excursion on the near-halo path. However, placing the maximum z point in both departure and arrival near-halos close to the time of periapsis of the primaries produces solutions that demonstrate the application of the algorithm in the elliptic case without introducing additional issues that are not relevant to the optimization problem.

The nominal transfers for this family and the associated primer histories are plotted in Figure V.1. Note that these plots show the path relative to a rotating, oscillating libration point centered coordinate frame. The general shape of each transfer is similar to the solution in the corresponding circular family. Since the slopes of the primers in the lower frame are non-zero at the terminal times, coast arcs will reduce the cost. The optimal time-free solutions for the family are plotted in Figure V.2. In each case, optimality is achieved with two impulses, and the endpoints remain relatively close to the nominal locations. Also, the optimal costs presented in Table V.2 are within three percent of the corresponding nominal ΔV's. A plot of the costs versus the approximate amplitude for the members of this family, Figure V.3, predicts a cost of approximately 45 to 50 m/s per 100,000 km change in the maximum z-excursion distance. Thus, the results are generally consistent with the solutions developed in the circular problem. Similar costs are possible in both systems, and the optimal transfer time in the elliptic problem is within two days of the time required in the transfers designed as solutions in the circular problem.

2. Negative z Family: 110,000 km A_z Departure Near-Halo Orbit

A second family of superior transfers in the elliptic problem is represented by solutions that depart from a near-halo orbit with amplitude of 110,000 km, along a path that is generally below the $x-y$ plane, in a negative $\dot{z}$ direction. The following target orbit amplitudes are considered: 200,000; 240,000; 300,000; 400,000; 500,000; and 600,000 km. The nominal costs for this family, computed for departure where the z component of position is zero and the y component of position is positive and arrival conditions such that position component z is zero and y is negative, are included in Table V.3. The nominal costs are significantly different than those seen in Table IV.3 for members of the corresponding transfer family assuming circular primary orbits. Also, the nominal transfer times differ from those computed for transfers in the negative $\dot{z}$ direction in the circular problem. The time of maximum z excursion, relative to periapsis of the primaries, used to construct the

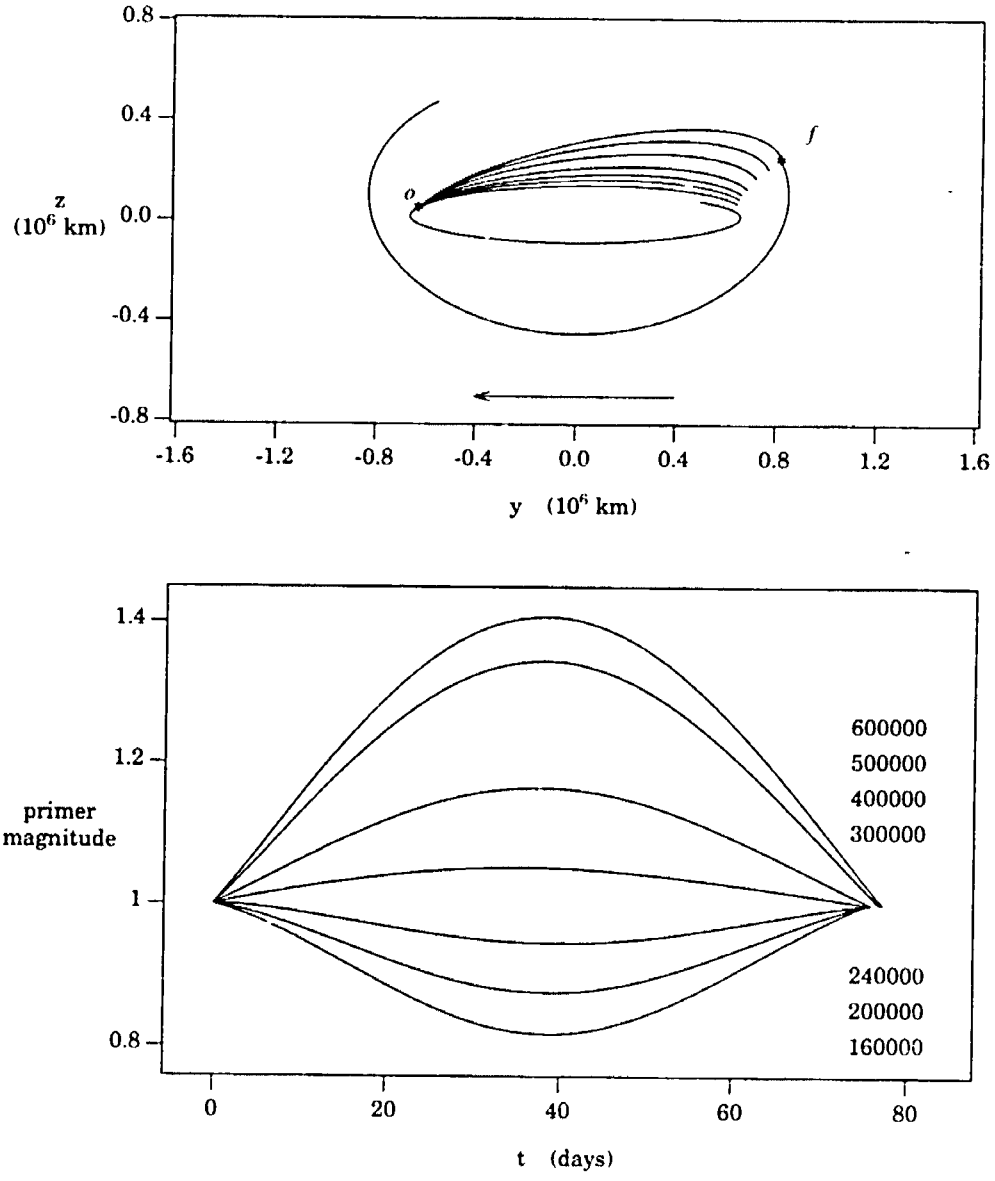

Figure V.1 110,000 km Positive z Elliptic Family Nominal Two-Impulse Solutions.

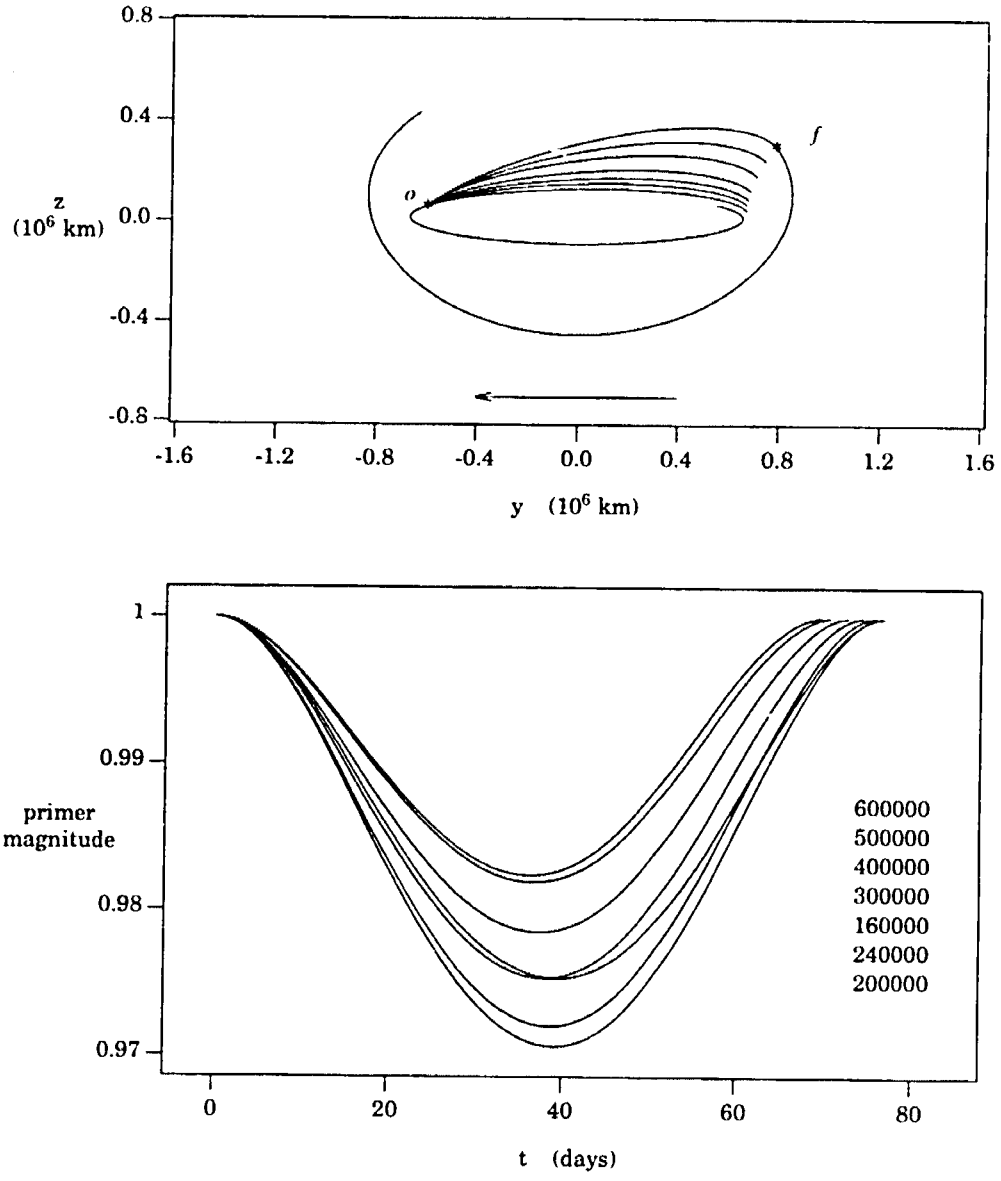

Figure V.2 110,000 km Positive z Elliptic Family: Optimal Two-Impulse Solutions.

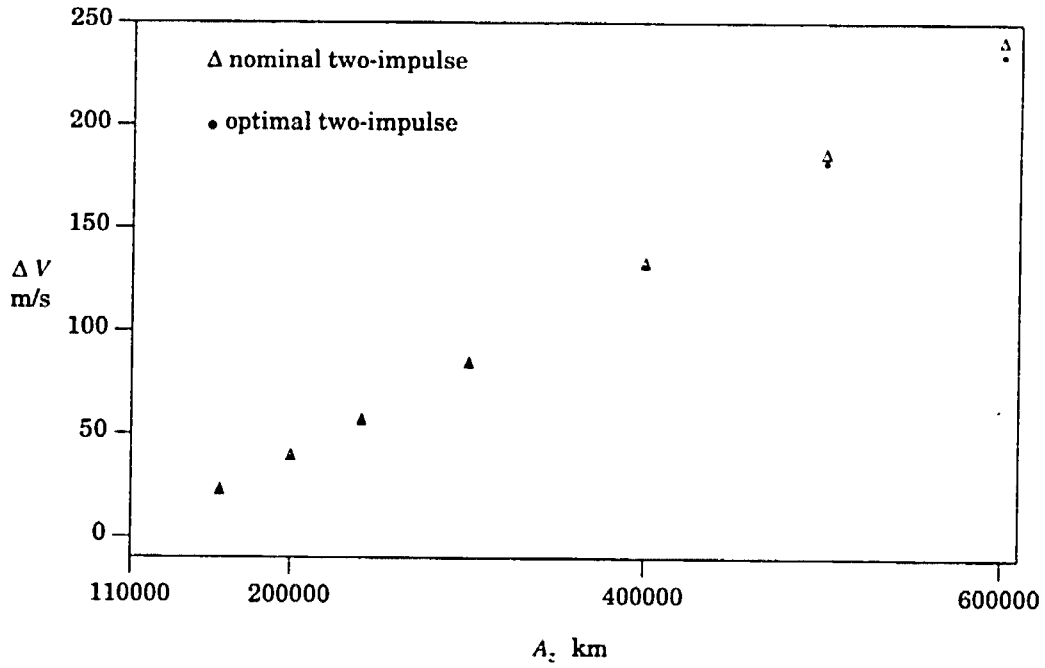

Figure V.3 110,000 km Positive z Elliptic Family: Arrival Amplitude — ΔV Relationship.

near-halo orbits is selected such that the time to transfer between positions on the near-halo orbits where the x component of acceleration is zero is similar to the time to transfer between positions where $\ddot{x}$ is zero on the halo orbits (that is, the halo orbits that are used to construct the near-halos). (Transfer times in the elliptic problem are similar to transfer times for solutions computed in the circular problem for transfers in the positive $\dot{z}$ direction.) Since the criterion used to construct the near-halo orbits defines transfer times for solutions that occur above the $x-y$ plane in the elliptic problem to be similar to transfer times for solutions above the plane in the circular problem, transfer times for solutions below the plane in the elliptic problem are notably different from transfer times for negative z transfers in the circular problem. (Note that negative z transfers are generally close to one-half revolution in length, but positive z transfers are generally less than one-half revolution. Thus, although the time to travel along the positive z arc of the near-halo halo is similar to the time required to travel along the negative z arc, the transfer times for the specific positions that have been considered here are not similar between the two cases.) Since the transfer times between the circular and elliptic problems are similar for positive z solutions that incorporate the specific positions that have been discussed, transfer times for negative z transfers in the elliptic problem are different from their circular problem counterparts (assuming that the same near-halo orbits are used in both cases, as has been assumed in this study). The optimal two-impulse transfer *costs* in the elliptic problem are, however, similar to those of the circular problem solutions. Also, in both systems, the primers for the optimal two-impulse solutions exceed one. Thus, an interior impulse is included.

The optimal three-impulse transfers and the primer histories are plotted in Figure V.4. Optimal three-impulse solutions are achieved for each of the destination near-halo orbits that are presented; however, for orbits with small amplitudes (such as the 200,000 km case), the optimization of the interior impulse, simultaneously with the terminal positions, requires large changes in the coast arcs that result in longer times of flight than that predicted by the trends exhibited by other members of the family. (The time of flight for the 200,000 km case is substantially longer than the transfer times for other members of the family.) The disparity in the orders of magnitude of the two types of gradient expressions that are employed (as discussed in section III.D.3) is particularly influential in the optimization of solutions of this type. Although optimal endpoints that produce transfer times that are consistent with the times of flight predicted by transfers to larger near-halo orbits are easily identified in the optimization process, continuity in the derivative of the primer and the Hamiltonian across the interior impulse is not achieved with those endpoints, to the tolerances that have been specified for the evaluation of optimality at the interior time. (The discontinuities are generally one to two order of magnitude larger than that which

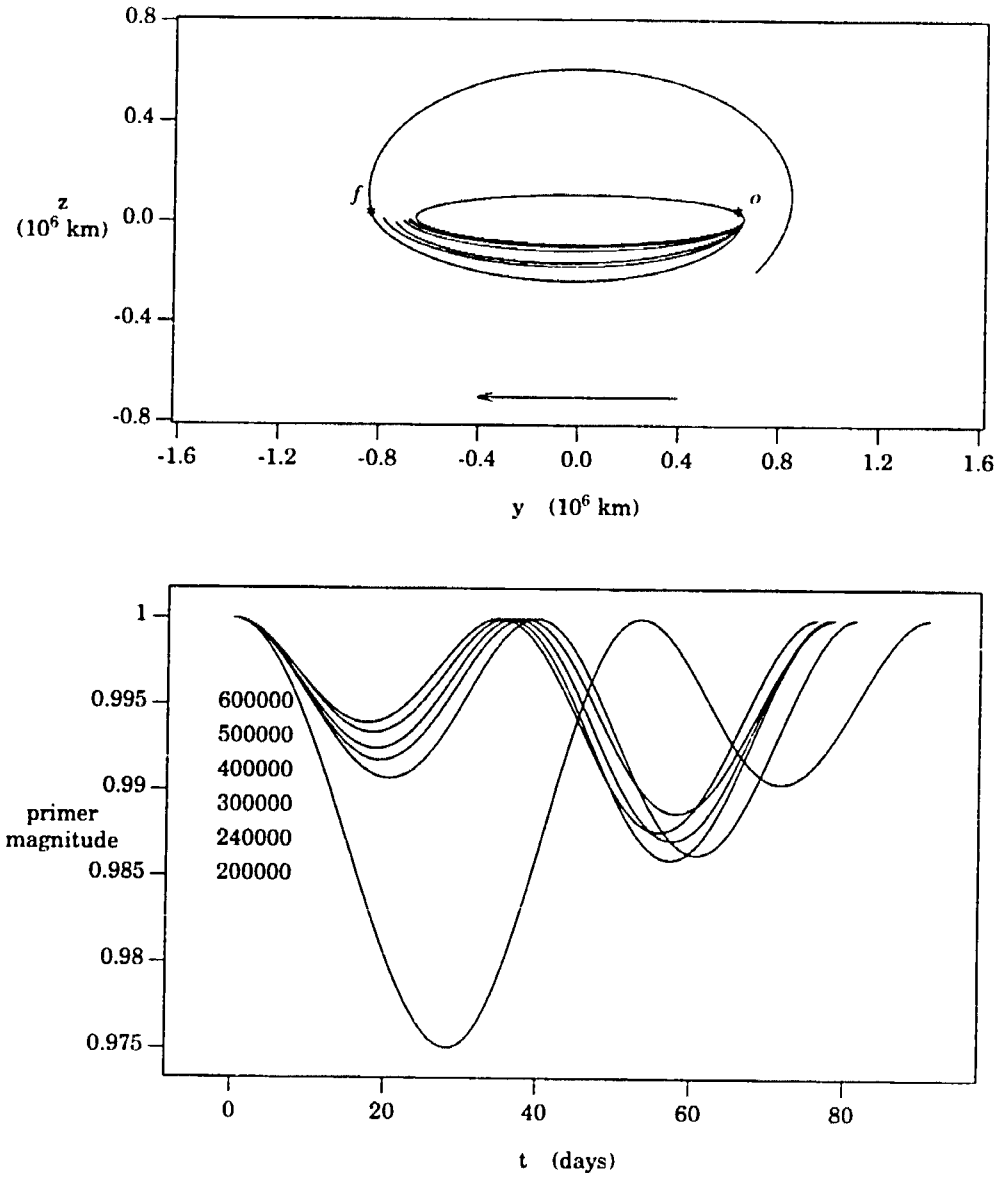

Figure V.4 110.000 Negative z Elliptic Family: Optimal Three-Impulse Solutions.

is considered acceptable.) To achieve optimality in the three-impulses simultaneously, in cases where the optimization algorithm fails to achieve an optimal interior impulse due to the disparity in the orders of magnitude of the elements of the gradient, an iterative procedure is employed that considers the terminal positions separately from the interior positions. If the algorithm that has been discussed to this point achieves a solution for which the interior impulse does not satisfy the tolerances, but further improvements in the time and position of the interior impulse are not possible due to the higher tolerance that is possible for those components of the gradient vector (relative to the tolerance that is possible for the terminal positions), an optimization problem is considered that reduces the cost by including additional coast arcs while constraining the interior position and time to the current locations. First, the endpoints are optimized assuming a fixed interior position and time. Although the actual coast arcs that are incorporated in this step are generally less than a few minutes in duration, the gradient of the cost function with respect to the time and location of the interior impulse in the resulting solution is generally several orders of magnitude larger than the gradient achieved in the solution that could not be further improved by considering all impulses simultaneously. Thus, the next step is to again attempt to improve the solution by considering all three impulses simultaneously. (For the transfer that includes the additional coast arcs, the gradient elements associated with the interior impulse are several orders of magnitude larger than the tolerance that is specified for those components; therefore, further changes in the interior impulse characteristics are possible). In this step, large changes in both the terminal positions and the interior quantities are possible; therefore, large changes in the time of flight are generally introduced. This process of iteratively optimizing only the terminal positions followed by the optimization of the three impulses is continued until no further reductions in the cost are possible in either step (or until the tolerances specified for each component of the gradient are satisfied). While this procedure generally converges to a solution that satisfies all of the tolerances, it may cause larger changes from the nominal solution than are expected. The characteristics of the first solution to which the algorithm converges (before the endpoints are optimized separately from the interior impulse) are generally consistent with the trends predicted by other members of the family for which the algorithm does achieve an acceptable optimal solution without the additional separate optimization steps, but the additional steps may produce substantial changes in that solution. However, the reduction in the cost that results from the additional steps is usually less than 0.1 m/s. Thus, the additional optimization does not substantially influence the cost, but it can have a significant impact on the shape of the transfer and, in particular, the total time of flight. (The 200,000 km near-halo orbit

optimal three-impulse transfer presented in Figure V.4 is the only transfer presented in this document that requires the application of these additional optimization steps.)

The total costs for the optimal solutions for this family are included in Table V.3. The

Final A_z	Nominal 2-Impulse		Optimal 2-Impulse		Nominal 3-Impulse		Optimal 3-Impulse	
	ΔV	TOF	ΔV	TOF	ΔV	TOF	ΔV	TOF
km	m/s	days	m/s	days	m/s	days	m/s	days
200000	50.50	83.65	37.90	64.21	37.90	64.21	37.48	90.95
240000	77.47	83.12	54.97	64.04	54.98	64.04	54.57	81.43
300000	206.41	83.12	81.55	63.63	81.56	63.63	80.94	78.14
400000	192.54	82.54	127.56	62.90	127.58	62.90	126.47	76.35
500000	276.38	81.96	175.98	60.90	176.03	60.90	173.46	78.19
600000	344.67	81.38	225.38	60.06	225.47	60.06	221.36	78.64

Table V.3 110,000 km Negative z Family: Transfer Costs — Elliptic Problem.

costs for this family are slightly higher than those for the corresponding negative z family in the circular problem; however, relative to the 110,000 km A_z positive z family in the elliptic problem, the costs associated with these transfers are smaller. (Recall, costs for negative z families in the circular problem are also smaller than costs for positive z families.) The costs for the family are plotted in Figure V.5 versus the target amplitude. For the optimal transfer costs, an approximately linear curve is established with a slope of 43 to 48 m/s per 100,000 km change in the amplitude; however, in this family, the nominal transfer costs do not follow an approximately linear curve. The Howell/Pernicka multi-state differential corrections algorithm that is used to define the departure/arrival near-halo orbits modifies the positions of a set of target points to achieve an orbit that is continuous in position and velocity, but, the algorithm is not specifically designed to produce a halo orbit. Given target points that approximate a halo orbit, a near halo-orbit is generally computed, but the closeness of the near-halo orbit to a true halo orbit cannot be specifically controlled. While the general shape of the resulting trajectory trajectory approximates the halo shape, the timing condition associated with any one individual position on the curve may be notably different than a position on the halo orbit that has a similar characteristic. The arrival position employed in the nominal transfer to the 300,000 km near-halo orbit in this family is located at the position where z is zero on the near-halo (consistent with the definition of the arrival positions for all members of this family), but the dislocation of the nominal cost for this case (evident in Figure V.5) is the result of an unusual timing condition

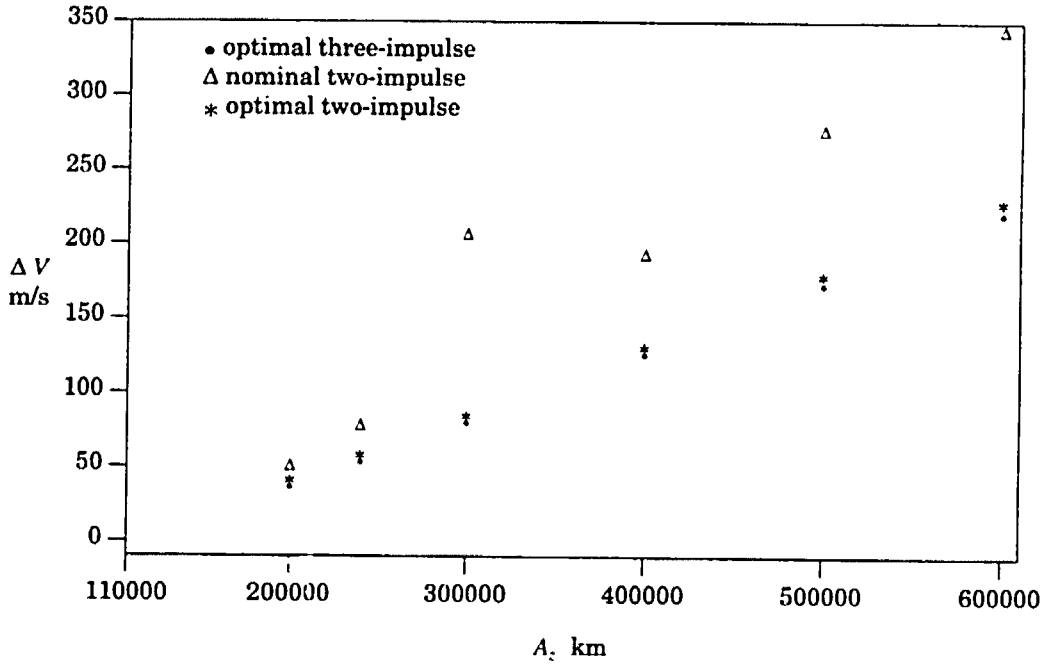

Figure V.5 110,000 km Negative z Elliptic Family: Arrival Amplitude — ΔV Relationship.

that is associated with that particular position as computed by numerically integrating the state vector defined by the Howell/Pernicka algorithm to the position where z is zero. The optimal cost for this case is consistent with the trend predicted by other members, reflective of the result that the general shape of the 300,000 km near-halo orbit is consistent with the 'halo shape,' although any one individual position may appear to be incompatible. The optimization algorithm searches over the entire near-halo orbit for appropriate arrival positions; therefore, the misalignment of specific intervals of the near-halo from an orbit that may be a better approximation of the original orbit does not substantially impact the search for an optimal transfer to the orbit. The nominal cost is associated with a specific, selected position. The optimal cost is also computed for a specific position, but that position is selected in the context of other positions on the orbit that produce larger costs.

While the optimal ΔV's are similar to their circular problem counterparts, the optimal trajectories are significantly different. Recall, optimal negative z transfers (where most of the motion occurs below the x – y plane) in the circular problem include a relatively small arc above the x – y plane (in the positive $\hat{z}$ direction) near arrival; however, the optimal arrival positions in the elliptic problem transfers are closer to the x – y plane crossing. Also, the transfer times are different in the two systems. Although disparate trajectory characteristics are achieved, the total ΔV, the objective in the minimization problem, that is computed for optimal solutions in the elliptic problem is close to that predicted by solutions computed in the circular case. This does not imply that the optimal transfer cost for any two near-halo orbits of approximately the sizes considered in a circular problem transfer will require approximately the same cost as the circular solutions. It does, however, indicate that similar transfer costs can be achieved in the two models.

VI. CONCLUSIONS

The application of primer vector theory to the optimal transfer problem between pairs of halo orbits, in conjunction with traditional numerical optimization techniques, yields impulsive transfers that satisfy all of the necessary conditions for optimality. Two classes of optimal impulsive transfers exist that are characterized by the direction of the out-of-plane motion along the trajectory and the number of impulses that are required to achieve optimality. Optimal solutions using two impulses include motion above the $x-y$ plane, in a positive $\hat{z}$ direction. Transfers in which the out-of-plane motion occurs in a negative direction, that is, below the $x-y$ plane along most of the trajectory, require three impulses. In both cases, an increase in the amplitude of the orbit of approximately 100,000 kilometers requires an additional cost of approximately 45 m/s. Transfers that exist in the negative out-of-plane direction have slightly smaller costs than transfers between the same halo orbits that are above the plane; however, the difference is generally less than two to three percent of the total ΔV. This result can be extended to larger changes in the amplitude by assuming a linear slope of approximately 45 to 50 m/s per 100,000 km change in the size of the target halo orbit. Similar results are achieved for both superior and inferior transfers. Optimal costs for transfers between near-halo orbits computed in the elliptic problem are also possible; if the departure and arrival near-halo orbits are similar in size to the periodic halo orbits used as the departure/arrival orbits in the circular problem, then the costs are also likely to be similar.

In the development of the algorithm that is used to compute the optimal transfers, two specific problems posed by earlier studies are addressed. The algorithm maintains the halo orbits throughout the optimization process. Also, all impulses are optimized simultaneously. This solution approach, however, introduces other issues that remain unresolved. The computation of time-free, two-impulse transfers in the circular problem, where the transfer time is not constrained by the definition of the halo orbits, requires the solution of a variable-time optimization problem at each step in the optimization procedure. A solution for the variable-time problem, possibly in the form of an additional analytic constraint that could be incorporated in the underconstrained differential corrections procedure, or an

analytic solution for the optimal transfer time, would eliminate the intermediate transfer computations that are required to solve the variable-time problem at each stage in the current algorithm.

The problem of achieving lower tolerances for the optimization of the coast arcs (compared with the order of magnitude of elements of the gradient vector that are associated with the interior impulse solution) is another unresolved issue. More accurate numerical integration techniques, or lower machine tolerances, that would permit the specification of lower tolerances at all stages of the computations (integration, differential corrections, and continuity specifications), are two options for reducing the tolerance that may be achieved; however, although all tolerances may be lowered with this approach, the smallest magnitudes that could be achieved for elements of the gradient vector that are associated with the interior impulse would still be higher than those for elements that are associated with the coast arcs. Thus, this approach does not solve the problem of unequal tolerance levels among different types of variables.

The solutions that have been considered in this work are computed for primary motion modeled consistent with the assumptions of the circular or elliptic restricted three-body problems. The primer vector theory, as developed, is not, however, applicable to a more general model of the primary motion. Although Hiday's development of the primer vector theory does not rely on the periodicity of the primary motion that exists in the elliptic problem, it does include several steps in which the specific form of the equations of motion, expressed in terms of the barycenter rotating coordinates, are employed. (For example, useful properties of the derivatives of the acceleration terms, such as $\partial\bar{g}/\partial\bar{r}$, are used in the development of the adjoint equation.) To consider the optimization of transfers between orbits computed assuming primary motion modeled using ephemeris data, such as the models employed in previous studies of halo and near-halo orbits [18], or using a model that includes solar radiation pressure, a solution for the optimization problem defined for equations of motion that do not possess the form employed by Hiday's derivation of the solution is required. Although Hiday assumed a more general form for the equations than Lawden's development, Hiday's development does not include the type of terms that exist in more general (ephemeris) models; therefore, an alternate derivative of the necessary conditions for optimality is required.

As the transfers that have been presented indicate, optimal impulsive transfers can be computed by combining the analytic primer vector analyses with numerical implementation techniques. By defining each departure and target orbit by a single state vector, and requiring the transfer trajectories to include positions that represent those states, transfers can be constructed that retain the specified orbits. Also, since numerical integration is used to

identify the new endpoints for the time-free aspects of the optimization problem, all transfers that are computed in the procedure connect the original orbits. Finally, the trajectory is optimized as a single solution, rather than a collection of segments, by considering all of the impulses simultaneously. By defining multi-state boundary value problems that incorporate the constraints on all of the variables of interest, trajectories can be constructed that satisfy all of the required conditions using differential correctors that are specifically designed to achieve those constraints. Thus, although numerical techniques form the basis for this aspect of the continuing effort to obtain optimal transfers in the restricted problem, the tools are successful because they are designed to satisfy the requirements of the analytic, primer vector solutions while utilizing the dynamics of the non-linear problem.

LIST OF REFERENCES

LIST OF REFERENCES

[1] V. Szebehely, *Adventures in Celestial Mechanics: A First Course in the Theory of Orbits*, University of Texas Press, Austin, 1989.

[2] K.W. Gatland ed., "Earth Gets A Halo," *Spaceflight*, vol. 21, pp. 195–196, May 1979.

[3] R.W. Farquhar, D.P. Muhonen, and D.L. Richardson, "Mission Design for a Halo Orbiter of the Earth," *Journal of Spacecraft and Rockets*, vol. 14, pp. 170–177, March 1977.

[4] D.L. Richardson and N.D. Cary, "A Uniformly Valid Solution for Motion About the Interior Libration Point of the Perturbed Elliptic-Restricted Problem," AAS Paper 75-021, AIAA/AAS Astrodynamics Specialists Conference, Nassau, Bahamas, July 28-30 1975.

[5] C. Marchal, *The Three-Body Problem*, Elsevier, Amsterdam, 1990.

[6] L.A. Hiday, "Optimal Transfers Between Libration-Point Orbits in the Elliptic Restricted Three-Body Problem," PhD Thesis, School of Aeronautics and Astronautics, Purdue University, West Lafayette, Indiana, August 1992.

[7] L.A. Hiday and K.C. Howell, "Transfers Between Libration-Point Orbits in the Elliptic Restricted Problem," AAS 92-126, AAS/AIAA Spaceflight Mechanics Meeting, Colorado Springs, Colorado, February 24-26 1992.

[8] D.F. Lawden, *Optimal Trajectories for Space Navigation*, Butterworths, London, 1963.

[9] H.J. Pernicka, "The Numerical Determination of Lissajous Orbits in the Circular Restricted Three-Body Problem," MS Thesis, School of Aeronautics and Astronautics, Purdue University, West Lafayette, Indiana, December 1986.

[10] F.R. Moulton, *An Introduction to Celestial Mechanics*, The Macmillan Company, New York, second edition, 1914.

[11] V. Szebehely, *Theory of Orbits: The Restricted Problem of Three Bodies*, Academic Press, New York, 1967.

[12] H. C. Plummer, *An Introductory Treatise on Dynamical Astronomy*, Cambridge University Press, New York, 1918.

[13] H.C. Plummer, "On Oscillating Satellites - 1," *Monthly Notices of the Royal Astronomical Society*, vol. 63, pp. 436–443, 1903.

[14] R.W. Farquhar, "The Control and Use of Libration-Point Satellites," PhD Thesis, Department of Aeronautics and Astronautics, Stanford University, Stanford, California, July 1968.

[15] R.W. Farquhar, "The Control and Use of Libration-Point Satellites," TR R-346, NASA, September 1970.

[16] R.W. Farquhar and A.A. Kamel, "Quasi-Periodic Orbits About the Translunar Libration Point," *Celestial Mechanics*, vol. 7, pp. 458–473, 1973.

[17] D.L. Richardson, "Analytic Construction of Periodic Orbits About the Collinear Points," *Celestial Mechanics*, vol. 22, pp. 241–253, 1980.

[18] J.L. Bell, "The Impact of Solar Radiation Pressure on Sun-Earth L1 Libration Point Orbits," MS Thesis, School of Aeronautics and Astronautics, Purdue University, West Lafayette, Indiana, August 1991.

[19] J.V. Breakwell and J.V. Brown, "The 'Halo' Family of 3-Dimensional Periodic Orbits in the Earth-Moon Restricted Three-Body Problem," *Celestial Mechanics*, vol. 20, pp. 389–404, 1979.

[20] K.C. Howell, "Three Dimensional, Periodic Halo Orbits in the Restricted Three-Body Problem," PhD Thesis, Department of Aeronautics and Astronautics, Stanford University, Stanford, California, March 1983.

[21] K.C. Howell, "Three Dimensional, Periodic 'Halo' Orbits," *Celestial Mechanics*, vol. 32, pp. 53–71, 1984.

[22] K.C. Howell and H.J. Pernicka, "Numerical Determination of Lissajous Trajectories in the Restricted Three-Body Problem," *Celestial Mechanics*, vol. 41, pp. 107–124, 1988.

[23] W. Hohmann, "The Attainability of Heavenly Bodies," NASA TT-F-44, Translation of "Die Erreichbarkeit der Himmelskorper," R. Oldenbourg (Munich-Berlin), 1925, November 1960.

[24] P.M. Lion and M. Handelsman, "Primer Vector on Fixed-Time Impulsive Trajectories," *AIAA Journal*, vol. 6, pp. 127–132, January 1968.

[25] J. E. Prussing, "Optimal Four-Impulse Fixed-Time Rendezvous in the Vicinity of a Circular Orbit," *AIAA Journal*, vol. 7, pp. 928–935, May 1969.

[26] J. E. Prussing, "Optimal Two- and Three-Impulse Fixed-Time Rendezvous in the Vicinity of a Circular Orbit," *AIAA Journal*, vol. 8, pp. 1221–1228, July 1970.

[27] S.S. Rao, *Optimization: Theory and Applications*, Wiley Eastern Limited, New Delhi, second edition, 1984.

[28] G.N. Vanderplaats, *ADS* – A Fortran Program for Automated Design Synthesis (Version 1.10)," May 1985.

[29] A.E. Roy, *The Foundations of Astrodynamics*, The Macmillan Company, London, 1965.

[30] R.W. Farquhar, "The Moon's Influence on the Sun/Earth Exterior Libration Point," *Celestial Mechanics*, vol. 2, pp. 131–133, 1970.

[31] H.J. Pernicka and K.C. Howell, "Sun-Earth Libration Point Trajectories that Avoid the Solar Exclusion Zone," *Journal of the Astronautical Sciences*, vol. 38, pp. 269–288, July-September 1990.

[32] B.T. Barden, "Using Stable Manifolds to Generate Transfers in the Circular Restricted Problem of Three Bodies," MS Thesis, School of Aeronautics and Astronautics, Purdue University, West Lafayette, Indiana, December 1994.

APPENDIX

APPENDIX
COST DISTRIBUTION

A. Superior Transfers: Positive A_z Families

1. Positive z Family: 110,000 km A_z Departure Halo Orbit

Final Halo A_z	Nominal 2-Impulse			Optimal 2-Impulse		
	ΔV_1	ΔV_2	ΔV	ΔV_1	ΔV_2	ΔV
km	m/s	m/s	m/s	m/s	m/s	m/s
160000	10.47	10.49	20.97	10.35	10.39	20.74
200000	19.08	19.15	38.23	18.95	19.08	38.02
240000	27.91	28.08	56.00	27.80	28.08	55.88
300000	41.61	42.04	83.65	41.51	42.14	83.65
400000	65.68	66.85	132.52	65.36	66.82	132.18
500000	91.18	93.42	184.59	90.21	92.69	182.90
600000	117.86	121.30	239.17	115.87	119.29	235.16
700000	145.44	149.98	295.42	142.17	146.22	288.38
800000	173.62	178.98	352.60	167.00	173.12	342.12

Table A.1 110,000 km Positive z Family: Two-Impulse Transfer Cost Distribution.

2. Positive z Family: 200,000 km A_z Departure Halo Orbit

Final Halo A_z	Nominal 2-Impulse			Optimal 2-Impulse		
	ΔV_1	ΔV_2	ΔV	ΔV_1	ΔV_2	ΔV
km	m/s	m/s	m/s	m/s	m/s	m/s
240000	8.92	8.94	17.87	8.92	8.95	17.86
300000	22.81	22.95	45.76	22.74	22.91	45.65
400000	47.26	47.90	95.16	46.79	47.42	94.21
500000	73.19	74.67	147.86	71.88	73.10	144.98
600000	100.32	102.80	203.12	97.78	99.51	197.29
700000	128.32	131.75	260.07	124.32	126.26	250.57
800000	156.87	161.04	317.91	151.36	153.01	304.37

Table A.2 200,000 km Positive z Family: Two-Impulse Transfer Cost Distribution.

B. Superior Transfers: Negative A_z Families

1. Negative z Family: 110,000 km A_z Departure Halo Orbit

Final Halo A_z	Nominal 2-Impulse			Optimal 2-Impulse		
	ΔV_1	ΔV_2	ΔV	ΔV_1	ΔV_2	ΔV
km	m/s	m/s	m/s	m/s	m/s	m/s
160000	10.34	10.36	20.70	10.33	9.69	20.02
200000	16.92	21.59	38.51	19.09	17.52	36.61
240000	28.84	28.26	57.10	28.13	25.55	53.68
300000	43.88	43.10	86.99	42.12	37.98	80.09
400000	70.78	70.03	140.81	66.27	59.74	126.01
500000	99.73	98.14	197.86	91.12	82.66	173.78
600000	132.11	124.01	256.12	116.29	106.58	222.87
700000	158.99	154.68	313.67	141.45	131.41	272.86
800000	187.52	182.08	369.60	166.35	157.11	323.46

Table A.3 110,000 km Negative z Family: Two-Impulse Transfer Cost Distribution.

Final Halo A_z	Nominal 3-Impulse				Optimal 3-Impulse			
	ΔV_1	ΔV_2	ΔV_3	ΔV	ΔV_1	ΔV_2	ΔV_3	ΔV
km	m/s	m/s	m/s	m/s	m/s	m/s	m/s	m/s
160000	10.30	0.06	9.66	20.02	10.07	0.58	9.37	20.02
200000	18.98	0.21	17.41	36.61	18.32	1.84	16.42	36.57
240000	27.91	0.42	25.34	53.67	26.62	3.76	23.18	53.57
300000	41.62	0.93	37.52	80.06	39.23	7.79	32.76	79.78
400000	65.00	2.26	58.67	125.92	61.26	17.15	46.60	125.00
500000	88.70	4.14	80.74	173.57	86.02	29.28	56.23	171.54
600000	112.45	6.46	103.59	222.50	117.09	43.84	57.79	218.72
700000	135.92	9.17	127.19	272.28	166.40	60.60	38.90	265.89

Table A.4 110,000 km Negative z Family: Three-Impulse Transfer Cost Distribution.

2. Negative z Family: 200,000 km A_z Departure Halo Orbit

Final Halo A_z	Nominal 2-Impulse			Optimal 2-Impulse		
	ΔV_1	ΔV_2	ΔV	ΔV_1	ΔV_2	ΔV
km	m/s	m/s	m/s	m/s	m/s	m/s
240000	9.43	9.40	18.84	8.62	8.47	17.08
300000	24.54	24.45	48.99	22.14	21.40	43.55
400000	51.87	51.43	103.31	45.81	43.76	89.57
500000	80.95	79.86	160.81	70.34	67.13	137.47
600000	110.70	108.67	219.37	95.27	91.43	186.70
700000	140.22	137.06	277.29	120.25	116.60	236.85
800000	168.87	164.58	333.45	145.00	142.61	287.61

Table A.5 200,000 km Negative z Family: Two-Impulse Transfer Cost Distribution.

Final Halo A_z	Nominal 3-Impulse				Optimal 3-Impulse			
	ΔV_1	ΔV_2	ΔV_3	ΔV	ΔV_1	ΔV_2	ΔV_3	ΔV
km	m/s	m/s	m/s	m/s	m/s	m/s	m/s	m/s
240000	8.48	0.26	8.33	17.08	7.70	1.88	7.41	17.00
300000	21.73	0.77	21.00	48.99	19.50	5.81	17.90	43.22
400000	44.62	2.17	42.67	89.46	40.17	14.91	33.37	88.45
500000	67.96	4.16	65.10	137.23	63.27	26.62	45.12	135.01
600000	91.41	6.64	88.23	186.28	91.28	40.46	50.48	182.22
700000	114.59	9.54	112.05	236.18	130.29	55.93	43.30	229.51

Table A.6 200,000 km Negative z Family: Three-Impulse Transfer Cost Distribution.

3. Negative z Family: 240,000 km A_z Departure Halo Orbit

Final Halo A_z	Nominal 2-Impulse			Optimal 2-Impulse		
	ΔV_1	ΔV_2	ΔV	ΔV_1	ΔV_2	ΔV
km	m/s	m/s	m/s	m/s	m/s	m/s
300000	15.11	15.07	30.18	13.35	13.12	26.47
400000	42.45	42.16	84.61	36.81	35.71	72.52
500000	72.04	70.21	142.26	61.21	59.25	120.46
600000	101.45	99.49	200.94	86.05	83.69	169.74
700000	130.90	128.09	258.99	110.97	108.97	219.94
800000	159.50	155.77	315.28	135.68	135.08	270.75

Table A.7 240,000 km Negative z Family: Two-Impulse Transfer Cost Distribution.

Final Halo A_z	Nominal 3-Impulse				Optimal 3-Impulse			
	ΔV_1	ΔV_2	ΔV_3	ΔV	ΔV_1	ΔV_2	ΔV_3	ΔV
km	m/s	m/s	m/s	m/s	m/s	m/s	m/s	m/s
300000	13.06	0.55	12.84	26.45	12.06	3.92	27.04	26.228
400000	35.73	1.97	34.72	72.41	31.49	12.93	27.04	71.46
500000	58.91	4.02	57.29	120.21	53.79	24.49	39.74	118.02
600000	82.21	6.58	80.51	169.30	80.45	38.08	46.73	165.25
700000	105.23	9.61	104.40	219.24	116.25	53.14	43.19	212.57

Table A.8 240,000 km Negative z Family: Three-Impulse Transfer Cost Distribution.

C. Inferior Transfers: Positive z Families

1. Positive z Family: 600,000 km A_z Departure Halo Orbit

Final Halo A_z	Nominal 2-Impulse			Optimal 2-Impulse		
	ΔV_1	ΔV_2	ΔV	ΔV_1	ΔV_2	ΔV
km	m/s	m/s	m/s	m/s	m/s	m/s
110000	121.30	117.86	239.17	119.29	115.87	235.16
160000	111.24	108.34	219.58	108.46	106.06	214.52
200000	102.80	100.32	203.12	99.51	97.78	197.29
240000	94.00	91.95	185.95	90.33	89.14	179.47
300000	80.14	78.68	158.82	76.17	75.56	151.73
400000	55.31	54.65	109.96	51.65	51.53	103.18
500000	28.48	28.32	56.80	26.19	26.20	52.39

Table A.9 600,000 km Positive z Family: Two-Impulse Transfer Cost Distribution.

2. Positive z Family: 700,000 km A_z Departure Halo Orbit

Final Halo A_z	Nominal 2-Impulse			Optimal 2-Impulse		
	ΔV_1	ΔV_2	ΔV	ΔV_1	ΔV_2	ΔV
km	m/s	m/s	m/s	m/s	m/s	m/s
110000	149.98	145.44	295.42	146.21	142.17	288.38
160000	140.07	136.15	276.22	135.27	132.51	267.78
200000	131.75	128.32	260.07	126.26	124.32	250.57
240000	123.08	120.13	243.20	117.03	115.75	232.78
300000	109.40	107.14	216.54	102.82	102.25	205.06
400000	84.85	83.58	168.44	78.26	78.29	156.56
500000	58.22	57.69	115.91	52.81	52.97	105.78
600000	29.80	29.68	59.48	26.67	26.74	53.41

Table A.10 700,000 km Positive z Family: Two-Impulse Transfer Cost Distribution.

3. Positive z Family: 800,000 km A_z Departure Halo Orbit

Final Halo A_z	Nominal 2-Impulse			Optimal 2-Impulse		
	ΔV_1	ΔV_2	ΔV	ΔV_1	ΔV_2	ΔV
km	m/s	m/s	m/s	m/s	m/s	m/s
110000	178.98	173.62	352.60	173.12	169.00	342.12
160000	169.23	164.54	333.77	162.08	159.47	321.55
200000	161.04	156.87	317.91	153.01	151.36	304.37
240000	152.51	148.85	301.36	143.74	142.86	286.60
300000	139.06	136.14	275.19	129.50	129.42	258.92
400000	114.90	113.07	227.97	104.95	105.51	210.46
500000	88.64	87.67	176.31	79.55	80.17	159.72
600000	60.48	60.09	120.57	53.49	53.88	107.37
700000	30.78	30.70	61.47	26.93	27.05	53.98

Table A.11 800,000 km Positive z Family: Two-Impulse Transfer Cost Distribution.

D. Inferior Transfers: Negative z Families

1. Negative z Family: 500,000 km A_z Departure Halo Orbit

Final Halo A_z	Nominal 2-Impulse			Optimal 2-Impulse		
	ΔV_1	ΔV_2	ΔV	ΔV_1	ΔV_2	ΔV
km	m/s	m/s	m/s	m/s	m/s	m/s
110000	98.14	99.73	197.86	82.66	91.12	173.78
160000	88.40	89.72	178.12	74.46	79.49	153.95
200000	79.86	80.95	160.81	67.13	70.34	137.47
240000	70.70	71.55	142.25	59.25	61.20	120.46
300000	55.87	56.43	112.29	46.62	47.43	94.05
400000	28.82	29.08	57.91	23.96	24.05	48.01

Table A.12 500,000 km Negative z Family: Two-Impulse Transfer Cost Distribution.

Final Halo A_z	Nominal 3-Impulse				Optimal 3-Impulse			
	ΔV_1	ΔV_2	ΔV_3	ΔV	ΔV_1	ΔV_2	ΔV_3	ΔV
km	m/s	m/s	m/s	m/s	m/s	m/s	m/s	m/s
110000	82.59	0.05	91.19	173.83	56.22	29.29	86.03	171.54
160000	74.39	0.05	79.56	154.00	50.27	28.18	73.11	151.55
200000	67.07	0.05	70.40	137.51	45.13	26.62	63.26	135.01
240000	59.19	0.04	61.26	120.50	39.73	24.50	53.79	118.02
300000	46.57	0.03	47.48	94.08	31.32	20.35	40.14	91.81
400000	23.94	0.02	24.07	48.03	16.45	11.24	18.87	46.57

Table A.13 500,000 km Negative z Family: Three-Impulse Transfer Cost Distribution.

2. Negative z Family: 600,000 km A_z Departure Halo Orbit

Final Halo A_z	Nominal 2-Impulse			Optimal 2-Impulse		
	ΔV_1	ΔV_2	ΔV	ΔV_1	ΔV_2	ΔV
km	m/s	m/s	m/s	m/s	m/s	m/s
110000	126.65	129.40	256.05	106.59	116.29	222.87
160000	117.08	119.44	236.52	98.60	104.53	203.14
200000	108.67	110.71	219.37	91.43	95.27	186.70
240000	99.62	101.33	200.94	83.69	86.05	169.74
300000	84.96	86.20	171.16	71.21	72.18	143.39
400000	57.50	59.52	117.02	48.69	48.71	97.40
500000	29.49	29.73	59.22	24.74	24.67	49.41

Table A.14 600,000 km Negative z Family: Two-Impulse Transfer Cost Distribution.

Final Halo A_z	Nominal 3-Impulse				Optimal 3-Impulse			
	ΔV_1	ΔV_2	ΔV_3	ΔV	ΔV_1	ΔV_2	ΔV_3	ΔV
km	m/s	m/s	m/s	m/s	m/s	m/s	m/s	m/s
110000	106.45	0.10	116.42	222.97	57.78	43.84	117.09	218.72
160000	98.48	0.10	104.66	203.23	54.00	42.31	102.44	198.75
200000	91.31	0.10	95.40	186.80	50.52	40.45	91.25	182.22
240000	83.58	0.09	86.17	169.83	46.73	38.08	80.44	165.25
300000	71.11	0.08	72.28	143.47	40.53	33.62	64.90	139.05
400000	48.63	0.06	48.78	97.46	29.02	24.18	40.63	93.83
500000	24.72	0.02	24.69	49.43	15.69	12.79	18.80	47.27

Table A.15 600,000 km Negative z Family: Three-Impulse Transfer Cost Distribution.

3. Negative z Family: 700,000 km A_z Departure Halo Orbit

Final Halo A_z	Nominal 2-Impulse			Optimal 2-Impulse		
	ΔV_1	ΔV_2	ΔV	ΔV_1	ΔV_2	ΔV
km	m/s	m/s	m/s	m/s	m/s	m/s
110000	154.81	158.86	313.67	131.41	141.45	272.86
160000	145.37	148.94	294.31	123.64	129.59	253.22
200000	137.06	140.23	277.29	116.60	120.25	236.85
240000	128.14	130.85	258.99	108.97	110.97	219.94
300000	113.63	115.78	229.41	96.61	2 97.04	193.65
400000	83.84	92.04	175.88	74.16	2 73.56	147.72
500000	58.71	59.35	118.05	50.17	0 49.59	99.76
600000	29.52	29.45	58.98	25.29	1 25.07	50.36

Table A.16 700,000 km Negative z Family: Two-Impulse Transfer Cost Distribution.

Final Halo A_z	Nominal 3-Impulse				Optimal 3-Impulse			
	ΔV_1	ΔV_2	ΔV_3	ΔV	ΔV_1	ΔV_2	ΔV_3	ΔV
km	m/s	m/s	m/s	m/s	m/s	m/s	m/s	m/s
110000	131.19	0.17	141.68	273.03	38.89	60.60	166.41	265.89
160000	123.42	0.17	129.80	253.39	42.46	58.27	145.27	246.00
200000	116.39	0.17	120.46	237.02	43.37	55.92	130.22	229.51
240000	108.77	0.16	111.17	220.10	43.26	53.13	116.18	212.57
300000	96.43	0.15	97.22	193.80	41.50	48.21	96.71	186.41
400000	74.03	0.12	73.69	147.84	35.75	38.27	67.24	141.25
500000	50.09	0.08	49.67	99.84	26.96	26.61	41.16	94.73
600000	25.25	0.03	25.10	50.38	15.03	13.72	18.72	47.47

Table A.17 700,000 km Negative z Family: Three-Impulse Transfer Cost Distribution.

E. Superior Transfers: Elliptic Problem

1. Positive z Family: 110,000 km A_z Departure Near-Halo Orbit

Final Halo A_z	Nominal 2-Impulse			Optimal 2-Impulse		
	ΔV_1	ΔV_2	ΔV	ΔV_1	ΔV_2	ΔV
km	m/s	m/s	m/s	m/s	m/s	m/s
160000	11.01	11.81	22.82	7.89	14.80	22.69
200000	19.40	20.06	39.45	16.20	23.17	39.37
240000	28.16	28.81	56.96	25.09	31.84	56.93
300000	41.79	42.71	84.49	38.92	45.49	84.41
400000	66.12	66.79	132.91	64.36	67.92	132.28
500000	91.74	94.55	186.29	87.99	94.93	182.92
600000	119.00	122.23	241.23	114.89	119.99	234.89

Table A.18 110,000 km Positive z Elliptic Family: Two-Impulse Transfer Cost Distribution.

2. Negative z Family: 110,000 km A_z Departure Near-Halo Orbit

Final Halo A_z	Nominal 2-Impulse			Optimal 2-Impulse		
	ΔV_1	ΔV_2	ΔV	ΔV_1	ΔV_2	ΔV
km	m/s	m/s	m/s	m/s	m/s	m/s
200000	13.82	36.68	50.50	8.13	29.77	37.90
240000	23.11	54.36	77.47	15.55	39.43	54.97
300000	82.59	123.82	206.41	28.07	53.48	81.55
400000	76.62	115.92	192.54	55.20	72.35	127.56
500000	110.09	166.29	276.38	75.27	100.71	175.98
600000	147.45	197.22	344.67	103.74	121.63	225.38

Table A.19 110,000 km Negative z Elliptic Family: Two-Impulse Transfer Cost Distribution.

Final Halo A_z	Nominal 3-Impulse				Optimal 3-Impulse			
	ΔV_1	ΔV_2	ΔV_3	ΔV	ΔV_1	ΔV_2	ΔV_3	ΔV
km	m/s	m/s	m/s	m/s	m/s	m/s	m/s	m/s
200000	8.13	0.00	29.76	37.90	1.18	3.83	32.47	37.48
240000	15.56	0.00	39.42	54.98	4.52	6.36	43.68	54.57
300000	28.08	0.00	53.47	81.56	12.69	10.43	57.82	80.94
400000	55.24	0.02	72.32	127.58	36.43	17.83	72.21	126.47
500000	75.35	0.05	100.63	176.03	43.37	30.46	99.63	173.46
600000	103.88	0.10	121.50	225.47	71.02	42.47	107.88	221.36

Table A.20 110,000 km Negative z Elliptic Family: Three-Impulse Transfer Cost Distribution.

VITA

VITA

Julia L. Bell, daughter of Dorothy and David Bell, was born on January 4, 1967. With her sisters, Jennifer and Deborah, Julia grew up in Minersville, Pennsylvania. She was educated in the Minersville Area public school system, where she attended the Llewellyn Elementary Center, the Minersville Area Middle School, and the Minersville Area Jr.-Sr. High School, graduating as the valedictorian of her class in 1984.

From 1984 to 1986, Julia attended the Schuylkill Campus of the Pennsylvania State University, where she was awarded the 1986 Schuylkill Campus Mathematics and Engineering Awards. She completed her degree requirements at the University Park campus of Penn State from 1986 to 1988, graduating with high distinction in 1988 with a B.S. degree in Aerospace Engineering and a B.S. degree in Mathematics, under the simultaneous dual-degree program.

Julia began graduate school in the School of Aeronautics and Astronautics at Purdue University in 1988 and completed the requirements for the M.S. degree in Aeronautical and Astronautical Engineering in 1991. During her work at Purdue, she was selected to receive the David Ross Fellowship, Purdue Research Foundation Fellowship, and a NASA Indiana Space Grant Consortium Fellowship.